SYNTHESIS AND STUDY OF PERYLENE-BRIDGE-ANCHOR DERIVATIVES FOR METAL OXIDES SEMICONDUCTOR SENSITIZATION

by

HAO FAN

A dissertation submitted to the

Graduate School – Newark

Rutgers, The State University of New Jersey

in partial fulfillment of requirements

for the degree of

Doctor of Philosophy

Graduate Program in Chemistry

Written under the direction of

Professor Elena Galoppini

and approved by

_____

_____

_____

_____

Newark, New Jersey

October 2018

ABSTRACT OF THE DISSERTATION

SYNTHESIS AND STUDY OF PERYLENE-BRIDGE-ANCHOR DERIVATIVES FOR METAL OXIDES SEMICONDUCTOR SENSITIZATION

By HAO FAN

Dissertation Director:
Professor Elena Galoppini

Electron transfer at the interface between a photoactive molecule and large-bandgap nanostructured metal oxide (MO_n) semiconductors remains at the center of intense research in numerous areas for solar energy conversion. Organic chromophore-bridge-anchor compounds are important to the studies of heterogeneous charge transfer on MOn semiconductors and are widely employed in various photochemistry researches. In this thesis, we report the synthesis of 2,5-di-*tert*-butylperylene (**DTBuPe**) and a series of **DTBuPe**-bridge-anchor compounds, and study their steady state photochemical properties in solutions as well as on nanostructured metal oxide semiconductor films.

The thesis described a practical pathway to synthesize the **DTBuPe**, and further modification of the **DTBuPe** framework. Two modification routes were employed; one starting from formylation, which can be followed by reduction, oxidation or other functional group transformation of the aldehyde group. The second route starts from bromination of the framework, followed by various palladium catalyzed cross-coupling reactions. Through these methods, a series of **DTBuPe**-bridge-anchor derivatives were synthesized.

The spectroscopic properties of **DTBuPe**-bridge-anchor derivatives in solution and bound to nanostructured semiconductor surfaces were also investigated by absorption and

emission spectra. 8,11-di-*tert*-Butylperylene-3-carboxylic acid (**DTBuPe-COOH**), 3-(8,11-di-*tert*-Butylperylen-3-yl)propanoic acid (**DTBuPe-Prop-COOH**), 4-(8,11-di-*tert*-Butylperylen-3-yl)benzoic acid (**DTBuPe-Ph-COOH**) and perylene-3-carboxylic acid (**Pe-COOH**) were bound to both TiO_2 and ZrO_2 films and characterized by absorption and emission spectra. A comparison of the properties of **DTBuPe**-bridge-anchor/TiO_2 and perylene/TiO_2 is made, and the influence of t-butyl spacing group as well as different bridge units is investigated. In addition, perylene was functionalized with an azide group (9-(4-azidophenyl)-2,5-di-*tert*-Butylperylene (**DTBuPe-Ph-N_3**)) for click chemistry. Copper-catalyzed azide-alkyne cycloaddition (CuAAC) reaction of **DTBuPe-Ph-N_3** was successfully performed in solution and on ZnO nanostructured surfaces which was functionalized with propiolic acid in a stepwise functionalization process. The sensitized ZnO surface was characterized by SEM, XPS and TA. The morphology of ZnO nanorod was preserved and strong electronic coupling between sensitizer and semiconductor film was obtained.

Acknowledgement

I would like to take this opportunity, first and foremost, to thank my supervisor, Professor Elena Galoppini, for sharing her knowledge on synthetic and physical chemistry. It has been a pleasure studying in her research group for her kindness, help, guidance, and patience during my studies.

I would like to thank my committee members, Prof. Michal Szostak, Prof. Jenny Lockard of Rutgers University, Newark and Prof. Andrew V. Teplyakov of the University of Delaware for their effort and time in reading and correcting my thesis.

It has been a pleasure working with members of the Galoppini group, both past and present, Dr. Andrew Kopecky, Dr. Yan Cao, Dr. Hao Tang, Dr. Runkun Sun, Xiuyuan Ma, Yuan Chen, Ian Weiss, and Ryan Harmer. I thank them for their constant support and motivation.

I would also like to thank Prof. Lars Gundlach, Prof. Andrew V. Teplyakov, Baxter Abraham, Chuan He and Joseph Avenoso for the great collaboration. Thanks for all the discussions on semiconductor films and ultrafast electron dynamics.

My sincere thanks also go to Prof. Jonathan Rochford and Dr. Ken T Ngo from the University of University of Massachusetts, Boston, for offering me the research opportunity in his group and leading me work on diverse exciting projects.

I wish to also thank the faculty members of the Department of Chemistry, Rutgers University for their guidance, excellent teaching and research advice, and also the staff of both the Department of Chemistry and Rutgers University for their helpfulness.

In addition, I greatly appreciate the Department of Energy – Basic Energy Science for financial support for this work and to the Dean's Office, Graduate School-Newark for the 2017-2018 Dissertation Fellow Award.

And a special thank goes to Chendi Gu for bearing with me during the completion of this manuscript.

Table of Contents

List of Figures

List of Schemes

List of Tables

Lists of Abbreviations

Ag/AgCl	silver/silver chloride electrode
ALD	atomic layer deposition
AM 1.5G	air mass 1.5 global
C.B.	conduction band
CuAAC	copper-catalyzed azide-alkyne cycloaddition
CT	charge transfer
CV	cyclic voltammetry
D_2O	deuterium oxide
DBO	2,3-diazabicyclo[2.2.2]oct-2-ene
DCE	1,2-dichloroethane
DDQ	2,3-Dichloro-5,6-dicyano-1,4-benzoquinone
DFT	density functional theory
DMSO	dimethyl sulfoxide
DSSC	dye-sensitized solar cell
E_{bg}	band gap
equiv.	equivalents
ESI-MS	electrospray ionization mass spectrometry
ET	electron transfer
Et	ethyl
eV	electron volt
fs	femtosecond

FTO	fluorine doped tin oxide
HBC	hexa-peri-hexabenzocoronene
HET	heterogeneous electron transfer
HOMO	Highest Occupied Molecular Orbital
Hz	Hertz
IR	infrared
J	coupling constant in Hz
LB	Langmuir-Blodgett
LUMO	Lowest Occupied Molecular Orbital
M	Molar concentration (mol per Litre)
m/z	mass-to-charge ratio
MALDI-TOF	Matrix Assisted Laser Desorption Ionization- Time Of Flight
Me	methyl
MLCT	metal-to-ligand charge transfer
MOCVD	metal-organic chemical vapor deposition
MOn	metal oxide nanoparticle
MS	mass spectrometry
NHE	normal hydrogen electrode
NMR	nuclear magnetic resonance spectroscopy
PAH	polycyclic aromatic hydrocarbon
PCE	power conversion efficiency
PDI	perylene diimide
ppm	parts per million

ps	picosecond
SB-CS	symmetry-breaking charge separation
SCE	standard calomel electrode
SEM	scanning electron microscopy
TA	transient absorption
t-Bu	*tert*-butyl
TfOH	trifluoromethanesulfonic acid
TLC	thin layer chromatography
TPA	triphenylamine
Trp	tryptophan
UV-Vis	Ultraviolet–visible spectroscopy
V.B.	valence band
wt. %	weight percent
XPS	X-ray photoelectron spectroscopy
δ	chemical shift in ppm
$\Delta\delta$	induced shift change in ppm
λ_{ex}	excitation wavelength
λ_{max}	wavelength of maximum absorbance

Chapter A Introduction

Overview and Thesis Organization

The objective of this Ph.D. research is to design and synthesize organic compounds that are used as models to study HET on the surface of nanostructured wide band gap metal oxides in collaboration with Prof. Andrew Teplyakov and Prof. Lars Gundlach at the University of Delaware.

In this thesis, the synthesis of 2,5-di-*tert*-butylperylene (**DTBuPe**) and a series of **DTBuPe**-bridge-anchor derivatives was completed, and their steady-state photochemical properties were studied in solutions as well as on metal oxide semiconductor films.

Chapter A provides some brief background of this work. First, some general aspects of heterogeneous electron transfer (HET) are introduced. Subsequently, the molecular design of dyes is discussed as one of the vital components for successful HET studies. The design of both chromophores and linkers is introduced. Lastly, the properties and limitations of perylene, which has been proven an ideal model dye for HET studies, are also discussed in this chapter.

Chapter B reports the synthesis. Perylene is an ideal model dye for the investigation of HET on nanostructured metal oxides. However, there are relatively few examples for its application in HET studies compared with other organic chromophores A method to prevent aggregation and further modification of the perylene framework are discussed in this chapter.

The photophysical properties of **DTBuPe**-bridge-anchor derivatives in solution and bound to semiconductor surfaces are reported in Chapter C. By comparing properties of **DTBuPe**-bridge-anchor derivatives and perylene derivatives, we investigated the influence of *t*-butyl groups, as well as different bridge units. In addition, for the first time

perylene was functionalized with an azide group for click chemistry. The CuAAC reaction was successfully performed with the azido perylene derivative in solution and on ZnO nanorod films. This can lead to promising applications of perylene in a variety of fields, as the CuAAC reaction is widely employed in surface modification methods. **DTBuPe-Ph-N$_3$** was also employed in a morphology preserving sensitization of ZnO nanorod surfaces.

Chapter D summarizes the results and gives some implications for applications utilizing **DTBuPe**-bridge-anchor derivatives.

A.1 Background

In homogenous electron transfer processes, electrons are usually transferred from a molecular donor to a molecular acceptor state. A different situation occurs if there are multiple acceptor states, as is the case for the interface between a photoactive molecule (a chromophore, a redox group or a photocatalyst) and large-bandgap nanostructured metal oxide semiconductors (MO_n), mostly TiO_2, SnO_2 or ZnO (Figure A-1) or core-shell materials prepared by various combinations of them. If the excited states of the photoactive molecules overlap in energy with the empty states of the substrate, e.g. the conduction band of semiconductor, photoexcitation of the molecule will be followed by electron transfer (ET) from the molecule to the substrate. This charge transfer process is also called sensitization, and in this context the chromophores are called sensitizers or dyes, because the first compounds studied were dyes absorbing in the visible. Heterogeneous electron transfer (HET) remains at the center of intense research in numerous areas of solar energy conversion. Such areas encompass photocatalysis and

solar fuels,[1-6] photovoltaics,[7-11] energy storage,[12] and artificial photosynthesis.[13-20] More broadly, HET is of interest to other scientific communities studying molecular electronics, photoswitches, photonics, catalyst, and other fields where ET in hybrid organic/inorganic systems plays a central role.

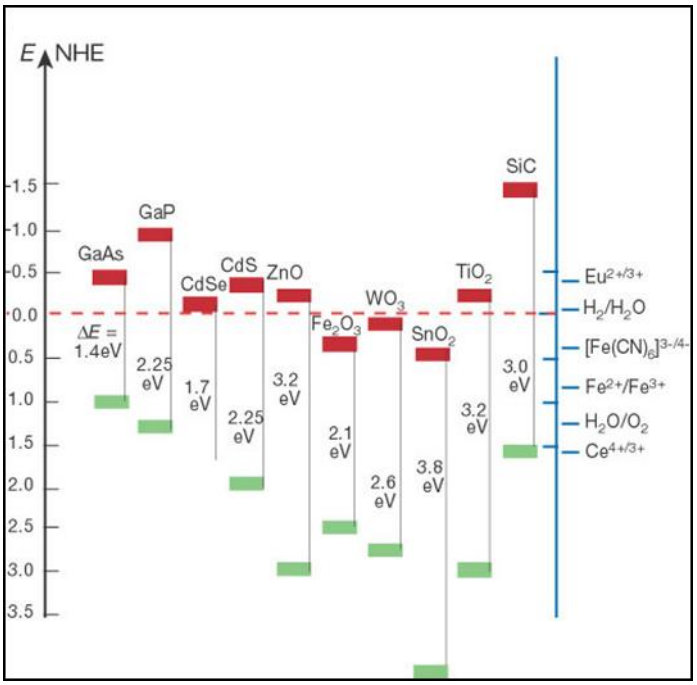

Figure A-1 Band positions of several semiconductors. Reproduced from ref[21] with permission. NHE = normal hydrogen electrode

Although molecule/semiconductor interfaces have been studied for decades, both experimentally and theoretically, there are numerous aspects of this process that remain poorly understood, and it is still not possible to control HET at the molecular level, because of the complexity associated with heterogeneity, the lack of electronic control of the interface and other challenges, including the need to control the binding of the molecule on the semiconductor. The kinetic process in DSSCs[22] can be a perfect example for this exceptional complexity. (Figure A-2)

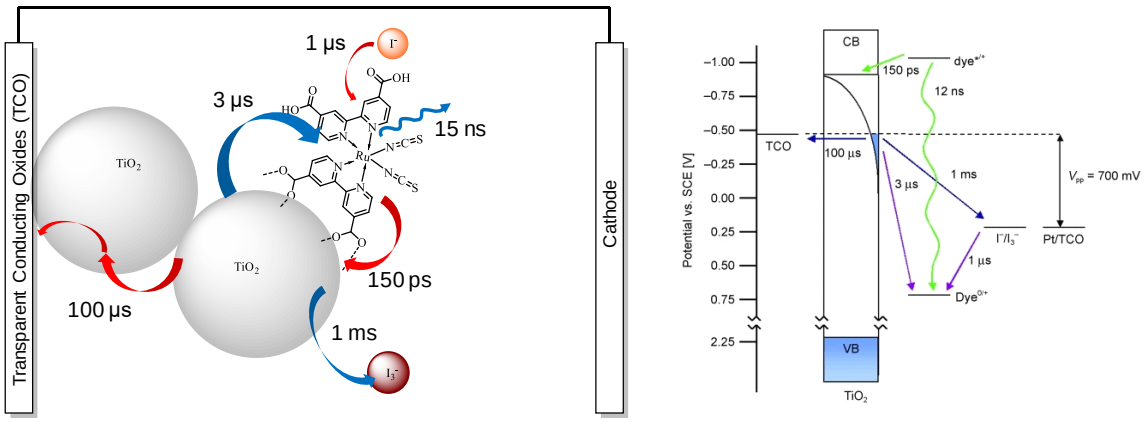

Figure A-2 Left: Schematic representation of kinetic processes in DSSCs. The Right panel shows the process on a modified energy level. Processes in kinetic competition have similar colors. Reproduced from ref[22] with permission.

A.2 Introduction to molecular design of dyes

The dye molecule is one of the key components that are necessary to carry out successful HET studies. For both fundamental and practical purposes, a dye should fulfill the following requirements.

1. Wide band gap semiconductors absorb in the UV region, therefore the dye should have a broad absorption spectrum and high molar extinction coefficient to allow efficient harvesting of incident solar photons. (Figure A-3)
2. The dye should have anchoring groups, typically -COOH or -$P(O)(OH)_2$, to ensure the covalent binding, and a strong attachment, to the semiconductor surface.

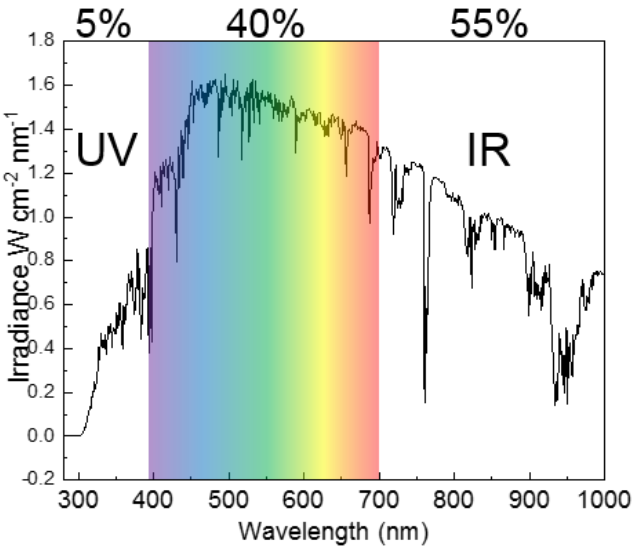

Figure A-3 The Air Mass 1.5 (AM 1.5) solar irradiance spectrum. Reproduced from ref[23]

3. The excited state of the dye should be sufficiently long lived (typically in the ns domain, although ps is sufficient), and the electron injection into the conduction band of the semiconductor should be fast (in the case of TiO_2 it is in the fs domain) to avoid the decay of the excited dye.
4. The excited state energy level of the dye should be at higher energy than the conduction band edge of the semiconductor to ensure an efficient ET process between the excited dye and conduction band of the semiconductor.
5. For possible dye-regeneration purpose, the oxidation state level of the dye should be more positive (by ca. 200–300 mV) than the redox potential of the electrolyte. This is necessary in the case of dye sensitized solar cells (DSSCs) where the dye/TiO_2 is coated on a transparent electrode and acts as the photoanode.

6. Dye aggregation on the semiconductor surface should be avoided because aggregation leads to hypo- or bathochromic shifts, fast relaxation, recombination and other processes competing with desired ET processes.[24]
7. The sensitizer should be electrochemically, photochemically and thermally stable in the ground and oxidized states.
8. The dye should have good solubility in a variety of solvents, and, for real-life applications, should be environmentally-friendly, low-cost, and abundantly available.

In this context, chromophore-bridge-anchor design allows to tune the dye properties and to probe specific scientific questions. The sophistication of the design of dyes as well as of surface attachment methods have significantly increased in the past two decades. In summary, molecular design has played, and continues to play, a key role in this field. In the next section we will discuss the progress in the design of each individual component of chromophore-bridge-anchor compounds.

A.2.1 Design of Chromophores

A.2.1.1 Metal-Containing Dyes

In 1991, O'Reagan and Gratzel first reported DSSCs employing films of nanostructured TiO_2 for increased dye uptake.[25] In DSSCs, nanostructured TiO_2 is usually sensitized by surface-bound ruthenium polypyridine dyes. Such systems are capable to convert sunlight into electricity with efficiencies that have now reached up to 15%[26]. This finding triggered an intense, worldwide research effort on a wide variety of inorganic transition metal complexes as well as porphyrins[27] and phthalocyanines[28-29] for

the preparation of more efficient DSSCs and to study their HET behaviors. Ruthenium(II) is the metal ion most commonly used in polypyridine complexes dyes. In the case of metalloporphyrins and metallophthalocyanines, the preferred metal ions are those with full or half-filled d-orbitals, such as Zn(II), Mg(II) and Al(III).

Among all transition metal complexes mentioned above, Ru(II) polypyridyl complexes have favorable excited-state properties, high redox reversibility and are photostable in the oxidized and reduced state. One of the most successful inorganic sensitizers, called N3 (Figure A-2), is cis-$Ru(LL)_2X_2$, where LL = 4,4´-dicarboxylic acid bipyridine (dcb) and $X = SCN^-$, with overall conversion efficiency ~10%.[30] The $Ru^{III/II}$ reduction potential of N3 is more negative compared to $Ru(bpy)_3^{2+}$, and the absorption and emission maxima are red-shifted. The electron density of the highest occupied molecular orbital (HOMO) shifts from the ruthenium metal center to the isothiocyanate ligands. The MLCT excited state is localized on the ligand substituted with the –COOH group. A similarly successful Ru-based sensitizer, prepared from terpyridine is called ‘black dye’ (Figure A-4) because it extends the spectral range of DSSCs significantly towards the IR region of the solar spectrum. (Figure A-3)

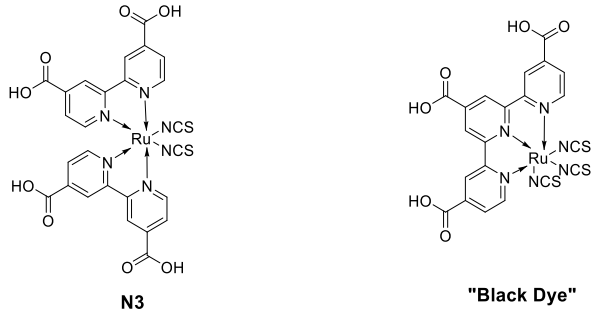

Figure A-4 Structure of some ruthenium polypyridyl type dyes.

One problem with Ru and other second and third row transition metals-based sensitizers is that these are rare metals, and are not ideal for large-scale application. Thus, using earth abundant metals, i.e. iron or copper (Figure A-5), instead of ruthenium in such complexes would be a significant step towards large-scale light-harvesting applications. Iron is an obvious choice as an earth-abundant and environmentally friendly replacement of ruthenium. However, iron polypyridine complexes have been found unsuitable for DSSCs applications, even if they have intense MLCT absorption, due to the low-lying metal-centered quintet high-spin state that rapidly (~ 100 fs) deactivates the MLCT manifolds[31-33], and because of their poor photostability as they disassociate during photoexcitation.

Thus, a possible solution for a longer lived MLCT states is to destabilize the metal-centered states. To this end, several Fe-N-heterocyclic carbene (NHC) complexes were synthesized,[34-37] and MLCT state time had been significantly extended up to 100 ps[38] as compared to previously known Fe-polypyridine complexes.[32-33] In recent work by Chábera et. al[38], carefully designed meso-ionic triazolylidene NHC ligands were employed due to their better σ-donor and π-acceptor electron properties compared to commonly used NHC ligands (Figure A-5 **I**). The meso-ionic triazolylidene NHC ligands stabilize the excited state resulting in a record long charge transfer lifetime (100 ps) and room-temperature photoluminescence. The absence of excited state energy loss was exploited to achieve an increased driving force in photochemical reactions on surfaces.

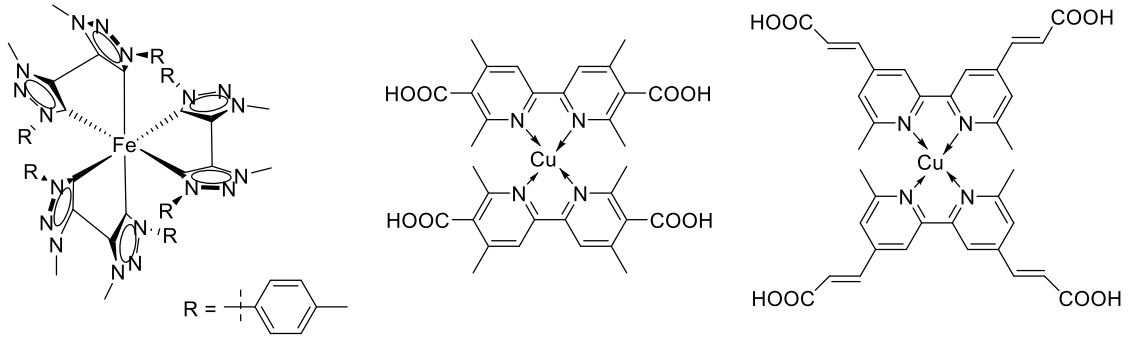

Figure A-5 Structure of other metal complexes[38-39]

Copper complexes are also potentially inexpensive and earth-abundant sensitizers for solar energy conversion and are receiving considerable interest.[39-41] They were first introduced into DSSCs by Sauvage and co-workers due to their similar photophysical properties to Ru(II) complexes. This system was further expended by Sakaki et al.[41] and Bessho et al.[39] via ligand modification. The MLCT states in these complexes are from a d^{10} electronic ground-state configuration, which circumvents the deactivation of MLCT states via low-energy ligand field states that is observed in d^6 complexes.

A.2.1.2 Organic Chromophores

Organic chromophores are attractive, in part, because it is possible to finely tune their properties via synthetic modifications. Earlier examples included polycyclic aromatic hydrocarbons (PAHs, such as pyrene,[42] perylene,[43] anthracene[44]), coumarins,[45-47] triphenylamines[48-49], and others[50-52]. In most cases, the electron injection rate was character to be ultrafast (10 fs).[53] However, many of the early organic dyes exhibited fast recombination kinetics, and their ground-state redox levels did not match favorably with

that of commonly used redox mediators for DSSCs. This had led to the design of new types of redox mediators[54-55].

In recent years, triphenylamine (TPA) based dye molecules have been widely reported as sensitizers in DSSCs, due to the favorable electron-donating properties of the TPA unit and their potential for low-cost DSSC production.[48-49] Furthermore, the nonplanar molecular configuration of TPA based dyes prevents aggregation.[48] In a recent breakthrough by Freitag et al.,[56] two TPA based sensitizers, **D35** and **XY1** (Figure A-3), were combined with the copper complex Cu(II/I)(4,4',6,6'-tetramethyl-2,2'-bipyridine(tmby)) as a redox mediator, and DSSCs prepared from them exhibited large open-circuit photovoltage (1.1 V). In standard air mass 1.5 global (AM 1.5G) sunlight, the power conversion efficiencies (PCEs) reached 11.3%. Moreover, under 1000 lux ambient lightning which corresponds to typical indoor illumination, the PCE of this new DSSC design was a strikingly 28.9% with a power output of 88.5 μW cm^{-2}.

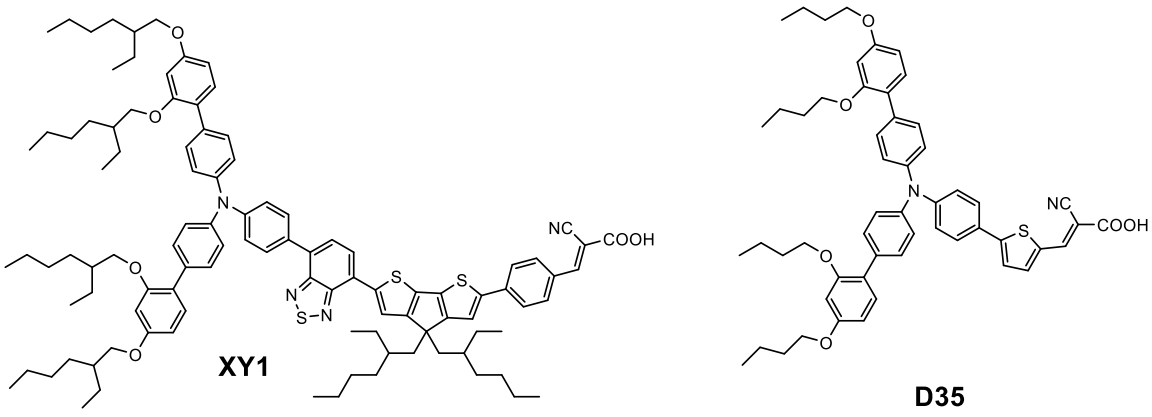

Figure A-6. Structure of two selected TPA based chromophores[56].

A.2.2 Linker Design

An enduring challenge in HET is the ability to control the chromophore/semiconductor interface at the molecular level. This is a key prerequisite to achieve a better control of the properties. For instance, an efficient solar cell requires fast electron injection and oxidized dye regeneration, as well as a slow competing recombination process. In photocatalysis applications, however, researches are focusing on achieving long-lived charge separation to allow catalysis to occur. To attain a good level of control of such complex photoinduced interfacial electronic processes, the careful design of the linker and its components, the bridge and anchor group, as schematically represented in Figure A-7, has received intense interest in the past 15 years. Modular approaches to linker design with tunable properties have led to systems that are important for photovoltaic devices, artificial photosynthetic systems and photocatalysts, and as models for fundamental HET studies..

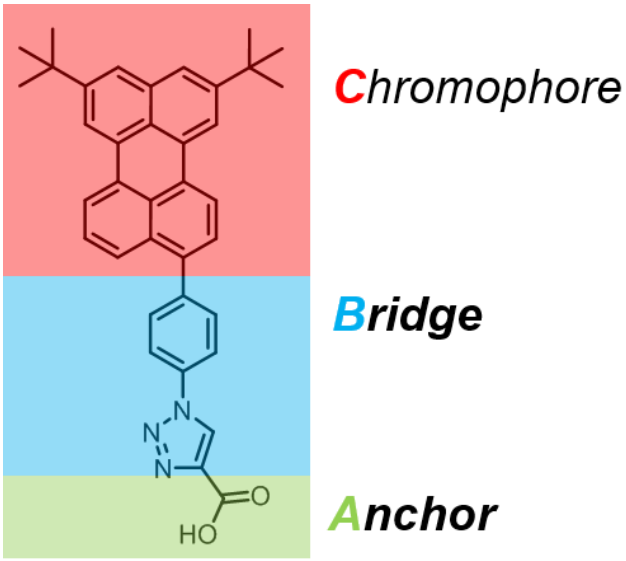

Figure A-7 Schematic representation of linker strategy

A.2.2.1 Anchor Strategy

Typically, an anchoring group for MO semiconductors forms covalent bonds with metal oxides by reacting with surface hydroxyl groups. The best anchoring groups for metal oxides are phosphonic acids ($P(O)(OH)_2$)[57-58], followed by carboxylic acids (COOH) and their derivatives, for instance acid chlorides, esters or hydroxyamides. Silanes (SiX_3, X = Cl[59] or OEt[60]), acetylacetonate and salicylates have also been employed. For the well-studied COOH group, the binding is reversible with high equilibrium binding constants ($K\sim 1 \times 10^5\ M^{-1}$) for Ru-polypyridine complexes attached through a single COOH group.[61] Saturation surface coverages are in the range of $\Gamma \sim 1\times10^{-10}$ mol cm^{-2}.[57] In basic conditions (usually pH $\geqslant$ 9), however, the dyes are easily desorbed from the films. For COOH groups, a variety of binding modes can occur (Figure A-8) and which one is prevalent depends on the type of metal (Zn, Ti), surface hydration, pH, structure of the linker, surface crystal facet and other factors[62]. It is generally accepted, following IR and computational studies, that bidentate bridging (circled in Figure A-8) is the most stable and prevalent binding mode on TiO_2.

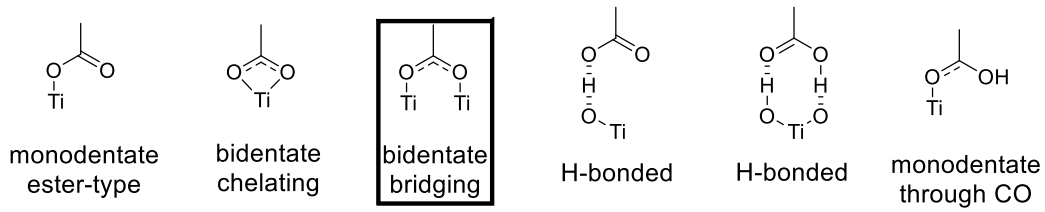

Figure A-8. Possible binding configurations of COOH on TiO_2.[63]

Several groups have developed advanced anchor strategies, involving multiple attachment points (Figure A-6). In early work made by Gray et al., the kinetic influence of alternative anchors and linkers for N3-type dyes on TiO_2 was characterized. Their

results suggested that binding through multiple groups would significantly influence both kinetic and stability properties.[64] Supported by Persson's computational study,[65] a design of tripodal anchors to match TiO_2 substrates were synthesized by Galoppini et al.[66-68] and spectroscopically characterized by Meyer et al.,[67] demonstrating that the three-point attachment and rigid geometry of the linker led to two-dimensional interfacial control on semiconductor surfaces. (Figure A-9) The study, however, also highlighted remaining problems of full functional control in mesoscopic films due to an abundance of "necking" (point of contacts) regions between neighboring nanoparticles. To achieve comprehensive sensitizer-substrate functional control also in nanostructured films, one approach is to use rigid linker groups radially arranged around the metal center for multiple, and symmetrical arrangement of the anchor groups ("Star" complexes) to shield the metal center from surface direct contacts and control metal-semiconductor distance.[69-72]

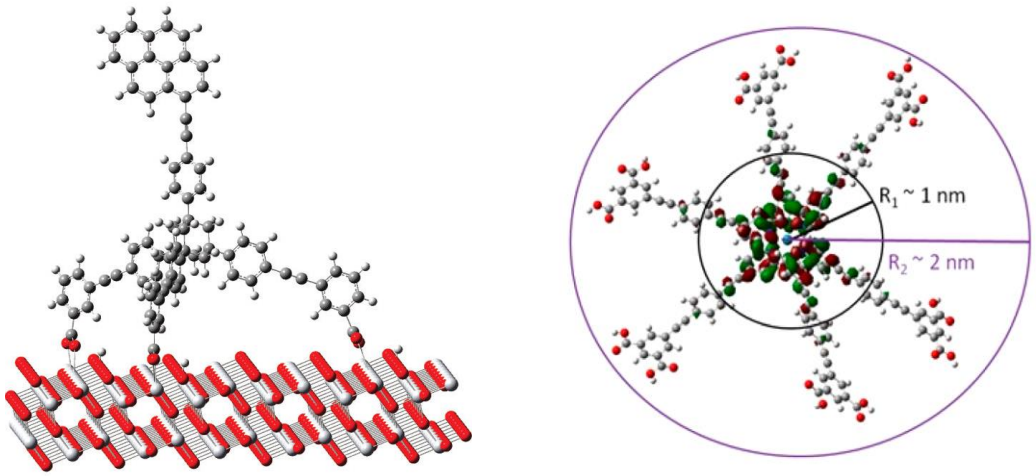

Figure A-9 Left: A tripodal anchor group achieving two-dimensional structural control of surface sensitization of semiconductor surfaces. Reproduced with permission from ref.[67] Copyright (2018) American Chemical Society. Right: HOMO level of a ruthenium star complex that effectively shields the metal core in all directions also in nanostructured films. Reproduced from ref. [69]

A.2.2.2 Bridge Strategy

Bridge units, i.e. the moieties between the anchoring group and the chromophore, are also important components in the molecular design of dyes. A well-designed bridge unit is highly useful in fundamental HET studies, as well as to obtain efficient DSSCs. For instance, the length of bridges can be systematically varied to control the distance between chromophores and semiconductor surfaces and inhibit recombination. Also, bridge variations can be used to tune the photophysical properties of chromophores (HOMO-LUMO gap for instance).

The earliest examples of bridge units were just simple saturated -CH_2- alkyl chains. In the pioneering work by Lian et al.[73], methylenic spacers were inserted between the bpy ligand and the carboxylic group in $Re(CO)_3Cl(dcbpy)$ to form ReC1A–ReC5A, respectively. These complexes were bound to TiO_2 thin films and femtosecond IR spectroscopy indicated that injection rate decreased exponentially with distance, in qualitative agreement with the change predicted for non-adiabatic electron transfer processes through a saturated bridge.[73]

Another approach that results in the attachment through flexible linkers, involves a two-step process involving surface modification of the metal oxide first, and subsequent binding of the chromophoric groups, was reported in a recent research by Yan et al.[74] This stepwise surface modification strategy was successfully employed on nanostructured ZnO films. The ZnO nanorod film was first functionalized with 10-azidodecanoic acid (N_3-$(CH_2)_9$-COOH). After the self-assembled monolayer (SAM) was formed on the surface through binding of the COOH group, CuAAC click reaction with the remaining

N_3 group was performed to bind either chromophore or bio-sensing probe (in both case ethynyl-substituted) to the film.

The use of a methylenic bridge between the anchoring group and the dye was dictated by convenience, but the flexibility of the attachment does not allow to fix the distance from the surface. Therefore, synthetic efforts in this area have been redirected towards synthetic bridges that are rigid and modular, as represented in Figure A-10. Rigid linkers that are synthetically very accessible are unsaturated rigid axial rods made of oligo-*p*-phenylenes (Figure A-10 **a**) and oligo-*p*-ethynylphenylenes. (Figure A-10 **b**) They are usually synthesized by Pd-catalyzed cross-coupling, such as Sonogashira and Suzuki reactions, and the number of rigid units can be systematically varied[75].The introduction of functional groups on the bridge is a more recent development. For instance, recent work by Galoppini et al. included the use of directed dipoles on rigid bridges[76-77] (Figure A-10 **c**) suggested a new pathway for improved control over the interfacial electron injection and recombination processes. A recent breakthrough investigated by Meyer, et al. also provided an alternative method to control kinetic pathways for interfacial electron transfer from a semiconductor to a molecule using steric modifications of rigid bridges that form transition dipole upon photoexcitation.[78] (Figure A-10 **d**) The use of rigid, saturated bicyclo[2.2.2]octane units was also reported[79]. (Figure A-10 **e**)

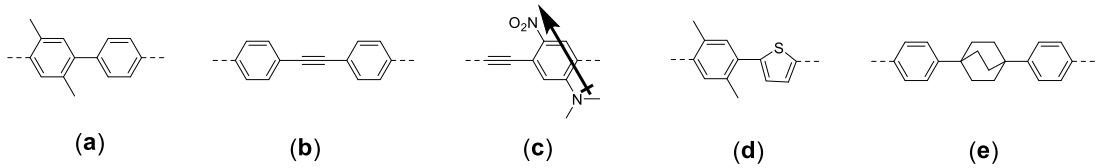

Figure A-10. Example of bridges that have the shape of rigid, axial rods.

An important example of functional rigid bridges are the so-called push−pull dyes[80]. By inserting conjugated bridge units between electron donor and electron acceptor groups, the redox level, HOMO-LUMO gap, can be tuned, and long-lived charge separation can be obtained, leaving the hole on the far side of the sensitizer facing the electrolyte for efficient dye regeneration by the external redox couple. A successful application of this strategy is the development of push-pull coumarin dyes. (Figure A-11) Coumarin based dyes are promising sensitizers because of their good photoresponse in the visible region and appropriate LUMO levels matching with the conduction band of TiO_2. However, the first coumarin based DSSC, which utilized the simple coumarin 343, only exhibited an efficiency of 0.9%.[45] Since then, a new class of dyes based on coumarins has been developed by connecting the coumarin core and anchor group with conjugated moieties, for instance vinylene[47, 81], thiophene[46, 82] or ethylenedioxythiophene,[83] (Figure A-11) and the efficiency was significantly improved (6.0 – 8.2%). Introduction of conjugated units in between coumarin and cyanoacrylic acid acceptor was proven to considerably expand the absorption to the visible region, and also improve device photovoltaic properties.

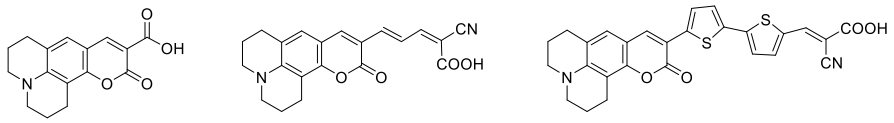

Coumarin 343 (**a**) (**b**)

Figure A-11 Structures of coumarin based dyes for DSSCs application. [45-43]

A.3 Perylene dyes

The PAH perylene, $C_{20}H_{12}$ in Figure A-12, is a historic organic molecule. Its synthesis was first reported by Scholl et. al. in 1910, via the oxidative cyclization of binaphthyl or naphthalene.[84] Perylene and its derivatives, for the most part perylene diimides, are widely used as dyes and pigments because of their high extinction coefficient (38,500 cm^{-1}/M for perylene[85]), excellent photo and chemical stability, high photoluminescence quantum yield, (See Table A-1). In the case of perylene diimides (PDIs), large range of colors can be obtained by variation of the substitution pattern on the perylene core through high yielding synthetic routes. Besides conventional uses, perylene are also key components of OFET,[86] fluorescent solar collectors,[87] photovoltaic cells, [88-89] and optical switches.[90-91]

Table A-1. Selected physical properties of perylene

$\lambda_{abs,max}$[a]	$\lambda_{em,max}$[b]	Φ_{PL}[c]	τ_{ex}[d]	$E_{1/2}$[e]
436 nm	438 nm	0.94	5.34 ns	3.8 V vs. Li/Li^+

[a] Wavelength of maximum absorbance in cyclohexane.[85]

[b] Wavelength of maximum emission in cyclohexane. [85] λ_{ex} = 410 nm

[c] Photoluminescence quantum yield in cyclohexane. [85]

[d] Excited state lifetime in cyclohexane. [85]

[e] Redox potential. Measured with cyclic voltammetry (CV) in ethylene carbonate: dimethyl carbonate (3:7 volume ratio) with 1 M $LiPF_6$. [92]

A.3.1 Properties of perylene dyes

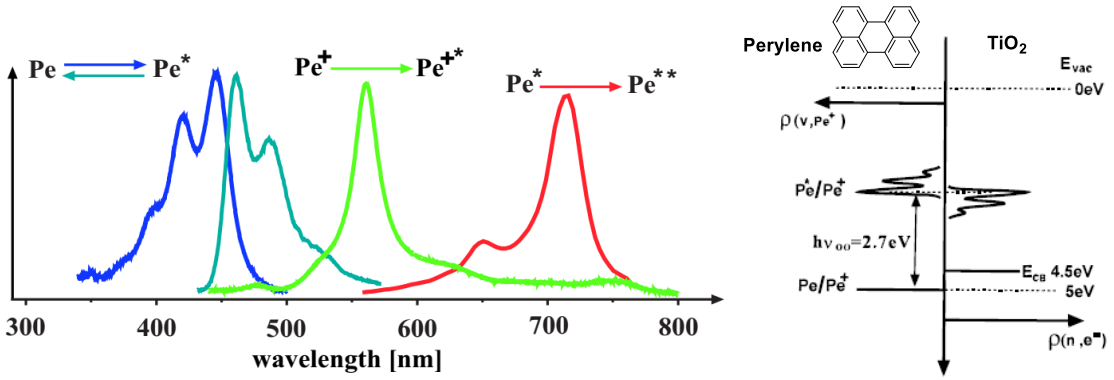

Figure A-12 Left: absorption and emission spectra of the relevant states: ground states absorption (blue), emission from S_1 (teal), cation ground state absorption (green) and excited state absorption (red). Adapted from ref[93]. Right: Energy level alignments of perylene comparing with TiO_2. Adapted from ref[94].

Perylene (Pe) is an ideal model dye for the investigation of HET on nanostructured metal oxides. First, the absorption spectra of the ground state Pe, the excited state, Pe^*, as well as the ground state of the oxidized form Pe^+ (the product of HET reaction), i.e. all the species involved in ET process, are well separated. Additionally, these transitions are all in visible range (Figure A-12). These absorption properties allow the direct spectroscopic investigation of the ET process with pump-probe spectroscopy. Also, photoexcitation of perylene has almost pure S_0 - S_1 character, and the first excited singlet state decays only radiatively with a long lifetime (about 5 ns in cyclohexane[85]). Finally, perylene is a good photo-reductant for TiO_2 and ZnO, as the energy of the donor state lies very high above the conduction band, resulting in efficient and ultrafast charge injection (13 to 200 fs depending on structure[53]). There is no ultrafast decay channel and electron injection is expected to be the only reaction for perylene/TiO_2. The combination of these favorable properties is rather exceptional and allows easier spectral identification and

monitoring of all species formed during the interfacial charge transfer process, making perylene/TiO_2 interfaces ideal substrates for pump-probe spectroscopic investigations of HET processes.

Although perylene has favorable electronic properties, there are only a few examples for its application in HET studies, with the exception of the pioneering work of Willig and coworkers[53, 79, 95-96]. One significant drawback for the application of perylene is the easy aggregation in solution and on surfaces due to the strong interaction of the π-system. Interchromophore electronic coupling can result in several processes competing with CT, for instance symmetry-breaking charge separation (SB-CS) and excimer formation, which may lead to rapid excited-state quenching.

In fact, perylene aggregation has been studied in the past for this very reason. Studies of molecular association of perylene, i.e., ground-state dimer and excimer, have been conducted in solution,[97] in crystals,[98-100] in thin polymer films,[101] and in Langmuir-Blodgett (LB) films.[102-104] In the study of Petty et al.,[104] perylene molecules were doped into LB films, and their aggregation was discussed in terms of steady-state and nanosecond time-resolved fluorescence spectroscopy. The temperature effect on the luminescence and its lifetime of excimers was extensively studied by Willig et al.[105] using 1:1 mixed layers of 12-(3-perylenyl) dodecanoic acid and arachidic acid. In this case the excimer emission occurs at 1.5 K. The excimer emission showed a significant red-shift (peak at 636 nm) with a lifetime of 69 ns, and can be generated through the partially forbidden transition to the lowest excited dimer state. Akimoto et al.[103] employed the same LB film model and investigated the concentration effect in the formation of dimers. By preparing LB monolayers containing Pe chromophores with

different concentrations and measuring the steady-state and picosecond time-resolved fluorescence spectra, they found the presence of two types of dimers, D1 and D2, which were assigned to the dimers where two chromophores are partially and fully overlapped, respectively. (Figure A-13) Their formation was closely dependent on the concentration of chromophores included in the LB films.

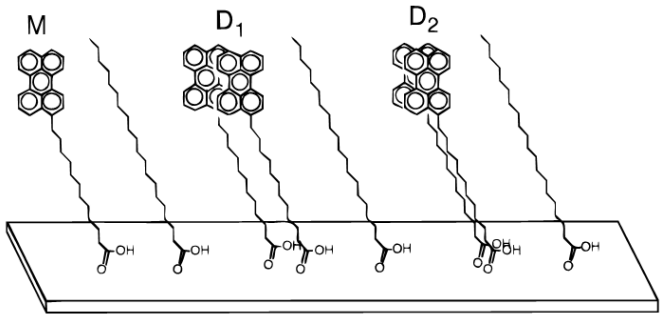

Figure A-13. Schematic drawing of different states of perylene in LB films. Adapted with permission from ref.[103] Copyright (YEAR) American Chemical Society.

A recent study by Cook et al.[106] probed the energy transfer dynamics of perylene dimers. With ultrafast transient absorption (TA) spectroscopy of dimers of perylene bound either directly or through a xylyl spacer to a xanthene backbone (Figure A-17), they were able to probe the effects of interchromophore electronic coupling on excimer formation and symmetry-breaking charge separation (SB-CS). Two different time constants for excimer formation in the 1-25 ps range were observed in each dimer. In highly polar solvent like acetonitrile, SB-CS competes with excimer formation in the weakly coupled isomers followed by charge recombination with τ_{CR} = 72-85 ps to yield the excimer.

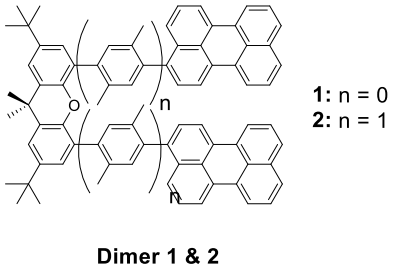

Figure A-14 The structure of Dimer 1 & 2.

In summary, an effective use of perylene for MO_n sensitization requires strategies that prevent the formation of aggregates. The substitution of the perylene framework with bulky alkyl groups has proven an effective strategy to prevent aggregation and increase solubility. Perylene derivatives disubstituted with *tert*-butyl (*t*-Bu) groups at position 2 and 5 were at the center of the pioneering studies of heterogeneous ultrafast charge transfer conducted by Willig and coworkers over two decades ago.[79, 95-96] However, this model molecule is, to this date, underutilized. In next chapter we will describe a practical, improved routes to the synthesis of **DTBuPe**-bridge-COOH derivatives that are currently being studied by our group, in collaboration with the groups of Prof. Andrew Teplyakov and Prof. Lars Gundlach at the University of Delaware, and of novel compounds suitable for click chemistry that we recently reported.[107]

Chapter B : Synthesis of 2,5-di-*tert*-Butylperylene-Bridge-Anchor Derivatives

B.1 Introduction

In this chapter we describe the synthesis of 2,5-di-*tert*-butylperylene (**DTBuPe**) derivatives and of **DTBuPe**-bridge-anchor compounds. Figure B-1 shows the chemical structures of the target compounds. The two bulky *tert*-butyl groups were introduced in the 2- and 5-position of the perylene (**Pe**) framework to prevent π-π stacking in solution and on surfaces. In addition, the *t*-Bu substituents resulted in excellent solubility in organic solvents of all **DTBuPe** derivatives.

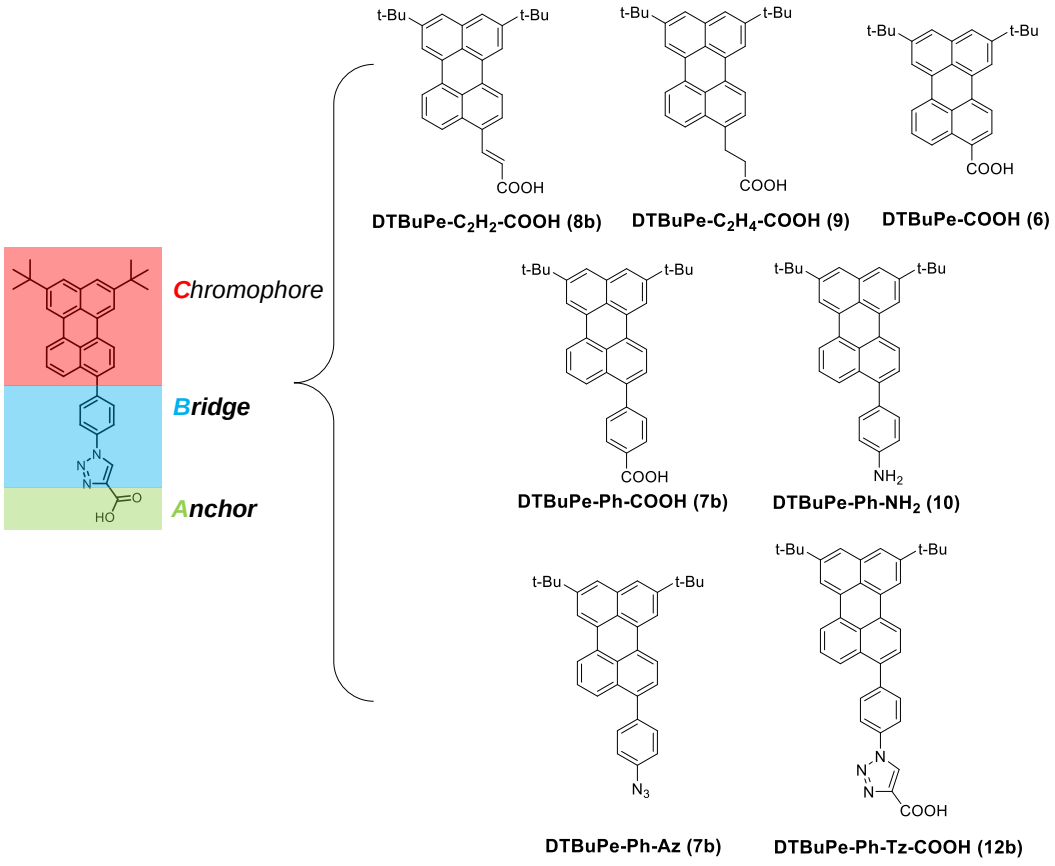

Figure B-1 Structure of **DTBu-Pe** derivatives synthesized.

Our strategy was to prepare **DTBuPe** and then introduce functional groups in position 9 for further functionalization. Direct Friedel-Crafts alkylation of perylene with *t*-BuCl

seemed a direct approach to **DTBuPe**, but the lack of regioselectivity led to an intractable mixture of alkylation products[96] (Scheme B-1, a). A longer, but ultimately successful, approach involved anionic cyclization of 1,1'-binaphthyl derivatives, effectively building the perylene framework using a North-South approach. (Scheme B-1, b)

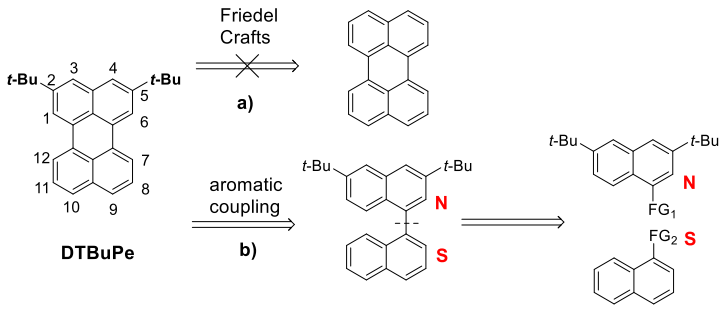

Scheme B-1 Retrosynthetic analysis of **DTBuPe 3.**

Once the **DTBuPe** was synthesized, functional group addition in the 9-position was carried out via two simple pathways. (Scheme B-2) The first approach involved formylation of **DTBuPe** in position 9 via Friedel-Crafts with dichloromethyl methyl ether to form **DTBuPe-CHO**[108], in a 1-C homologation. The aldehyde group in **DTBuPe-CHO 4** can undergo numerous functional group transformations, for instance oxidation to form the carboxylic acid, which is the anchor group necessary for surface binding. The second path involves the formation of bromo-derivative **DTBuPe-Br** (**6**) via *N*-bromosuccinimide (NBS) bromination, leading to as an easy entry to Pd-catalyzed cross coupling reactions. The combination of both approaches led to the synthesis of known as well as previously unreported perylene-bridge-anchor compounds.

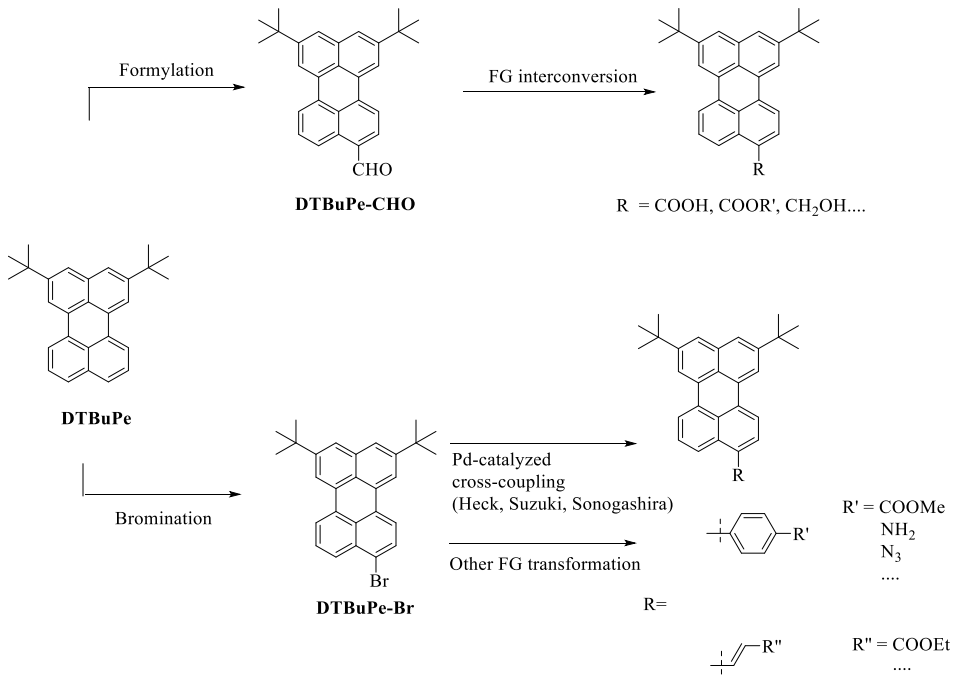

Scheme B-2 Functionalization of **DTBuPe**

In summary, intramolecular aromatic coupling is the key step in the synthesis of **DTBuPe** derivatives. In the next section we will describe the scope and mechanism of this reaction.

B.2 Dehydrogenative Intramolecular Aromatic Coupling Reaction

Methods for the selective formation of aryl-aryl bonds between unfunctionalized aryl groups constitute an exciting area in the field of organic chemistry. Other than palladium-catalyzed oxidative aromatic cross-coupling and dehydrogenative coupling by C-H activation by organometallic catalysts, the formation of aryl-aryl bonds can also be achieved by aromatic coupling of electron-rich arenes. Such reactions can occur either

via catalysis of non-oxidizing Brønsted or Lewis acids,[109-111] (Figure B-2a) or mediated by oxidants.[112-115] (Figure B-2b). In the literature, both kinds of coupling reactions of electron-rich aromatic substances are often referred to the Scholl reaction.

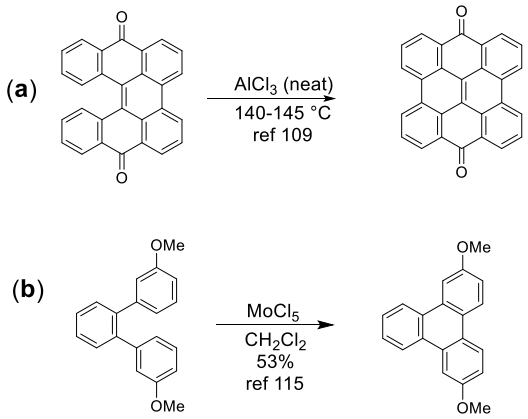

Figure B-2 Examples of two Scholl reactions under different conditions.

This reaction was first reported in 1868[116], then pioneered by Scholl[117] and Kovacic[118], and attracted considerable attention after the discovery of the application of oxidative aromatic coupling in the industrial synthesis of many antraquinone-derived dyes.[119] The intramolecular adaptation by Müllen et al. for the synthesis of structurally well defined, nanosized graphene substructures,[120-123] and the potential of this reaction for the application towards the synthesis of polyaromatic hydrocarbons for organic electronics with well-defined structures, has spurred an increasing interest in Scholl-type reactions. Different mechanisms were proposed for these two major conditions: processes which proceed with strong Lewis acid undergo an arenium cation pathway, while processes that occur at room temperature with a one-electron oxidant proceed through aryl radical cation intermediates. In some cases, it is proposed that both mechanisms exist.[119, 124]

The arenium cation mechanism was first proposed by Baddeley[125], and then investigated by Nenitzescu and Balaban[126]. It implies the electrophilic attack to the aryl species, for example, **A**, to form an electrophilic σ complex **A'** (shown H^+ for simplicity, but could also be a Lewis acid). The attack from the other aromatic ring forms a new carbon–carbon bond (Scheme B-3, **A''**). Hydrogen elimination regenerates the aromatic system, finally giving **B**, as described in Scheme B-3.

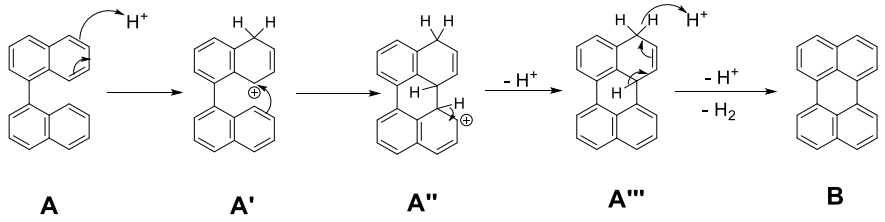

Scheme B-3 Schematic representation of arenium cation mechanism.

The radical cation mechanism for the Scholl reaction was first proposed by Kenner and later supported by several studies that probed the presence of aryl radical intermediates.[127-128] Later, Rathore and co-workers studied the reaction of electron-rich aromatic compounds in the presence of various oxidants in detail, especially on 2,3-dichloro-5,6-dicyano-1,4-benzoquinone (DDQ)-$MeSO_3H$ system.[129] The same system had been used previously by these authors to efficiently synthesize a number of triphenylenes and hexa-peri-hexabenzocoronenes under mild conditions.[130-131] They presented some important evidence suggesting that, for many *o*-terphenyls, the reaction indeed proceeds via radical cation intermediates, as shown in Scheme B-4.

It should be noted that Scholl reactions often occur with a rearrangement. It has long been known that alkyl- or arylsubstituted benzenes can interconvert in the presence of

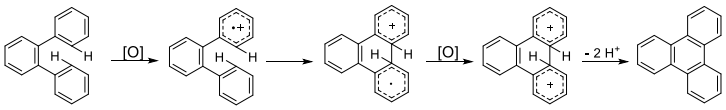

Scheme B-4 Schematic representation of radical cation mechanism for the Scholl reaction.

acid catalysts.[127, 132-133] (Scheme B-5a) Similar rearrangement was observe during the synthesis of exa-peri-hexabenzocoronene (HBCs) by Müllen and co-workers.[114] The reaction of a *p*-dimethoxy-substituted precursor with $FeCl_3$ in $MeNO_2$ provided a mixture of *m*-dimethoxy-HBC product and bis(spirocyclic) dienone. (Scheme B-5b) This rearrangement behavior was further investigated by Johnson et al. using aryl naphthalene system.[134] In the presence of 1 M trifluoromethanesulfonic acid (TfOH) in 1,2-dichloroethane (DCE), 1,1'-binaphthyl isomerized to 1,2'-binaphthyl and 2,2'-binaphthyl rapidly, and formed multiple cyclization products other than perylene. (Scheme B-5c)

Other noncatalytic intramolecular aromatic coupling methods have also been investigated. One example is the stilbene photocyclization developed by Mallory and coworkers[135]. Upon UV-irradiation in solution, *cis*-stilbene undergoes reversible photocyclization reaction. The resulting *trans*-4a,4b-dihydrophenanthrene intermediate can be oxidized with oxidants such as I_2 to give phenanthrene in high yield.[136-137] (Scheme B-5a) Another example is the thermal cyclodehydrogenation by flash vacuum pyrolysis (FYP)[138], which entails heating a precursor molecule in vacuum at high temperature (over 1000 °C) and briefly. This method was employed by Scott and coworkers in a series of syntheses of bowl-shaped PAHs and C_{60}.[139-141](Scheme B-5b)

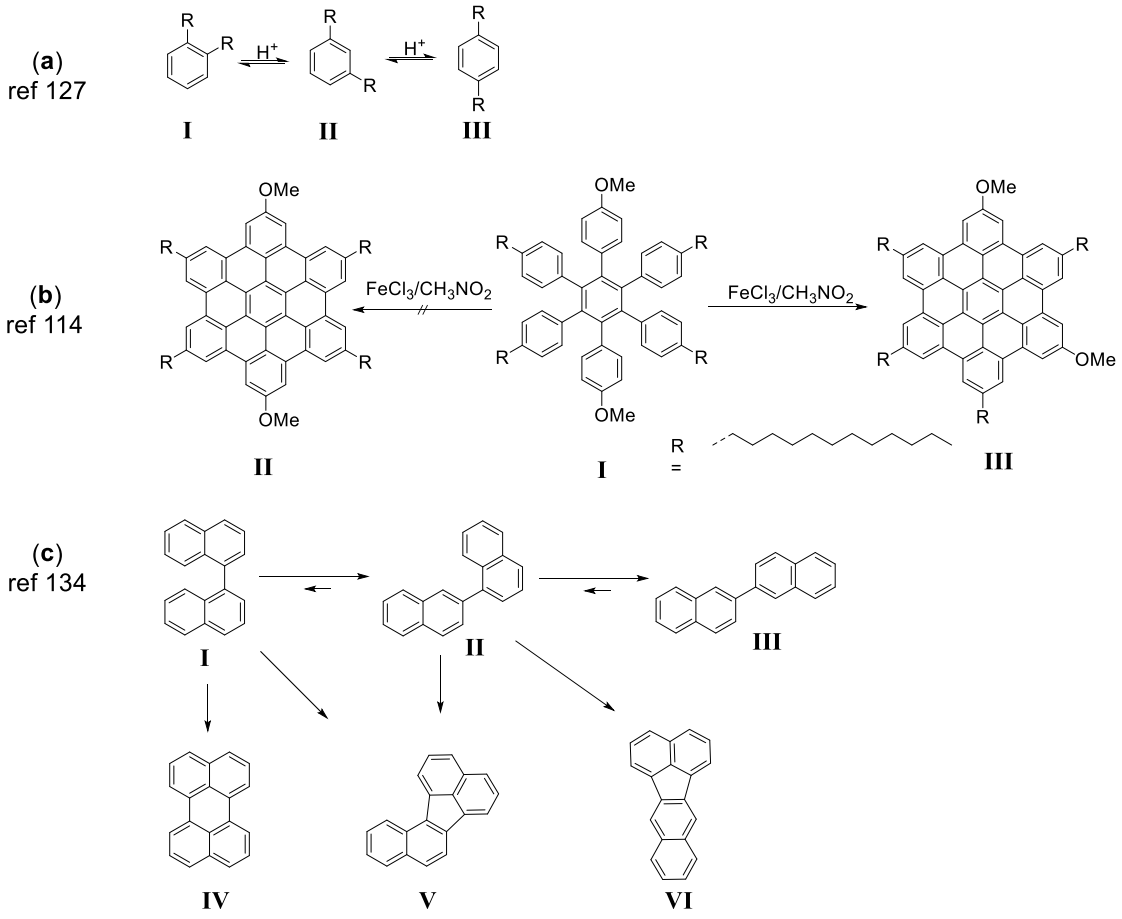

Scheme B-5 Rearrangements of aromatic compounds under Scholl reaction conditions.

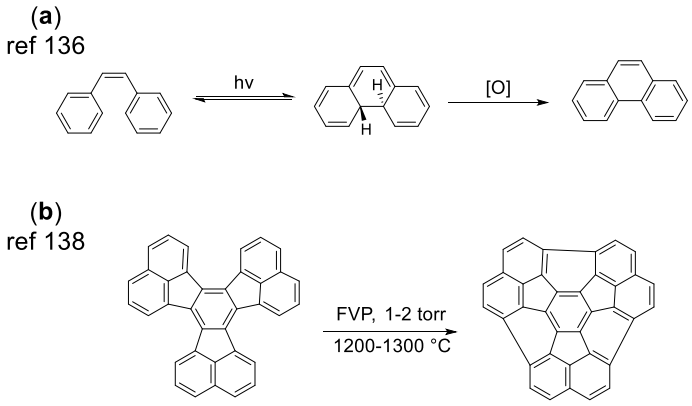

Scheme B-6 Examples of (**a**) stilbene photocyclization and (**b**) flash vacuum pyrolysis.

However, the most efficient conversion of 1,1'-binaphthatyl to perylene remains, to this date, the anionic cyclization of aromatic hydrocarbons by alkali metals.(Figure B.3) The anionic cyclization synthesis of perylene from 1,1'-binaphthyl was accidentally discovered in 1967 by Solodovnikov and coworkers during a study of 1,1'-binaphthyl radical anion[142]. In this study, 1,1'-binaphthyl was reduced in 1,2-dimethoxyethane (0.1 M) with potassium metal at room temperature. The ESR signal of 1,1'-binaphthyl anion radicals was observed growing rapidly in the first hour but then decayed slowly. After 72 h, the mixture was exposed to oxygen, and perylene was isolated in 39% yield. The experiment was then repeated in the same condition except that potassium was removed after 1 h, at which point the ESR signal had reached the maximum intensity, producing perylene in 10% yield. Hydrogen gas was also observed during the reaction (GC analysis).

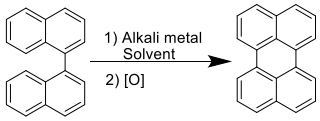

Figure B-3. Anionic cyclization synthesis of perylene.

This reaction is, to date, underutilized. The most noticeable applications are probably the synthesis of rylene[143] by Müllen et al. and the preparation of 2,5-di-*tert*-butylperylene dyes[96] by Willig et al. There was no mechanistic research published until Scott et al.[144] proposed a mechanism in 2010 which accounted for Solodovnikov's observations.

In this proposed mechanism, illustrated in Scheme B-7, 1,1'-dinaphthyl (**I**) is first reduced to the radical anion (**II**) by the alkali metal. This intermediate then cyclizes to form dihydroperylene radical anion (**III**) or is reduced to the dianion of 1,1'-binaphthyl (**IV**). Single-electron reduction of **III** results in the dianion of dihydroperylene, which can

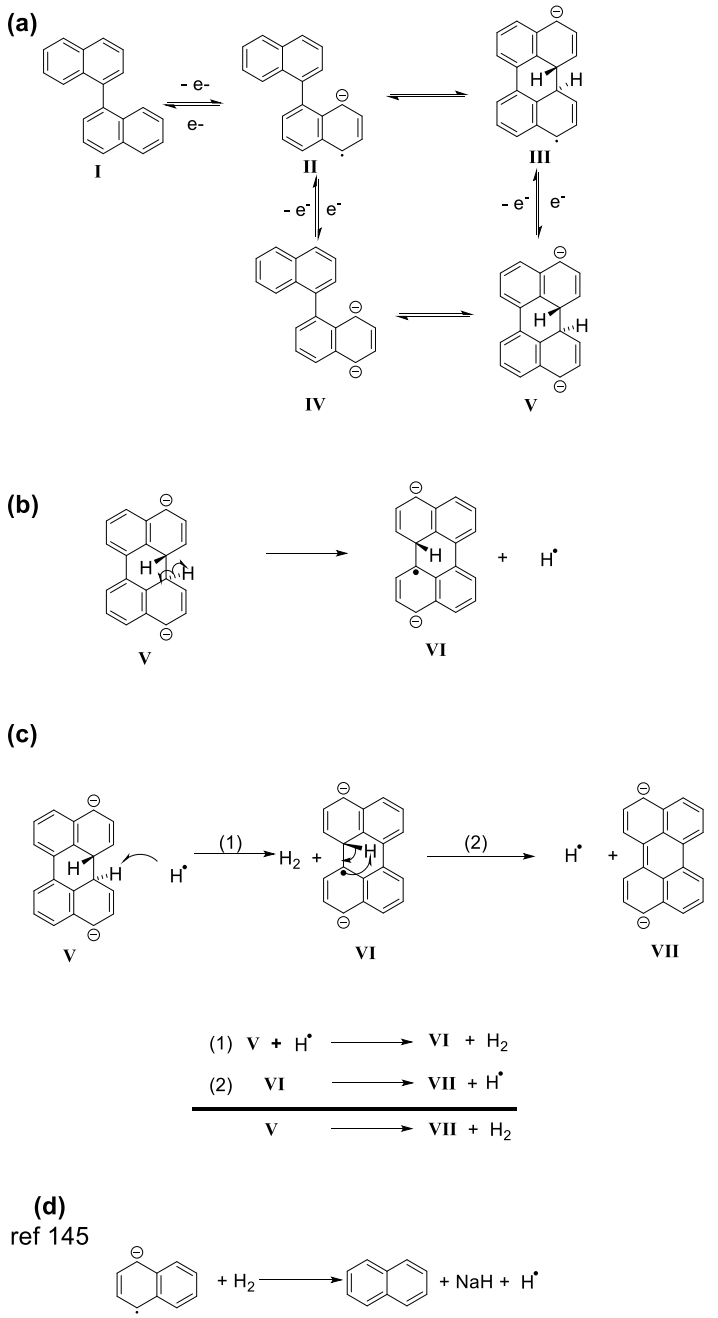

Scheme B-7 Mechanism proposed by Scott et al. **a**: C-C bond forming step. **b**: Initiation step in the proposed radical chain mechanism. **c**: Two-step propagation cycle in the proposed radical chain mechanism. **d**: Mechanism for the reduction of H_2 to NaH by sodium naphthalenide.[145]

be obtained also by the cyclization of **IV**. (Scheme B-7a) All these steps are reversible, unless the C-H bonds breaks, as in the conversion from **IV** to **VII**. The weak C-H bond in

V can undergo homolytic cleavage, thermally, to generate **VI** and free hydrogen atoms. (H·) The resulting $\mathbf{C}^-$ and H· can undergo a radical chain reaction producing **VII** and H_2. (Scheme B-7 b&c) H_2 formed in the cycle can be reduced by the aromatic radical anions, according to a well-studied mechanism,[145] generating more H· for the radical chain reaction. (Scheme B-6d)

Scott et al. also investigated the conditions for this reaction. By screening solvents, alkali metals, reaction temperature and time, quantitative yield was achieved using an optimized condition: three or more equivalents of potassium metal in tetrahydrofuran (THF), 85 °C in a pressure vessel overnight.[144]

To summarize, several types of intramolecular aromatic coupling reactions, for instance Scholl reaction and anionic cyclization, can be utilized to synthesize the **DTBuPe** framework. However, there is no published high-yield record utilizing Scholl reaction on the synthesis of perylene framework. Furthermore, 1,1'-binaphthatyl can undergo complicated rearrangement under typical Scholl reaction conditions; this could be even more complex as our precursor is a disubstituted 1,1'-binaphthatyl. Considering all these factors, we selected anionic cyclization for the intramolecular aromatic coupling step.

B.3 Synthesis of 2,5-di-*tert*-butylperylene

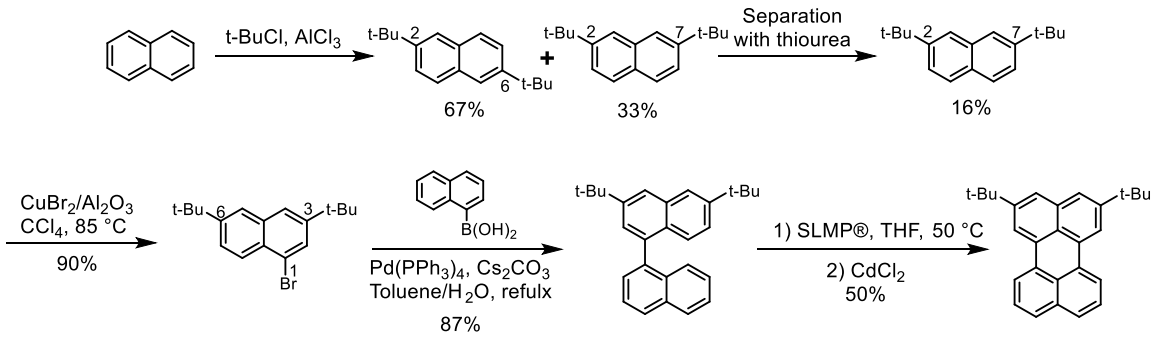

Scheme B-8 Synthesis of **DTBuPe**

The synthesis of **DTBuPe** proceeds through the anionic aromatic cyclization as the key step and it is described in Scheme B-8. The first step in this synthesis is the Friedel-Crafts alkylation of naphthalene. This procedure is utilized for the synthesis of 2,6-di-*tert*-butylnaphthalene, which is a commonly used precursor in polymer industry for the synthesis of valuable poly(ethylene naphthalenedicarboxylate) (PEN). However, in our case, the minor product, 2,7-di-*tert*-butylnaphthalene, is the desired target. This reaction was repeated in large scale (~30 g naphthalene) several times and consistently generated a 1:2 mixture of the 2,7- and 2,6- regioisomers.

Due to their similar physical properties, these two regioisomers could not be separated through conventional purification methods, i.e. silica gel column chromatography; however, 2,6-substitued naphthalene, which has a more elongated shape, has a much stronger tendency to form crystalline adducts with thiourea and can be separated from the 2,7-regioisomer which remains in the mother liquor. This phenomenon was first studied by Takayoshi Shindo et al[146]. By growing the single crystal of 2,6-diethyl naphthalene thiourea adduct, they investigated the crystal structure of the

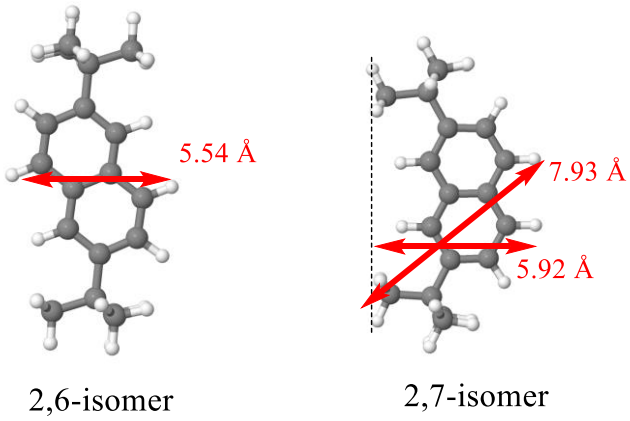

Figure B-4 Optimized geometries of 2,6-di-*tert*-butylnaphthalene (left) and 2,7-di-*tert*-butylnaphthalene (right). Calculated by Gaussian 16 using B3LYP/6-311G(d).

adduct and the crystallization process. Thiourea forms a stable monoclinic $P2_1/c$ space group lattice, and plate-like guests, like 2,6-substituted naphthalene, can be embedded into the hexagonal channel of the lattice without disrupting the crystal (Figure B-5). In a later study[147], they further investigated the equilibrium constant of this process for different dialkylnaphthalene. According to their result, 2,6-di-*tert*-butylnaphthalene showed much stronger tendency to precipitate as a crystalline adduct with thiourea compared with 2,7-di-*tert*-butylnaphthalene. This selectivity can also be supported by computational results (Figure B-4): the optimized geometry of the 2,7-isomer is much more hindered to fit into a crystal channel compared to the 2,6-isomer. Therefore, pure 2,7-di-*tert*-butylnaphthalene was isolated from the crude with this separation method. (Scheme B-9) The isolated yield of 2,7-di-*tert*-butylnaphthalene is very low (~ 15%) due to the separation and the fact that 2,7-regioisomer is the minor product. However, this reaction can be performed in very large scale, and gram-amount of 2,7-di-*tert*-butylnaphthalene was obtained.

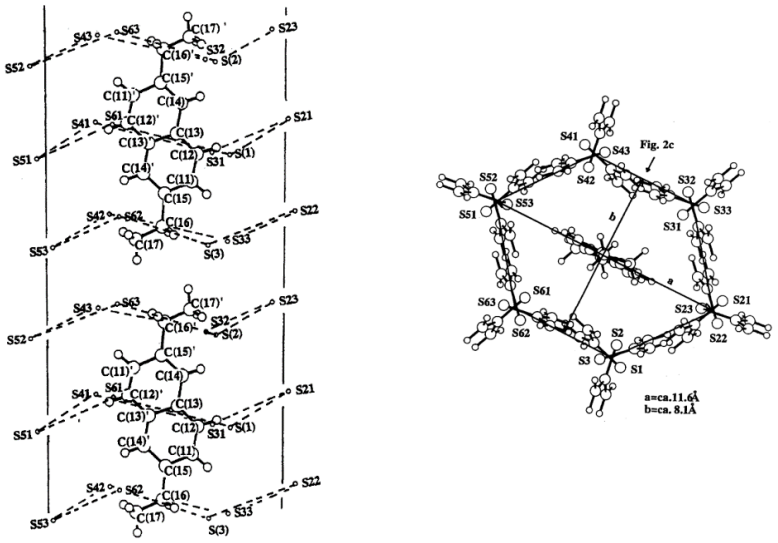

Figure B-5 Two views of inclusion behavior of 2,6-diethylnaphtalene in thiourea crystal channel. Reproduced from ref. [146]

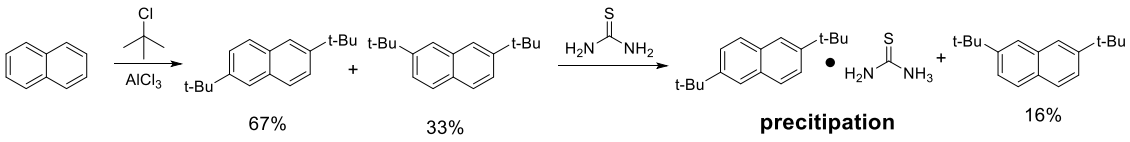

Scheme B-9 Synthesis of 2,7-di-*tert*-butylnaphthalene

The second step, a bromination in the 1-position of 2,7-di-*tert*-butylnaphthalene, proceeds regioselectively and in almost quantitative yield to afford 1-bromo-2,7-di-*tert*-butylnaphtalene (Scheme B-8). We found that the use of $CuBr_2$ physiosorbed on Al_2O_3[148] led to almost quantitative yields in the bromination step and the crude product was considerably easier to purify (by filtration) than the crude obtained from electrophilic aromatic bromination reaction with bromine. The mechanism is not clear for this condition; it is suggested that the reaction proceed through an aromatic radical cation which is formed by single electron transfer (SET) from an aromatic hydrocarbon to copper(II) bromide. Activated alumina has electron-acceptor properties, and formation of

a radical cation of an aromatic hydrocarbon adsorbed on alumina has been observed by ESR.[149] Therefore, it is likely that alumina as a support facilitates the generation of the radical cation of the aromatic hydrocarbon.

To synthesize the binaphthyl precursor, commercially available naphthalen-1-ylboronic acid was used in a Suzuki Pd-Catalyzed cross coupling reaction with 1-bromo-2,7-di-tert-butylnaphtalene (**1b**), to afford 3,6-di-*tert*-butyl-1,1'-binaphthyl (**2**) in good (~ 90%) yields. (Scheme B-8)

The key step in Scheme B.8 is the anionic cyclization of 1,1'-binaphthyl (**2**) in the presence of alkali metal to form the perylene framework [150]. This reaction, which proceeds via an air-sensitive radical anion, required rigorously degassed (freeze-pump-thaw) and anhydrous (freshly distilled over sodium and benzophenone) solvent, in our case THF. A test reaction, performed with binaphthyl in the presence of potassium metal following a modified procedure from Storck et al[144]. (Scheme B.10) afforded perylene with 34% yield.

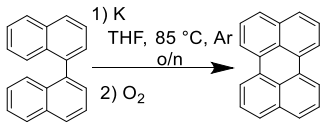

Scheme B-10 Anionic Cyclization of binaphthyl.

However, when we employed an identical procedure on 3,6-di-tert-butyl-1,1'-binaphthyl produced an inseparable crude mixture. Although the side products were not separated and characterized, we suspect that the high temperature (85 °C), which is required to melt the potassium metal for the exposure of fresh reactive surface, may lead to radical side reactions involving the *tert*-butyl group. Same phenomenon was observed

in the published result by Willig: large amount of high melting by-product was formed if the cyclization was performed at temperature > 50 °C.

Therefore, an alkali metal which can maintain a large reactive surface and that reacts at a relatively low temperature is preferable for this reaction. We found Stabilized Lithium Metal Powder (SLMP, FMC Corporation), which is used in lithium battery industry. It is made of spherical particles with controlled particle size (25~60 μm diameter) made by high-speed dispersion of molten lithium[151]. (Figure B-5) Generally, SLMP contains 97% lithium metal by weight; the remaining 3% is composed of the protective coating layer, e.g. Li_2CO_3. The protective layer is homogenously coated on the metallic lithium particle surface and provides both air and solvent stability to lithium metal, allowing SLMP to be safely handled in a dry room atmosphere. By using this lithium source, the reaction was successfully conducted at 50 °C and afforded 2,5-di-*tert*-butylperylene (**DTBuPe, 3**) in 50% yield.

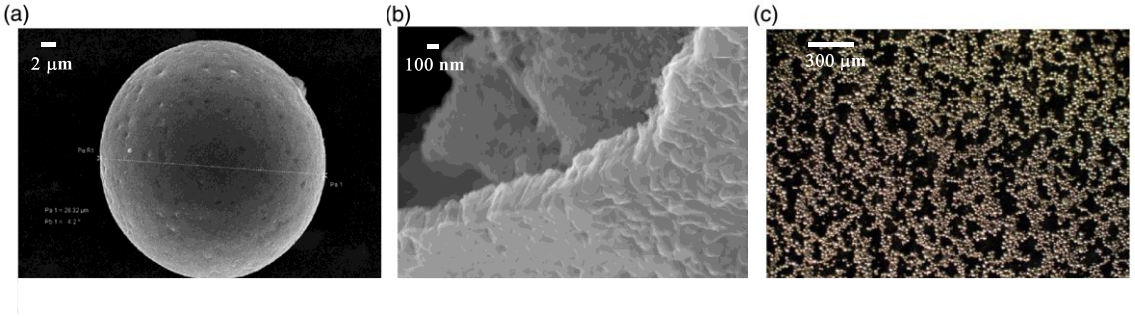

Figure B-6 (a) SEM image of single spherical SLMP particle; (b) high magnification SEM image of the broken edge of the surface skin of the reacted SLMP particle; (c) microscopic image of sprayed SLMP on a prefabricated anode sheet. Reproduced from ref[151]with permission.

B.4 Synthesis of 2,5-di-*tert*-butylperylene derivatives

The modification of **DTBuPe** is described in Schemes B-11 and B-12. As we discussed before, the distance between a chromophore and the semiconductor surface is crucial for heterogeneous ET studies. To obtain a well-defined distance from semiconductor to perylene, the bridge anchor must position the perylene as normal as possible to the surface. Thus, the 9-position of **DTBu-Pe** would be the most ideal position. This is also the most reactive position of perylene in reactions involving a radical cation.

The bromination of **DTBu-Pe** produced 9-bromo-2,5-di-*tert*-butylperylene (**6)** in 83% yield (Scheme B-11). The reaction was conducted in the dark and in controlled experimental conditions (room temperature, stoichiometric amount of NBS) to prevent bromination on other positions and possible homolytic cleavage of the N-Br bond in NBS, which would lead to radical reaction.

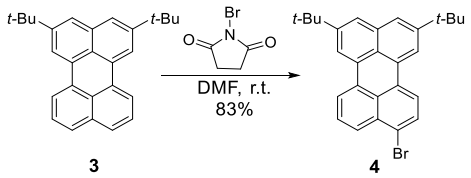

Scheme B-11 Synthesis of **DTBuPe-Br**.

The formylation via Friedel-Crafts with dichloromethyl methyl ether to prepare **4** (Scheme B-11b) was also straightforward and proceeded in acceptable yields[108] (~ 50%). However, the direct synthesis of 8,11-di-*tert*-butylperylene-3-carboxylic acid (**5**) by metal-halogen exchange of **6** with *tert*-butyllithium, followed by CO_2 and subsequent hydrolysis produced a mixture of **3** and unreacted **6**. (Scheme B-12) The same sequence repeated, however, on 1-bromonaphthalene readily produced 1-naphthoic acid. The

reason for this difference is not obvious, but we think it could be due to the lower solubility of the lithium salt derived from **6** compared to that derived from 1-bromonaphthalene, or to the delocalization of the lone pair on perylene radical anion. A method reported by Hlavac et al. for the synthesis of **5**,[152] involved reaction of **4** with phenyl hydrazine, followed by reaction with potassium trimethylsilanolate (TMSOK) and oxidization by air, requires a complex purification procedure, and Zeng and Wu[153] reported the oxidative esterification with 4-ethyl-1-methyl-4H-[1,2,4]triazol-1-ium iodide (EMTI). We found that a more facile and direct approach to the acid than these methods is the oxidation of aldehyde **4** to **5** with $KMnO_4$ at room temperature over three days. (Scheme B-12) When the reaction mixture was heated to 100 ºC, however, we observed a mixture of products assigned to oxidation of the perylene ring or of the *tert*-butyl groups.

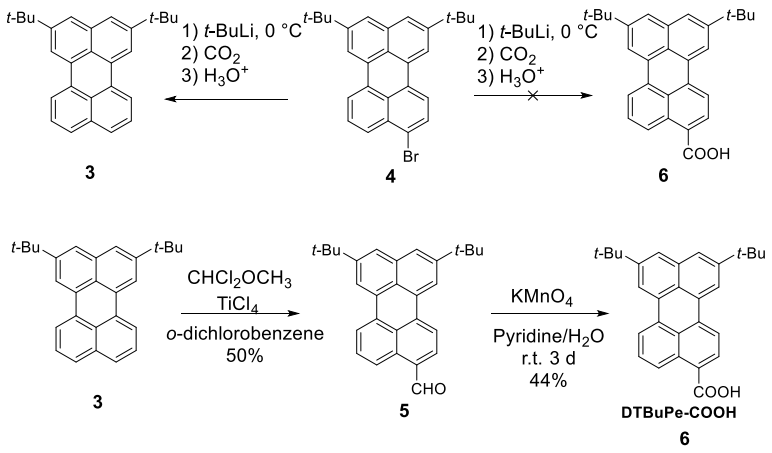

Scheme B-12 Synthesis of **DTBuPe** derivatives **5** & **6**

Bromoderivative **6** is an entry to previously unreported perylene-bridge-anchor compounds via Pd-catalyzed cross coupling procedures (Scheme B-13 and Scheme B-14). Suzuki cross-coupling reaction of **6** with (4-(methoxycarbonyl)phenyl) boronic acid gave methyl benzoate **7a** which was hydrolyzed to the corresponding acid **7b**, Scheme B.4-1,

and cross-coupling of **4** with 4-(4,4,5,5-tetramethyl-1,3,2-dioxaborolan-2-yl)aniline led to **10**, Scheme B.4-2. Finally, Heck reaction of **4** is a considerably easier approach to the synthesis of ethyl (*E*)-3-(8,11-di-*tert*-butylperylen-3-yl)acrylate (**8a**) which was previously prepared by Wittig reaction of the **4**[96]. Hydrolysis of **8a** afforded 3-(8,11-di-*tert*-butylperylen-3-yl)acrylic acid (**8b**) in high yields. Hydrogenation of **8b** with H_2 and Pd/C afforded 3-(8,11-di-*tert*-butylperylen-3-yl)propionic acid. (**9**)

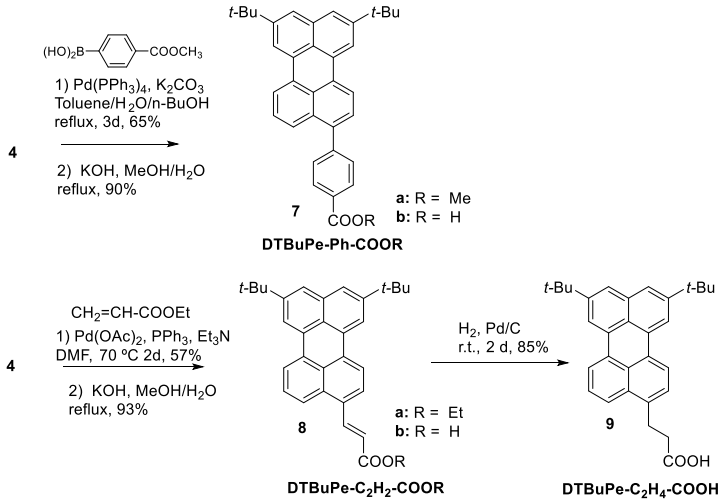

Scheme B-13 Synthesis of **DTBuPe**-bridge-anchor derivatives **7**-**9**.

The azido derivative, 9-(4-azidophenyl)-2,5-di-*tert*-butylperylene (**11**) was prepared by Sandmeyer reaction of **10** in H_2O/1,4-dioxane. 1,4-Dioxane was used as cosolvent[154] due to the highly hydrophobic **DTBuPe** moiety. 9-(4-azidophenyl)-2,5-di-*tert*-Butylperylene is a useful click-ready perylene derivative that can be used to prepare alkyne-bridge-anchor species by CuAAC, as demonstrated by the successful CuAAC of **11** and ethyl propiolate for the synthesis of **12a**, and for surface click reactions, as described in Chapter C.

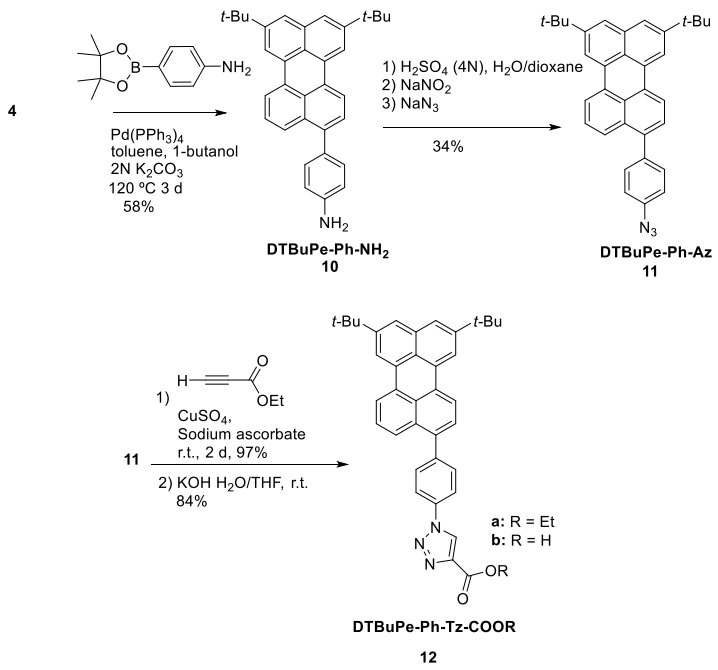

Scheme B-14 Synthesis of **DTBuPe** derivatives **10**-**12**.

B.5 Conclusions

2,5-di-*tert*-Butylperylene (**DTBuPe**) and a series of **DTBuPe**-bridge-anchor derivatives compounds were synthesized through practical pathways. We demonstrated that **DTBuPe** was brominated regioselectively, and the bromo group allowed palladium-catalyzed cross-coupling reactions to access several derivatives. Therefore, the functionalization potential of **DTBuPe** was significantly expanded. Moreover, for the first time, perylene was successfully functionalized with an azide group, and copper-catalyzed click reaction (CuAAC) was performed with **DTBuPe-Ph-N3** in high yield. This could lead to promising applications of perylene in a variety of field, as the CuAAC reaction is widely employed in surface modification. In next chapter, we will describe the studies of these **DTBuPe**-bridge-anchor derivatives both in solution and on

nanostructured TiO_2, ZrO_2 and ZnO films. An application of **DTBuPe-Ph-N3** for morphology preserving sensitization of ZnO nanorod surfaces will also be introduced.

B.6 Experimental Section

General: All reactions involving air- and moisture-sensitive reagents were performed under nitrogen or argon and in oven-dried or flame-dried glassware. All reactions involving perylene were conducted in the dark by protecting the vessels from ambient light with aluminum foil. Perylene samples were stored cold and protected with aluminum foil. Reagents (naphthalene, thiourea, copper (II) bromide, anhydrous $CdCl_2$, *O*-Dichlorobenzene, $TiCl_4$, 1,1-dichlorodimethyl ether, ethyl acrylate, sodium azide and ethyl propiolate) were purchased from VWR and used as received. Boron reagents were purchased from BTC and used without further purification. $Pd(PPh_3)_4$ and $Pd(OAc)_2$ catalysts were purchased from Strem and kept in a glovebox under N_2. NBS was purchased and then recrystallized with water and dried under air. Solvents (dichloromethane, (DCM) chloroform, ethyl acetate, (EA) methanol, toluene, 1-butanol, 1,4-dioxane and acetone were HPLC grade unless otherwise indicated. Hexanes employed for column chromatography was glass distilled. THF (anhydrous, stabilizer free) was first purified with an MBRAUN Solvent Purification System, then freshly distilled from sodium/benzophenone ketyl under nitrogen immediately prior to use. Alumina-supported $CuBr_2$ was prepared following a published procedure with activated neutral aluminum oxide.[148] Flash column chromatography was performed using silica gel (230-400 mesh) either in glass column or with a Sorbtech EZ Flash system. Thin layer chromatography was carried out on silica gel aluminum-backed sheets (200 μm thick) using UV light as developing agent. NMR spectra were collected on a Varian INOVA

NMR spectrometer operating at 599.896 MHz for ^{1}H and at 151 MHz for ^{13}C. Chemical shifts (δ) are reported relative to the central line of the solvent[155]: $CDCl_3$ (δ 7.26 ppm for ^{1}H and δ 77.16 ppm for ^{13}C); DMSO (δ 2.50 ppm for ^{1}H and δ 39.52 ppm for ^{13}C), Methanol-d4 (δ 3.31 ppm for ^{1}H and δ 49.00 ppm for ^{13}C) and spin-spin coupling constants (*J*) are reported in Hz. ESI spectra were collected on an Apex-ultra 70 hybrid Fourier transform mass spectrometer (Bruker Daltonics). Fourier transform infrared (FTIR) spectra in were collected on a Thermo Electron Corporation Nicolet 6700 FTIR utilizing the SMART MIRacle-single bounce attenuated total reflection (ATR) accessory (ZnSe crystal, with spectral resolution of 8 cm^{-1}). Samples for UV-Vis spectroscopy were dissolved in CH_3CN (unless otherwise indicated) and all have concentrations of 50 μM. Each solution was spectroscopically measured in 1 mm cuvettes using an Edmund Optics BDS130 UV/VisNIR Light Source and averaged 100 times to reduce noise.

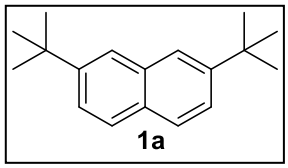

2,7-di-*tert*-Butylnaphthalene:[143] A flame-dried one-neck r.b. flask equipped with a magnetic stirrer and a drying tube charged with calcium hydroxide was charged with naphthalene (20 g, 156 mmol) and tert-butyl chloride (27.8 g, 624 mmol). Upon heating to 40 °C naphthalene and *tert*-butyl chloride formed a melt. $AlCl_3$ (250 mg, 1.2 mol%) was then added in small portions while stirring. A vigorous reaction with evolution of gaseous hydrogen chloride occurred. The reaction mixture turned to brown and solidified within minutes, and then was maintained at 40° C for 1 h. After that, unreacted *tert*-butyl chloride was removed *in vacuo*. The crude solid was refluxed in ethanol (300 mL) until dissolved, forming a deep violet solution. Thiourea (21 g) was added and heated to reflux with stirring until fully

dissolved. After cooling, a white crystalline adduct of thiourea and 2,6-di-*tert*-butylnaphthalene was separated by filtration. After this separation, the filtrate was treated again with thiourea twice (first 21 g and then 8 g) to separate the two regioisomers. The filtrate was collected and the solvent was removed *in vacuo*. The resulting crude residue from the filtrate was sonicated and triturated with H_2O, and the resulted suspension was extracted several times with hexanes. The combined organic layer was washed with H_2O and brine, dried with $MgSO_4$ and filtered. Evaporation of the solvent yielded a yellow solid, which was recrystallized with MeOH to afford compound **1a** as off-white crystals (6.2 g, 16%); m.p. 101 -103 °C. ^{1}H NMR (Chloroform-d) δ 7.75 - 7.73 (m, 4H), 7.51 (dd, *J* = 8.5, 1.9 Hz, 2H), 1.41 (s, 18H). ^{13}C NMR (Chloroform-d) δ 148.67, 133.46, 130.02, 127.18, 124.33, 123.10, 35.02, 31.49. GC-MS: m/z (%) = 240 (37) [M^+], 225 (100) [M^+-CH_3], 57 (11) [$C(CH_3)_3^+$]

bromo-3,6-di-*tert*-butylnaphthalene:[148] A flame dried r.b. flask equipped with a magnetic stirrer and condenser was charged with **1a** (1 g, 4.17 mmol), alumina-supported $CuBr_2$ (20.8 mmol of $CuBr_2$ in 14 g of mixture) and CCl_4 (anhydrous, 40 mL). The reaction vessel was then charged with N_2 and heated to 85 ºC for 2 h. Analysis by TLC and GC-MS indicated complete conversion. The mixture was then filtered, and the solid residue was rinsed with $CHCl_3$ to wash off any absorbed product. The combined filtrate was dried *in vacuo,* and **1b** was obtained as a pale-yellow oil (1.2 g, 90%). It was directly used in the next step. ^{1}H NMR (Chloroform-d) δ 8.09 (d, *J* = 8.9 Hz, 1H), 7.79 (d, *J* = 1.8 Hz, 1H), 7.73 (d, *J* = 1.9 Hz, 1H), 7.71 (s, 1H), 7.62 (dd, *J* = 8.9, 2.0

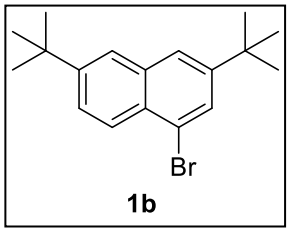

1b

Hz, 1H), 1.42 (s, 9H), 1.40 (s, 9H). ^{13}C NMR (Chloroform-d) δ 149.68, 149.56, 134.65, 128.72, 128.39, 126.62, 125.79, 123.55, 123.34, 122.51, 35.10, 35.00, 31.40. GC-MS: m/z (%) = 318 (45), 320 (45) [M^+], 303 (100), 305 (100) [M^+-CH_3], 57 (22) [$C(CH_3)_3^+$]

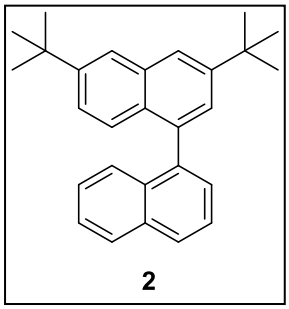

3,6-di-*tert*-butyl-1,1'-binaphthalene: A flame-dried r.b. flask equipped with a magnetic stirrer and condenser was charged with **1b** (2.0 g, 6.26 mmol), naphthalen-1-ylboronic acid (1.29 g, 7.51 mmol), toluene (10 mL), 1-butanol (5 mL) and 2N aq. Cs_2CO_3 (6.3 mL, 12.6 mmol) under N_2. $Pd(PPh_3)_4$ was added under N_2 flow and the mixture was refluxed with vigorous stirring for about 3 d. After cooling to room temperature, the mixture was diluted with brine and extracted with ethyl acetate (20 mL x 3). The combined organic layer was washed with brine, dried with Na_2SO_4, filtered, and the solvent was removed *in vacuo*. After column chromatography (silica gel, hexanes), compound **2** was obtained as a colorless glass (2.0 g, 87%) ^{1}H NMR (Chloroform-d) δ 7.99 (d, *J* = 8.3 Hz, 2H), 7.96 – 7.91 (m, 2H), 7.68 – 7.62 (m, 1H), 7.61 (d, *J* = 1.7 Hz, 1H), 7.54 (td, *J* = 14.6, 14.0, 7.1 Hz, 3H), 7.43 – 7.31 (m, 3H), 1.51 (d, *J* = 0.7 Hz, 9H), 1.46 (d, J = 0.8 Hz, 9H). ^{13}C NMR (Chloroform-d) δ 148.68, 148.26, 139.31, 137.86, 133.83, 133.21, 129.58, 128.37, 128.11, 127.95, 126.97, 126.55, 126.15, 126.08, 125.99, 125.61, 124.51, 123.41, 123.17, 35.17, 35.00, 31.58, 31.51.

2,5-di-*tert*-Butylperylene (DTBuPe) This procedure was carried out under argon and with rigorous exclusion of moisture and oxygen. The anhydrous THF used in this reaction was freshly distilled anhydrous THF, degassed by freeze-pump-thaw and then

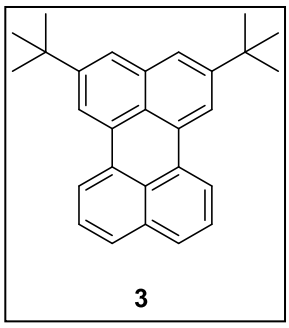
3

charged with argon. A glass coated stirring bar was used. *(CAUTION: Lithium metal may react with Teflon to form explosive carbon powder).* To a flame-dried r.b. flask equipped with a condenser, compound **2** (500 mg, 1.37 mmol) and stabilized lithium powder (SLMP® from FMC Co., 288 mg, 41.1 mmol) were added under positive argon flow. Then anhydrous THF (41 mL) was added to the flask via cannula. The mixture was then gradually (45 min) heated to 50 °C and maintained at 50 °C for 5 h. The color changed from yellow, to green, red-brown and finally deep violet, indicating the formation of the radical anion. After cooling to room temperature, anhydrous $CdCl_2$ (3.76 g, 15 mmol) was added in small portions under positive argon flow to oxidize the formed **DTBuPe**$^{2-}$ and any unreacted lithium. The color of the suspension changed to yellow with a detectable fluorescence. The suspension was stirred for 1 h and then carefully acidified with 5N $H_2SO_{4\,(aq)}$ while cooling with a water bath. The resulting suspension was filtered, and the metallic cadmium powder was rinsed with acetone to collect any physisorbed product. The filtrates were combined, evaporated *in vacuo* and the resulting orange crude solid was triturated with ethyl acetate. The aqueous layer was then extracted by ethyl acetate (20 mL x 3) and the combined organic layers were washed with diluted (~ 1M, aq) HCl, brine and dried (Na_2SO_4). The solvent was then removed *in vacuo*. Column chromatography (silica gel, hexanes: ethyl acetate = 30:1) yielded **3** as a yellow solid. (250 mg, 50 %) ^{1}H NMR (Chloroform-d) δ 8.24 (d, *J* = 1.4 Hz, 2H), 8.23 – 8.19 (m, 2H), 7.66 (d, *J* = 8.1 Hz, 2H), 7.63 (d, *J* = 1.4 Hz, 2H), 7.48 (t, *J* = 7.8 Hz, 2H), 1.47 (s, 18H). ^{13}C NMR (Chloroform-d) δ 148.98,

134.90, 134.75, 131.61, 130.41, 127.59, 126.37, 125.39, 123.46, 119.82, 118.28, 34.93, 31.31.

9-Bromo-2,5-di-*tert*-butylperylene (DTBuPe-Br)[108]: A two-neck r.b. flask equipped with a magnetic stirrer and condenser was charged with a solution of **3** (250 mg, 0.69 mmol) in DMF (anhydrous, 30 mL). After a few vacuum/ N_2 cycles a solution of NBS (122 mg, 0.69 mmol) in anhydrous DMF (7 mL) was injected via syringe. The reaction vessel was protected from ambient light with aluminum foil and the reaction mixture was stirred at r.t. in the dark under N_2 for 26 h., then water (60 mL) was added and the resulting suspension was stirred for 1 hour. The suspension was extracted with CH_2Cl_2 multiple times, and the combined organic layers were washed with H_2O and brine. After drying over $MgSO_4$ and filtration, the solvent was removed *in vacuo* and purification of the crude product by column chromatography (silica gel, hexanes: ethyl acetate = 100:1) yielded compound **4** as an orange solid (250 mg, 83%). ^{1}H NMR (Chloroform-d) δ 8.22 (m, 3H), 8.01 (dd, J = 28.4, 8.3 Hz, 1H), 7.72 (d, *J* = 8.0 Hz, 1H), 7.65 (d, *J* = 4.1 Hz, 2H), 7.54 (t, *J* = 7.9 Hz, 1H), 1.47 (s, 18H). ^{13}C NMR (Chloroform-d) δ 149.17, 149.12, 134.62, 133.20, 131.97, 131.56, 130.51, 130.27, 129.92, 129.74, 127.55, 126.67, 124.90, 123.99, 123.89, 122.16, 120.65, 120.12, 118.85, 118.56, 34.97, 31.34.

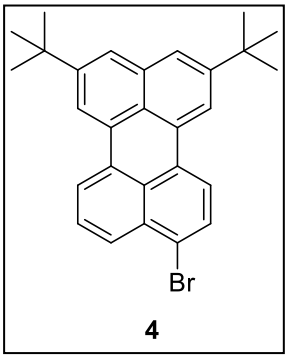

4

8,11-di-*tert*-Butylperylene-3-carbaldehyde (DTBuPe-CHO)[156]: A flame-dried 2-neck r.b. flask equipped with a

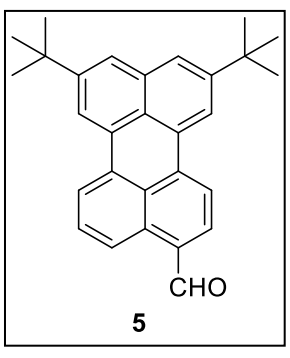

5

magnetic stirrer was charged with **4** (200 mg, 0.274 mmol) under nitrogen. *O*-dichlorobenzene (60 mL) was added via syringe. The solution was then cooled in an ice /water bath and $TiCl_4$ (90 uL, 0.357 mmol) and 1,1-dichlorodimethyl ether Cl_2CHOCH_3 (65 uL, 0.357 mmol) were added via syringe. After stirring for 1h, the ice bath was removed and the reaction mixture was stirred at r.t. for an additional 2 hours. The reaction mixture was diluted with ethyl acetate (50 mL), washed with 5% HCl (50 mL), H_2O (4 x 20 mL) and brine (20 mL). The combined organic layers were dried with Na_2SO_4, filtered and the solvent was removed *in vacuo*. The crude residue was purified via column chromatography (silica gel, hexane: ethyl acetate; 9:1) to yield **5** as a bright red solid (114 mg, 50%) ^{1}H-NMR (Chloroform-d) δ 10.33 (s, 1H), 9.18 (d, *J* = 8.4 Hz, 1H), 8.41 – 8.31 (m, 4H), 7.96 (d, *J* = 7.8 Hz, 1H), 7.81 – 7.75 (m, 1H), 7.75 – 7.68 (m, 2H), 1.50 (d, *J* = 5.4 Hz, 18H).

8,11-di-*tert*-Butylperylene-3-carboxylic acid (DTBuPe-COOH)[157]: A 2-neck r.b. flask equipped with a magnetic stirrer and a condenser was charged with **5** (50 mg, 0.128 mmol), H_2O (5 mL), pyridine (2.5 mL) and $KMnO_4$ (61 mg, 0.383 mmo) and the mixture was stirred at room temperature for about 3 d. Pyridine was removed in *vacuo*, and water (10 mL) was added to the crude residue. The resulting suspension was heated to 100 °C to dissolve any carboxylate salt and then filtered. The filtrate was cooled to r.t. and carefully acidified with conc. HCl to form a red suspension. After filtration, the solid was washed with H_2O and *n*-pentane, then dried under vacuum to yield **6** as a red solid (23 mg, 44%). ^{1}H NMR (DMSO-d6) δ 8.81 (d, J =

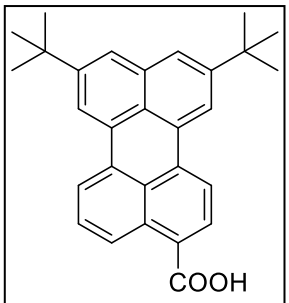

6

8.5 Hz, 1H), 8.56 (d, *J* = 7.5 Hz, 1H), 8.53 (d, *J* = 8.1 Hz, 1H), 8.45 (d, *J* = 1.4 Hz, 1H), 8.42 (d, *J* = 1.4 Hz, 1H), 8.12 (d, *J* = 7.9 Hz, 1H), 7.83 (d, *J* = 1.2 Hz, 1H), 7.78 (d, *J* = 1.2 Hz, 1H), 7.69 – 7.64 (m, 1H), 1.46 (d, *J* = 1.4 Hz, 18H). ^{13}C NMR (DMSO-d6) δ 174.49, 149.25, 149.11, 134.70, 134.15, 132.52, 130.90, 130.36, 129.57, 128.95, 128.63, 127.85, 125.44, 124.81, 124.23, 123.82, 120.92, 120.06, 119.63, 119.30, 34.84, 30.99. IR (FTIR): 700.0334, 719.3181, 765.6013, 784.886. 831.1692, 873.5955, 894.8086, 912.1648, 960.3765, 983.5181, 1035.587, 1093.441, 1118.511, 1137.795, 1201.435, 1218.791, 1251.575, 1270.86, 1317.143, 1357.641, 1374.997, 1392.353, 1403.924, 1434.779, 1463.706, 1500.347, 1521.56, 1571.7, 1598.699, 1625.698, 1673.909, 2848.345, 2917.77, 2950.554 cm^{-1}

Methyl 4-(8,11-di-*tert*-butylperylen-3-yl)benzoate: A flame-dried 2-neck r.b. flask equipped with a magnetic stirrer and a condenser was charged under nitrogen with **4** (340 mg, 0.77 mmol), (4-(methoxycarbonyl)phenyl)boronic acid (207 mg, 1.15 mmol), toluene (1.5 mL), 1-butanol (0.75 mL) and 2N aq. Cs_2CO_3 (0.75 mL,). $Pd(PPh_3)_4$ (44.5 mg, 0.039 mmol) was added under positive N_2 flow and the reaction mixture was refluxed with vigorous stirring for 3 d. After cooling to room temperature, brine was added and the mixture was extracted with ethyl acetate (20 mL x 3). The combined organic layers were washed with H_2O and brine, dried over Na_2SO_4, filtered, and the solvent was removed *in vacuo*. After column chromatography (silica gel, hexanes: ethyl acetate = 10:1), compound **7a** was obtained as a bright yellow solid (232 mg, 61 %). ^{1}H NMR

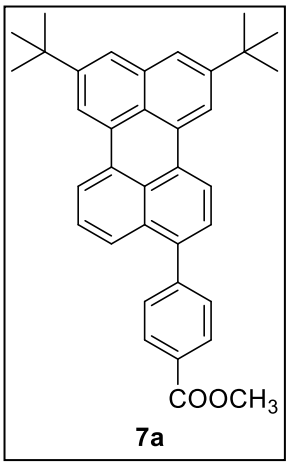

7a

(Chloroform-d) δ 8.30 – 8.24 (m, 4H), 8.18 (d, *J* = 8.4 Hz, 2H), 7.70 – 7.65 (m, 3H), 7.62 (d, *J* = 8.4 Hz, 2H), 7.47 – 7.41 (m, 2H), 3.99 (s, 3H), 1.49 (s, 9H), 1.49 (s, 9H). HRMS (ESI): calculated for $C_{34}H_{35}O_2$, 499.2637 $[M+H]^+$; found, 499.2640 $[M+H]^+$

4-(8,11-di-*tert*-Butylperylen-3-yl)benzoic acid (DTBuPe-Ph-COOH): To a solution of **7a** (100 mg, 0.2 mmol) in methanol (5 mL), 1N KOH (aq.) solution (5 mL) was added in one portion with stirring. The mixture was heated to reflux and stirred overnight. After cooled to room temperature, 10% HCl (aq.) was added dropwise to the flask until the solution became acidic and a bright yellow suspension formed. This fine powder was collected by filtration and washed with water and n-pentane to obtain **7b** as a yellow solid (90 mg, 90%).

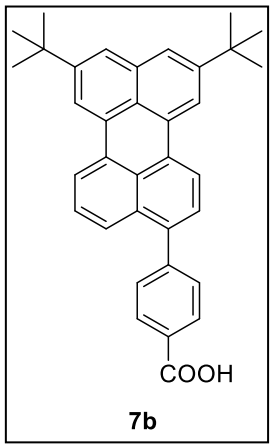

7b

^{1}H NMR (Chloroform-d) δ 8.31 – 8.25 (m, 6H), 7.71 (d, *J* = 8.3 Hz, 1H), 7.69 – 7.65 (m, 4H), 7.50 – 7.44 (m, 2H), 1.50 (d, *J* = 2.7 Hz, 18H). ^{13}C NMR (Chloroform-d) δ 171.57, 149.18, 149.16, 146.77, 138.29, 134.68, 132.71, 131.95, 131.83, 130.40, 130.23, 130.17, 129.45, 128.10, 127.67, 126.75, 125.28, 125.24, 123.78, 123.65, 120.17, 119.47, 118.64, 118.50, 34.99, 31.35. HRMS (ESI): calculated for $C_{33}H_{32}O_2$, 484.2402 $[M]^+$; found, 484.2407 $[M+H]^+$ IR (FTIR-ATR): 707, 727, 763, 798, 841, 878, 924, 933, 960, 977, 1018, 1043, 1087, 1101, 1126, 1176, 1234, 1259, 1275, 1286, 1311, 1369, 1415, 1462, 1564, 1601, 1624, 1684, 1734, 2856, 2865, 2923, 2952 cm^{-1}

Ethyl (*E*)-3-(8,11-di-*tert*-Butylperylen-3-yl)acrylate: A flame-dried 2-neck r.b. flask equipped with a magnetic stirrer and a condenser was charged with **4** (293 mg, 0.66

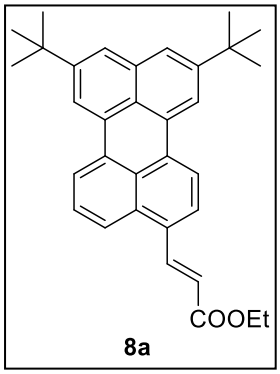

8a

mmol), $Pd(OAc)_2$ (3.7 mg, 0.017 mmol), and PPh_3 (21.6 mg, 0.083 mmol) under N_2 atmosphere. To the solution, ethyl acrylate (132 mg, 1.32 mmol), triethylamine (73.5 mg, 0.73 mmol) and DMF (anhydrous, 5 mL) were added with a syringe while stirring. The mixture was heated to 80 °C and stirred for 3 d. After cooling to room temperature, brine was added, and the mixture was extracted with ethyl acetate (20 mL x 3). The combined organic layers were washed with H_2O and brine, dried over Na_2SO_4, filtered, and the solvent was removed *in vacuo*. After column chromatography (silica gel, hexanes : ethyl acetate = 5:1), **8a** was obtained as a red solid (165 mg, 54%) 1H NMR (600 MHz, Chloroform-d) δ 8.46 (d, *J* = 15.7 Hz, 1H), 8.32 – 8.23 (m, 3H), 8.19 (d, *J* = 8.0 Hz, 1H), 8.03 (d, *J* = 8.4 Hz, 1H), 7.76 (d, *J* = 7.9 Hz, 1H), 7.67 (d, *J* = 12.4 Hz, 2H), 7.58 (t, *J* = 7.9 Hz, 1H), 6.54 (d, *J* = 15.7 Hz, 1H), 4.33 (q, *J* = 7.2 Hz, 2H), 1.49 (d, *J* = 1.4 Hz, 18H), 1.39 (t, *J* = 7.1 Hz, 3H). 13C NMR (151 MHz, Chloroform-d) δ 167.06, 149.23, 149.14, 141.40, 134.59, 133.78, 133.01, 132.08, 130.74, 130.19, 129.89, 129.29, 127.11, 125.65, 125.01, 124.32, 123.80, 122.88, 120.26, 119.96, 119.60, 119.03, 118.87, 60.58, 34.97, 31.32, 29.71.

(*E*)-3-(8,11-di-*tert*-Butylperylen-3-yl)acrylic acid (DTBuPe-C_2H_2-COOH) To a solution of **8a** (50 mg, 0.11 mmol) in methanol (5 mL), 1N aq. KOH (5 mL) was added in one portion. The mixture was heated to reflux and stirred overnight. After cooling to room temperature, diluted 10% aq. HCl was added dropwise until the solution became acidic. A red fine suspension formed. The powder was

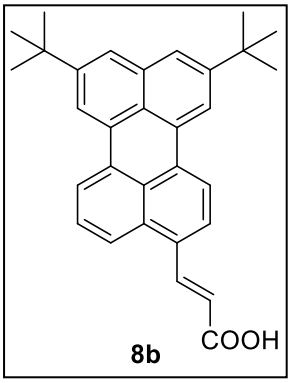

8b

collected by filtration and washed with water and *n*-pentane to obtain **8b** (42 mg, 87%) as a red powder. ^{1}H NMR (DMSO-d6) δ 8.56 (d, *J* = 7.7 Hz, 1H), 8.51 (d, *J* = 8.0 Hz, 1H), 8.41 (s, 2H), 8.33 (d, *J* = 15.6 Hz, 1H), 8.07 (d, *J* = 8.5 Hz, 1H), 7.96 (d, *J* = 7.9 Hz, 1H), 7.78 (d, *J* = 10.6 Hz, 2H), 7.66 (t, *J* = 8.0 Hz, 1H), 6.64 (d, *J* = 15.6 Hz, 1H), 1.45 (s, 18H). ^{13}C NMR (DMSO-d6) δ 167.99, 149.65, 149.61, 140.40, 134.69, 133.24, 132.80, 131.73, 130.76, 130.05, 129.78, 128.91, 128.12, 126.54, 124.78, 123.27, 121.82, 121.56, 121.03, 119.87, 119.63, 35.30, 31.47.

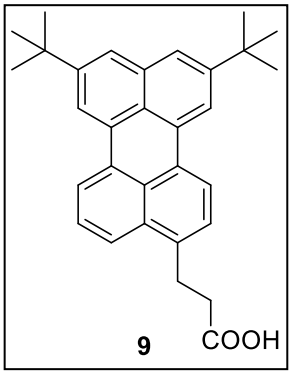

9

3-(8,11-di-*tert*-Butylperylen-3-yl)propanoic acid (DTBuPe-C_2H_4-COOH): A flame-dried 2-neck r.b. flask equipped with a magnetic stirrer was charged with **8b** (20 mg, 0.02 mmol) and Pd/C (4 mg, 10 mol%), and methanol (2 mL) were added. The reaction vessel was degassed with N_2 three times, and then charged with H_2 using a balloon and vigorously stirred at room temperature overnight. After column chromatography (silica gel, sequentially eluted with CH_2Cl_2; then CH_2Cl_2: acetone: formic acid = 66:33:1), **9** was obtained as a yellow solid (17 mg, 85%) ^{1}H NMR (Chloroform-d) δ 8.26 (d, *J* = 7.0 Hz, 2H), 8.22 (s, 1H), 8.16 (d, J = 7.9 Hz, 1H), 7.85 (d, *J* = 8.4 Hz, 1H), 7.66 – 7.59 (m, 2H), 7.54 (t, *J* = 8.0 Hz, 1H), 7.39 (d, *J* = 7.6 Hz, 1H), 3.43 – 3.32 (m, 2H), 2.86 – 2.78 (m, 2H), 1.47 (d, *J* = 3.5 Hz, 18H). IR (FTIR): 700.0334, 719.3181, 761.7444, 817.6699, 877.4524, 935.3064, 1024.016, 1043.301, 1087.655, 1151.295, 1201.435, 1230.362, 1257.36, 1288.216, 1363.426, 1461.778, 1652.696, 1708.622, 2852.202, 2923.555, 2954.411 cm^{-1}

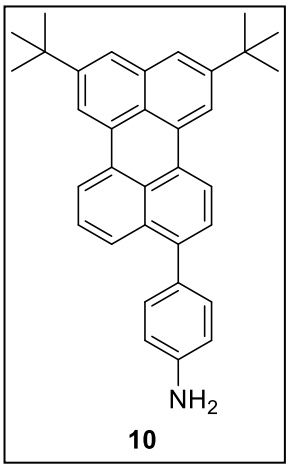

10

4-(8,11-di-*tert*-Butylperylen-3-yl)aniline (10): A flame-dried 2-neck r.b. flask equipped with a magnetic stirrer and a condenser was charged with **4** (330 mg, 0.746 mmol), 4-(4,4,5,5-tetramethyl-1,3,2-dioxaborolan-2-yl)aniline (196 mg, 0.896 mmol), toluene (1.41mL), and 1-butanol (0.71mL), and a 2 N aq. K_2CO_3 (0.72 mL). After a few vacuum/ N_2 cycles, $Pd(PPh_3)_4$ (71.6 mg, 8.3%) was added under N_2 flow and the reaction was heated to reflux (120 °C) for 3 days. The reaction mixture was cooled to r.t., filtered through Celite and extracted with ethyl acetate (5 ml x 3). The combined organic layers were washed with brine and dried with Na_2SO_4 and the solvent was removed in vacuo. The crude residue was purified via column chromatography (silica gel, hexanes: ethyl acetate = 10:1) to form product **10** as a brown solid (197 mg, 58%). ^{1}H NMR (Chloroform-d) δ 8.31 – 8.22 (m, 4H), 7.85 (d, *J* = 8.4 Hz, 1H), 7.66 (dd, *J* = 4.1, 1.4 Hz, 2H), 7.48 – 7.41 (m, 2H), 7.35 (d, *J* = 8.3 Hz, 2H), 6.83 (d, *J* = 8.3 Hz, 2H), 3.83 (s, 2H), 1.53 – 1.48 (m, 18H). ^{13}C NMR (Chloroform-d) δ 149.12, 149.08, 145.81, 139.97, 134.77, 133.36, 131.74, 131.07, 130.98, 130.80, 130.67, 130.39, 129.55, 127.49, 126.18, 126.15, 125.38, 123.38, 123.23, 119.99, 119.74, 118.33, 118.03, 115.01, 35.01, 31.40.

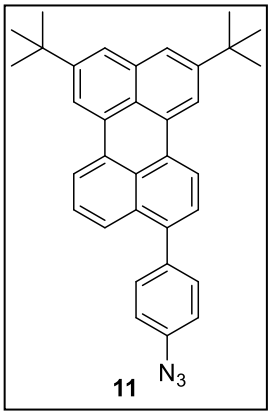

11

9-(4-azidophenyl)-2,5-di-*tert*-Butylperylene (DTBuPe-Ph-N3): A flame-dried 2-neck r.b. flask equipped with a magnetic stirrer and a condenser was charged with a solution of **10** (100 mg, 0.220 mmol) in dioxane (2 mL) followed by 4N H_2SO_4 (aq., 2mL) to form a suspension of the sulfate salt as a yellow solid. The flask

was then equipped with an addition funnel, degassed and charged with N_2. The suspension was stirred in an ice bath, until cold (about 30 min) and 0.5 N $NaNO_2$ solution (aq., 5ml, 0.263 mmol) was added dropwise (15 mins) with vigorous stirring to ensure that the reaction mixture stays cold. Upon addition the reaction mixture became darker. The reaction mixture was stirred for an additional 45 min while cold and 0.5 N NaN_3 solution (aq., 5mL, 0.263 mmol) was added dropwise via an addition funnel and allowed to stir while cold for an additional 30 min, at which point separation of a clear aqueous layer and a dark yellow organic layer was observed. The reaction mixture was left stirring in a large ice bath overnight during which time it slowly reached room temperature, then extracted with ethyl acetate, washed with brine, dried over Na_2SO_4 and filtered. The solvent was removed *in vacuo*. The crude residue was purified via column chromatography (silica gel, hexanes: ethyl acetate = 10:1) to obtain product **11** as a dark brown glassy solid (36 mg, 34%). *CAUTION: organic azides and sodium azide may decompose explosively. Azide waste should not come in contact with concentrated acids or metals.* ^{1}H NMR (Chloroform-d) δ 8.29 – 8.23 (m, 4H), 7.71 (d, *J* = 8.4 Hz, 1H), 7.66 (s, 2H), 7.52 (d, *J* = 8.4 Hz, 2H), 7.44 (t, *J* = 7.9 Hz, 1H), 7.40 (d, *J* = 7.6 Hz, 1H), 7.18 (d, *J* = 8.4 Hz, 2H), 1.51 – 1.46 (18H). ^{13}C NMR ($CDCl_3$) δ 149.13, 139.16, 138.57, 137.70, 134.73, 133.05, 131.90, 131.40, 131.26, 130.54, 130.35, 129.49, 127.63, 126.52, 125.48, 125.30, 123.58, 120.09, 119.54, 119.07, 118.53, 118.31, 35.00, 31.37. HRMS (ESI): calculated for $C_{34}H_{31}N_3$, 481.2518 $[M]^+$; found, 481.2524 $[M]^+$ IR (FTIR): 821.5269, 836.9546, 877.4524, 908.3079,958.448 977.7327, 1089.584, 1110.797, 1130.082, 1182.15, 1209.149, 1259.289, 1290.144, 1347.998, 1363.426, 1374.997,

1392.353, 1427.065, 1465.635, 1477.206, 1504.204, 1600.627, 1623.769, 2088.53, 2121.313, 2856.059, 2867.63, 2925.484, 2962.125 cm^{-1}

Ethyl 1-(4-(8,11-di-*tert*-butylperylen-3-yl)phenyl)-1H-1,2,3-triazole-4-carboxylate (12a): A flame-dried 2-neck r.b. flask equipped with a magnetic stirrer and a condenser was charged with a solution of **11** (30 mg, 0.062 mmol) in a 2:1 H_2O:THF mixture (6 mL) followed by ethyl propiolate (12.22 mg, 0.124 mmol). To the resulting suspension, sodium ascorbate (2.46 mg, 20 mol%) and copper(II) sulfate pentahydrate (1.55 mg, 10 mol%) were added under nitrogen. The reaction was stirred under nitrogen for 5 days. The reaction mixture was diluted with water, extracted with ethyl acetate, washed with brine, and dried with Na_2SO_4 and filtered. The solvent was removed in vacuo. The crude residue was purified via column chromatography (silica gel, hexanes: ethyl acetate = 10:1) to afford compound **12a** (35 mg, 97%) as a brown glassy soild. ^1H NMR (Chloroform-d) δ 8.59 (s, 1H), 8.33 – 8.24 (m, 4H), 7.89 (d, *J* = 8.5 Hz, 2H), 7.72 – 7.67 (m, 5H), 7.54 – 7.39 (m, 2H), 4.51 (q, *J* = 7.1 Hz, 2H), 1.52 – 1.45 (m, 21H). ^{13}C NMR (Chloroform-d) δ 160.59, 149.10, 149.07, 142.38, 140.89, 137.48, 135.34, 134.59, 132.71, 131.91, 131.74, 131.40, 130.25, 130.02, 129.36, 127.62, 126.70, 125.39, 125.12, 124.98, 123.73, 123.61, 120.72, 120.09, 119.36, 118.58, 118.40, 61.48, 34.89, 31.25, 14.29. HRMS (ESI): calculated for $C_{39}H_{37}N_3O_2$, 580.2964 $[M+H]^+$; found, 580.2969 $[M+H]^+$ IR (FT-IR): 3133, 2954, 2919, 2850, 1704, 1599, 1541, 1462, 1365, 1252, 1173, 1147, 1090, 1038, 874, 835 cm^{-1}.

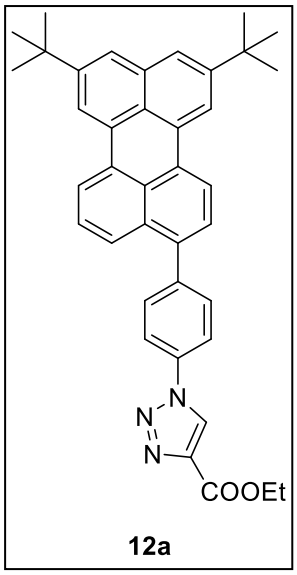

12a

1-(4-(8,11-di-*tert*-butylperylen-3-yl)phenyl)-1H-1,2,3-triazole-4-carboxylic acid (DTBuPe-Ph-Tz-COOH, 12b): A flame-dried 2-neck r.b. flask equipped with a magnetic stirrer was charged with a solution of **12a** (11 mg, 0.02 mmol) in THF (10 mL), and then LiOH (8 mg, 0.2 mmol) was added under N_2. The reaction was stirred at r.t. overnight and then 1 M HCl (aq.) was added dropwise. until the solution became acidic. A brown fine suspension was formed. The precipitate was filtered, washed with water, and then with *n*-pentane to give product **12b** (8.5 mg, 81%) as a dark brown solid. ^{1}H NMR (Methanol-d4) δ 9.04 (s, 1H), 8.36 – 8.25 (m, 4H), 7.93 (d, *J* = 8.0 Hz, 2H), 7.67 (d, *J* = 2.8 Hz, 2H), 7.63 (d, *J* = 8.3 Hz, 1H), 7.60 (d, *J* = 7.9 Hz, 2H), 7.43 (t, *J* = 7.9 Hz, 1H), 7.38 (d, *J* = 7.6 Hz, 1H), 1.48 (d, *J* = 3.0 Hz, 18H). ^{13}C NMR (Methanol-d4) δ 172.97, 150.46, 150.43, 143.44, 139.10, 136.29, 134.03, 133.09, 132.79, 132.40, 131.57, 131.36, 130.57, 128.98, 127.97, 126.40, 126.16, 124.92, 124.81, 124.21, 121.78, 121.36, 120.73, 119.71, 119.54, 48.71, 34.75, 31.73. HRMS (ESI): calculated for $C_{37}H_{33}N_3O_2$, 552.2651 $[M+H]^+$; found, 552.2647 $[M+H]^+$

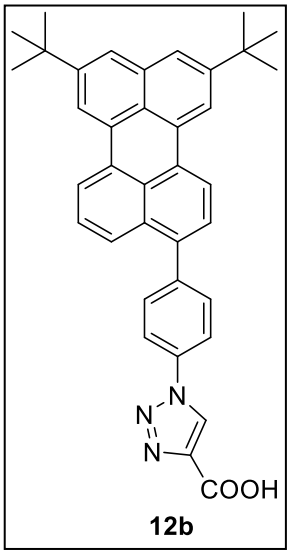

12b

3-Formylperylene (Pe-CHO, 13)[156]: A flame dried 2-neck r.b. flask equipped with a rubber septum, an N_2 adapter, and a magnetic stir bar was charged with perylene (1.00 g, 3.96 mmol) and dichlorobenzene (60 mL) under nitrogen. The solution was cooled in an ice/water bath, and then $TiCl_4$ (0.65 mL, 5.94 mmol) and 1,1-dichlorodimethyl ether (0.47 mL,

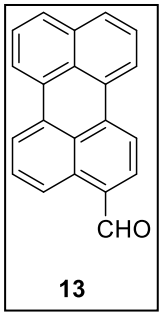

13

5.15 mmol) were added via syringe dropwise. The reaction mixture was stirred at 0 °C for one hour under nitrogen, then the ice bath was removed, and the reaction mixture was let reach room temperature, and then stirred for an additional 2 hours. The reaction mixture was diluted with chloroform (200 mL), washed with 5% HCl (200 mL), water (4 x 100mL) and brine (75 mL). The organic layer was dried over Na_2SO_4, filtered, and the solvent was removed *in vacuo*. The crude residue was purified via silica gel column chromatography (hexane: ethyl acetate; 9:1) to yield 3-formylperylene **13** (0.777 g, 70%). ^{1}H-NMR ($CDCl_3$) 7.53 (1H, t, J=7.57 Hz), 7.54 (1H, t, J=7.69 Hz), 7.68 (1H, t, J=7.98 Hz), 7.74 (1H, d, J=8.04 Hz), 7.81 (1H, d, J=8.04 Hz), 7.92 (1H, d, J=7.80 Hz), 8.26 (1H, d, J=7.44 Hz), 8.26 (1H, d, J=7.80 Hz), 8.29 (2H, d, J=7.56 Hz), 9.15 (1H, d, J=8.46 Hz), 10.31 (1H, s). ^{13}C NMR (151 MHz, Chloroform-d) δ 192.91, 137.83, 137.33, 134.56, 132.49, 131.45, 130.87, 130.25, 130.15, 130.05, 129.51, 129.15, 128.69, 128.34, 127.16, 126.85, 124.80, 122.98, 121.72, 121.28, 119.28.

Perylene-3-carboxylic acid (Pe-COOH, 14)[157]: A 2-neck r.b. flask equipped with an addition funnel, a nitrogen adapter, a condenser and a magnetic stir bar was charged with **13** (0.50 g, 1.79 mmol), water (8 mL), and pyridine (8 mL) under nitrogen. The reaction mixture was heated to 100 °C and 0.3 N $KMnO_4$ (aq., 10 ml) was added dropwise over 10 min. The reaction mixture was stirred at 100 °C for additional 12 h and then pyridine was removed in vacuo. Water (50 mL) was added to the resulting suspension and then heated to 100 °C and filtered. The filtrate was acidified by adding conc. HCl dropwise to form a red suspension. After filtration, the crude solid was washed with

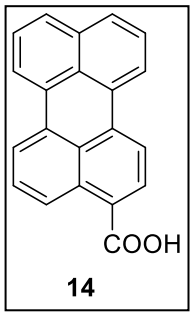

14

water and dried under vacuum to yield Perylene-3-carboxylic acid (40 mg, 15%) as a dark red solid. ^{1}H NMR (600 MHz, DMSO-d6) δ 8.79 (d, J = 8.5 Hz, 1H), 8.45 (d, J = 7.5 Hz, 2H), 8.42 (t, J = 7.6 Hz, 2H), 8.13 (d, J = 7.9 Hz, 1H), 7.89 (d, J = 8.1 Hz, 1H), 7.84 (d, J = 8.0 Hz, 1H), 7.66 (t, J = 8.0 Hz, 1H), 7.59 (q, J = 7.5 Hz, 2H). ^{13}C NMR (151 MHz, DMSO-d6) δ 169.06, 135.30, 134.71, 133.08, 131.38, 131.29, 130.88, 130.20, 129.95, 129.01, 128.99, 128.79, 128.13, 127.82, 127.69, 127.44, 126.23, 123.04, 122.24, 121.71, 120.38. IR (FTIR): 759.8159, 808.0276, 838.8831, 867.8101, 898.6655, 946.8772, 1008.588, 1124.296, 1151.295, 1201.435, 1253.503, 1313.286, 1380.782, 1428.994, 1500.347, 1519.632, 1567.844, 1583.271, 1621.841, 1670.052 cm^{-1}

Chapter C : Solution Properties and Binding of 2,5-di-*tert*-Butylperylene-Bridge-Anchor Derivatives to Metal Oxide Surfaces

C.1 Introduction

Three types of nanostructured metal oxide thin films were used for our studies: titanium dioxide (TiO_2), zinc oxide (ZnO) and zirconium dioxide (ZrO_2). Both ZnO and TiO_2 are well-known n-type semiconductors (Figure A-1) that can generate photocurrent under ultraviolet light irradiation or under visible light following sensitization with a dye.[158-161] The reason for using metal oxide semiconductors is that they have excellent stability, low-cost, and nontoxicity.[162-163] The excited state kinetics, like electron injection, intermolecular charge transfer, charge separation, and charge recombination of dyes bound to TiO_2 and ZnO surfaces, have been investigated by research groups worldwide. The band gap of nanostructured ZrO_2 is 5.0 eV, thus the ZrO_2 film behaves as an insulator precluding possible electron injection (TiO_2 anatase band gap is about 3.2 eV[164-165]) from the photoexcited sensitizers. However, the morphology of nanostructured ZrO_2 films is quite similar to that of the TiO_2 film[166]. Therefore, ZrO_2 films are an excellent substrate to study the fluorescence emission of sensitizers on metal oxide film in an environment that closely similar to TiO_2 films.

Surface sensitization with covalently attached dye-molecules requires a large surface area per volume that is provided by employing mesoporous thin films made of nanostructured metal oxide, most commonly nanocolloides, nanotubes, and nanowires.[167-168] TiO_2 nanocolloidal films are by far the most frequently used metal-oxide substrates in fundamental research and practical applications because they are very easily prepared by solution methods. An important reason for the dominance of TiO_2 is the inherent chemical stability of its surface, which is inert against strong acids at room temperature and requires boiling sulfuric acid for etching. Consequently, covalent modification by

attaching sensitizers via carboxylic (COOH) or phosphonic ($P(O)(OH)_2$) groups is often used.

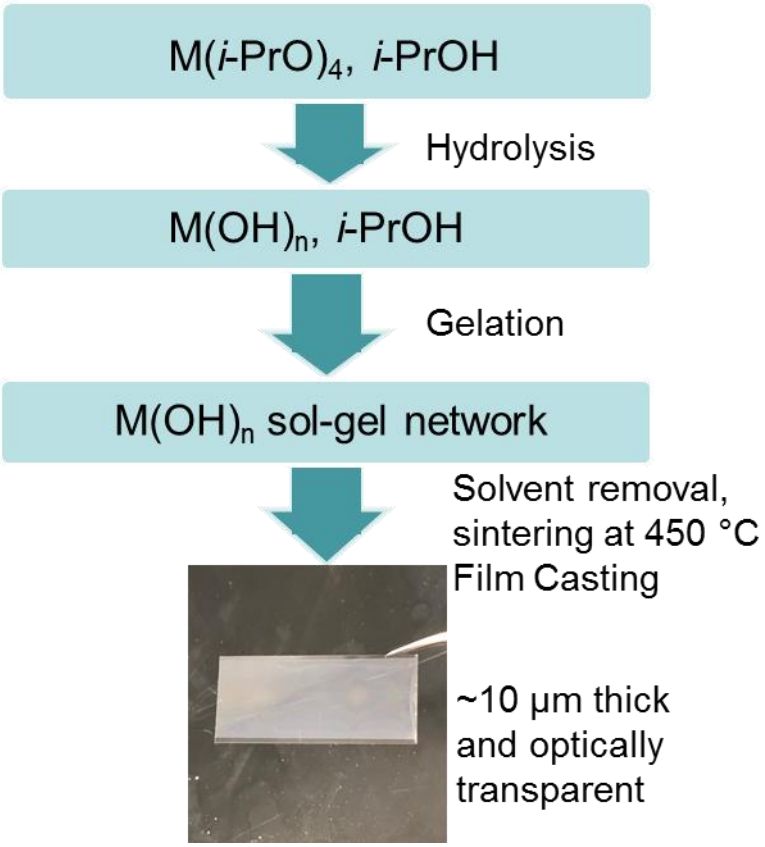

Figure C-1 Steps of film preparation of nanocrystalline MO_n in this study.

Metal oxide nanoparticles are often prepared using the sol-gel method, where the hydrolysis reaction is stopped right before gelation occurs, (Figure C-1).[169] Typically it involves hydrolysis and condensation of a metal alkoxide in an alcoholic solution. During the process a gel is formed consisting of a metal oxide network, which results in a nanoporous structure after calcination. Autoclaving of the sol-gels allows controlled growth of crystalline particles. Pore size, distribution and "necking" are determined by the reaction conditions. To improve the porosity and allow deposition on a substrate, a polymeric binder, polyethylene glycol (PEG), is added to form a homogeneous paste.

After the deposition of the MO_n paste on a suitable substrate, which can be a normal glass slide or conducting fluorine SnO_2 (FTO) glass substrate for conducting electrodes. The films are sintered at 450 °C, the organic polymer is burned, leading to film coatings with a high surface area and optical transparency. The properties of the nanoparticles are determined by the nucleation, growth and aging. The resulting nanocrystalline films of ZrO_2 or TiO_2 have a typical thickness of 10 μm and average particle size of 10 to 20 nm.[170]

ZnO has very similar band gap properties compared to TiO_2 (3.2 eV) and about a decade ago attracted considerable attention as a viable alternative to TiO_2 for DSSCs application. ZnO can easily be grown as highly crystalline (wurtzite), vertically aligned nanowires, and a variety of other ordered morphologies.[171] Highly ordered morphologies are advantageous in many electronic applications and fundamental interfacial charge transfer studies where it is important to better control the sensitization process. Also, ZnO nanorod electrodes exhibited higher electron mobility, a property that is attractive for applications in solar energy conversion.[172] However, the fact that ZnO is etched by the acidic anchor groups used to bind the sensitizers greatly limits its applicability,[173-175] leading to the formation of zincate salts that may deposit onto the surface. The binding may be further complicated when multiple surface anchors are present on the same molecule. Strategies aiming at preserving the integrity of ZnO nanostructure surface include the development of ZnO materials alloyed with MgO (such as $Zn_{(1-x)}Mg_xO$)[176] , but this requires metal-organic chemical vapor deposition (MOCVD) methods and for high doping (>5%) the band gap is affected. Modification of surface stoichiometry, which is realistic only on a defect-free surface in vacuum,[177] atomic layer deposition (ALD) of

thin layers of aluminum oxide,[178] and chemical stabilization of the surface with additional reagents, such as alkylammonium alkylcarbamates,[179] are additional strategies to prevent etching.

Liquid phase chemical modification of ZnO nanorods and nanostructures can also be carried by stepwise procedures, where the initial surface functionalization step involves attachment of a bifunctional linker with anchor group on an end, and it is followed by a second step involving reaction with a functional group on other end.[175, 180] The potential of click chemistry[181-184] as the second step in ZnO surface modification cannot be underestimated; however, the fact that the first step is carried out in a liquid phase does lead to ZnO surface etching even in most successful ZnO surface modification schemes.[175] A solution to this issue is presented in this chapter. A novel azido **DTBuPe** derivative (**DTBuPe-Ph-N3, 11**) was synthesized and bound via click chemistry (specifically via CuAAC) to a morphology preserving sensitization of ZnO nanorod surfaces. This two-step sensitization process is building on a recent finding by Teplyakov et al[185] and will be discussed in this chapter.

As discussed in Chapter A, one significant drawback for the application of perylene is its easy aggregation in solution and on surfaces due to the strong interaction of the π-system. Formation of excimer on the film would decrease the excited state energy level and compete with the desired HET process. In this chapter, we will describe the solution properties and binding of several 2,5-di-*tert*-butylperylene (**DTBuPe**) bridge-anchor derivatives to metal oxide surfaces (Figure C-2). By investigating their various photophysical properties and comparing with neutral perylene (**Pe**) and perylene-3-

carboxylic acid (**Pe-COOH**), the effects of *t*-butyl spacing groups and a variety of bridge units are probed.

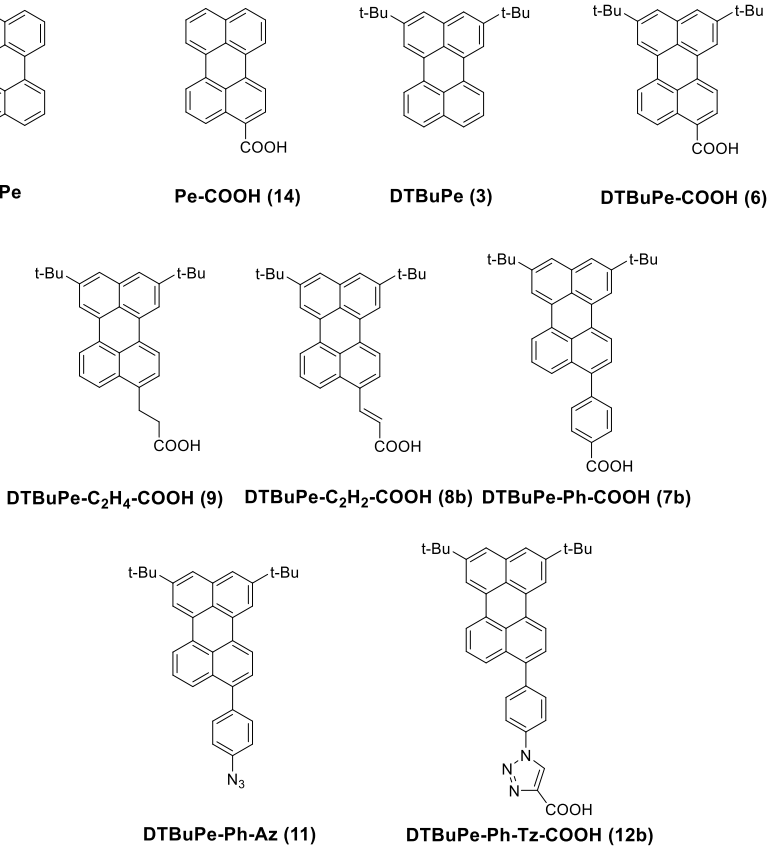

Figure C-2. Perylene and **DTBuPe**-bridge-anchor derivatives used in this study.

C.2 Results and discussion

C.2.1 UV-Vis Absorption and Fluorescence Emission Measurements in Solution

The absorption and emission of **DTBuPe** and **Pe** in MeCN solution are shown in Figure C-3. The 0-0 transition energies are estimated from the intersection of normalized absorption and emission spectra. From the spectra we notice that the absorption of the

two molecules are nearly identical, while the emission spectra of **DTBuPe** was slightly red-shifted by about 7 nm. Both spectra show very clear Franck–Condon progression. These results suggested that *t*-butyl groups only slightly influence the electronic properties of the perylene core.

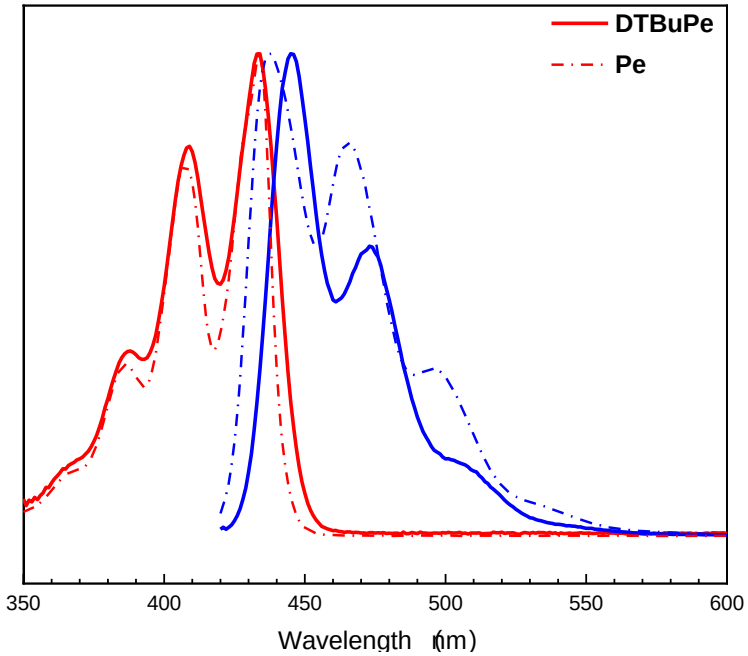

Figure C-3 Normalized absorption (red) and emission (blue) spectra of **Pe** (dash-dotted line) and **DTBuPe** (solid line) in 0.1 M CH_3CN. λ_{ex} = 410 nm.

The absorption and emission spectra of **DTBuPe**-bridge-anchor derivatives are shown in Figure C-4. The 0-0 transition energies are estimated from the intersection of normalized absorption and emission spectra and are listed in the Table C-1. All derivatives showed red-shift spectra when compared with **DTBuPe**. The spectra of derivatives **DTBuPe-COOH** and **DTBuPe-C_2H_4-COOH** show the characteristic spectrum of perylene and a small red-shift, indicating that, as expected, the electronically saturated bridge does not significantly alter the electronic properties of perylene. For derivative **8b** with the

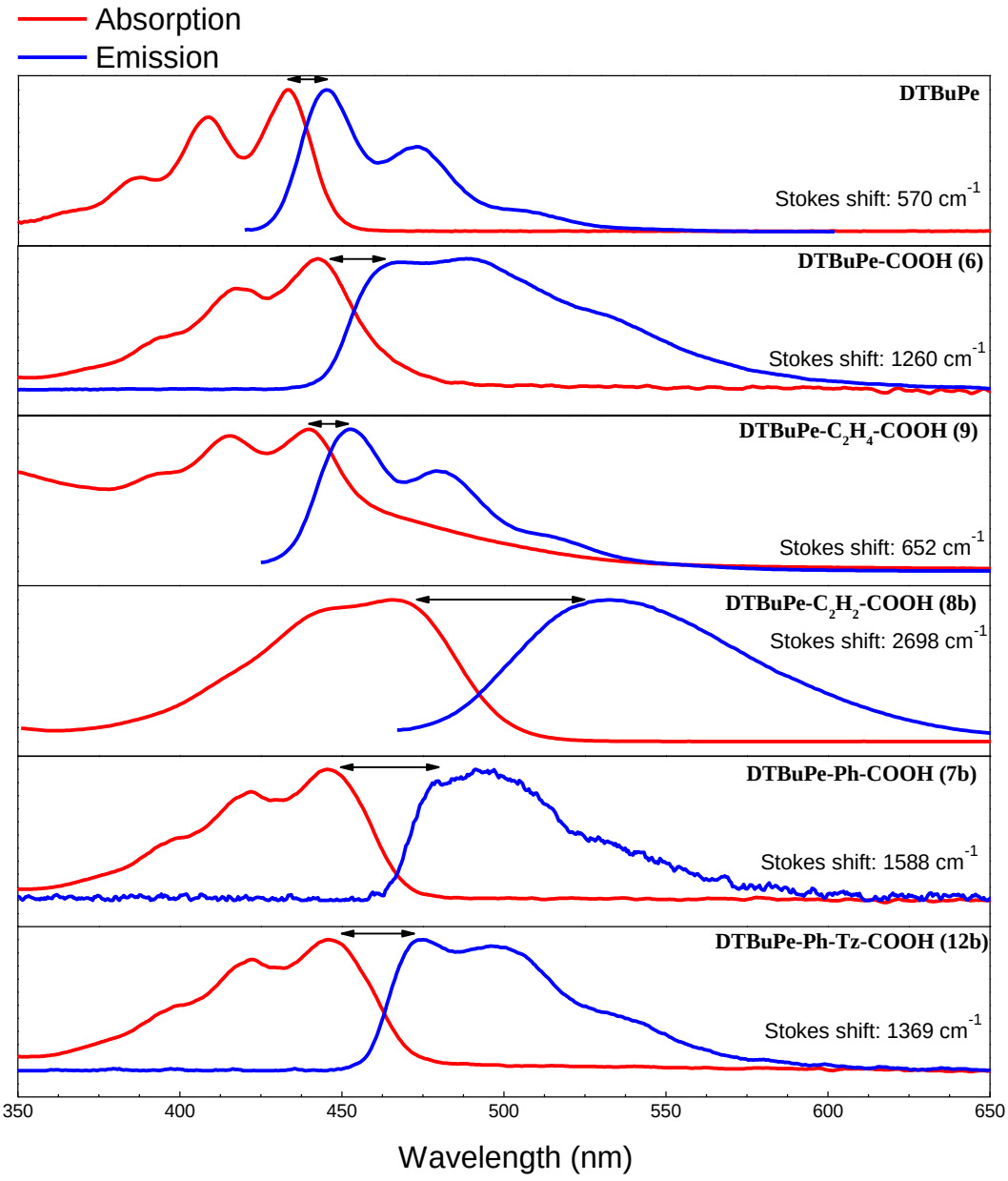

Figure C-4 Normalized UV-vis absorption (red) and emission (blue) spectra of DTBuPe derivatives in 0.1 mM CH_3CN solutions. $\lambda_{ex} = \lambda_{abs,max}$

conjugated ethylene bridge, a large red-shift (~30 nm) is observed. Moreover, the vibronic structure is almost washed out, and both absorption and emission band are significantly broadened. These results suggest that the unsaturated double bond is

strongly coupled with the perylene core; the excited wavefunctions spread into the bridge unit and form a larger delocalization system, results in a red-shift of the optical transition and bigger Stokes shift. Moreover, this expanded π-conjugation system may introduce new aggregation site and lead to dimer or excimer formation. DFT calculations (Figure C-4) are in good agreement with spectra, and indicate that the acrylic group is coplanar with the perylene core.

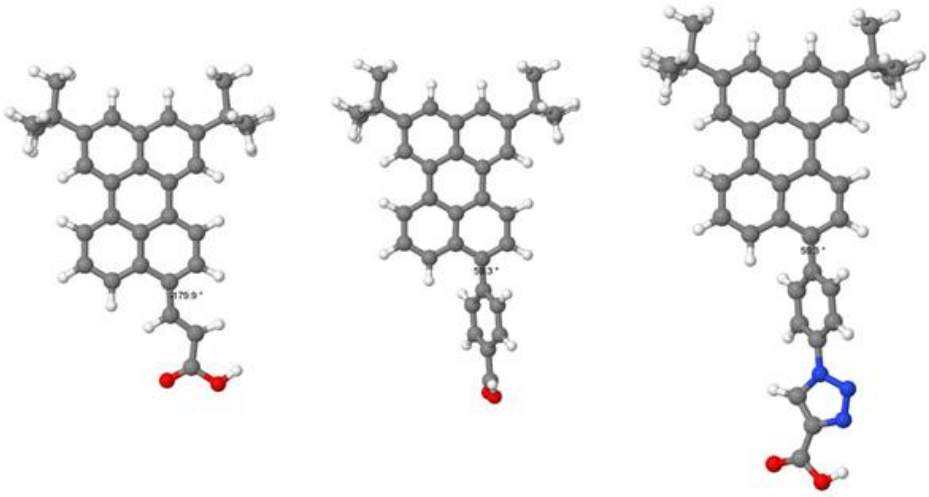

Figure C-5 Optimized ground state geometries of **8b** (**a**), **7b** (**b**) and **12b** (**c**). Calculated using Gaussian 16 with B3LYP pseudopotential and 6-311+g(d) basis set.

The absorption and emission spectra of derivatives **7b** and **12b**, which have an unsaturated phenyl ring connected to the perylene, are very similar to the spectra of **DTBuPe-COOH** and **9**. This similarity suggests that the π system of the phenyl ring is not strongly coupled with the π system of perylene. The calculation results (Figure C-5 (**b**) and (**c**)) are consistent with this observation, as both **7b** and **12b** show a 59.3° dihedral angle between the phenyl ring and perylene core, due to the hinderance between the

hydrogen atoms of phenyl ring and the H on C_{10} of perylene. Obviously, the electronic coupling between perylene and phenyl group would be disrupted by this conformation. Selected photophysical data of **Pe** and **DTBuPe** derivatives are reported in Table C-1.

Table C-1 Photophysical properties of **Pe** and **DTBuPe** derivatives in CH_3CN.

	$\lambda_{abs,max}$, nm	$\lambda_{em,max}$, nm	Stokes shift, cm^{-1}	0-0 transition energy, cm^{-1}
Pe	434	438	210	22,988
DTBuPe	434	445	570	22,779
DTBuPe-COOH, 6	443	468	1206	22,039
DTBuPe-Ph-COOH, 7b	446	480	1588	21,413
DTBuPe-C_2H_2-COOH, 8b	466	533	2698	20,325
DTBuPe-C_2H_4-COOH, 9	440	453	652	22,422
DTBuPe-Ph-Tz-COOH, 12b	446	475	1369	21,598

C.2.2 Binding of DTBuPe Bridge-Anchor Derivatives onto MO_2 Surfaces

All films used in this study were cast by "doctor blade" method on glass slides from nanostructured TiO_2 (E_{bg} = 3.2 eV) and from ZrO_2, an insulator (E_{bg} = 5 eV) with a morphology similar to TiO_2. Binding to metal oxide nanostructured thin films was done by immersing the films cast on glass substrates in 0.5 mM CH_3CN solutions of molecules. The functionalized films were rinsed with CH_3CN and dried under N_2 flow, then absorption, fluorescence and FT-IR-ATR spectra were collected.

C.2.2.1 Influence of *t*-Butyl Group

The binding study was first conducted on **Pe-COOH** and **DTBuPe-COOH (6)** to investigate the influence of the *t*-butyl substituents in preventing the aggregation of perylene on the nanostructured metal oxide film. The UV-vis absorption spectrum of the bare TiO_2/glass film (reference), **Pe-COOH** and **DTBuPe-COOH** bound TiO_2/glass are shown in Figure C-6.

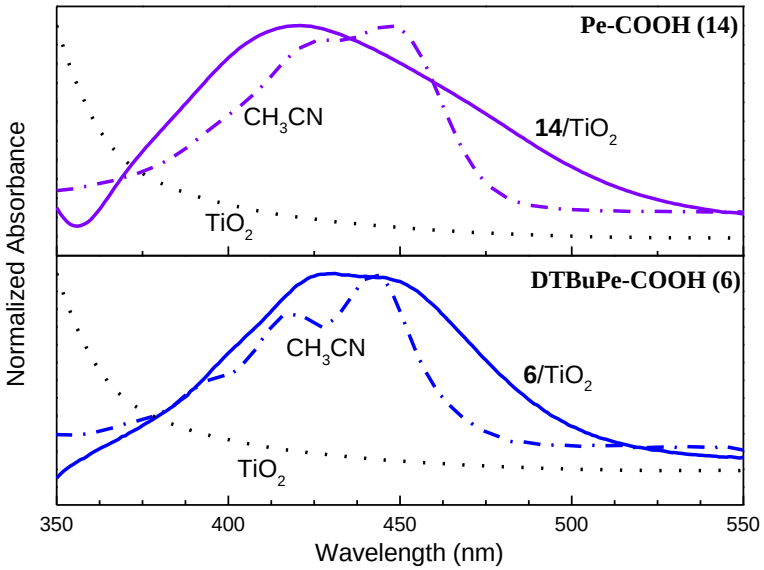

Figure C-6 Normalized absorption spectra of **Pe-COOH** (violet solid line) and **DTBuPe-COOH** (blue solid line) bound onto TiO_2 film in comparison to the normalized spectrum of **Pe-COOH** and **DTBuPe-COOH** in CH_3CN (dash-dotted line). Normalized absorption spectra of the TiO_2 film (black dotted line) is also included.

The spectrum of the reference TiO_2 films showed the fundamental absorption edge at 380 nm, corresponding to a band gap of 3.2 eV. Surface binding of **Pe-COOH** and **DTBuPe-COOH** onto TiO_2 nanoparticle films resulted in broadened spectra. The broadening of the absorption spectrum of **Pe-COOH** and **DTBuPe-COOH** upon binding to TiO_2 might be due to dye-TiO_2, dye-dye interactions or both[186]. Organic dyes strongly coupled to TiO_2 surfaces often display dye-to-particle charge-transfer (CT) absorption bands[187-188]. This direct $\pi \rightarrow$ conduction band transition could result in new absorption bands. Another source for the broadening in the absorption spectrum could be the mixing of the molecular state with the semiconductor states.[53] This mixing is induced by the

strong electronic coupling, resulting in a spread of the energy eigenvalues around the energy of the undisturbed molecular state. Moreover, the multiplicity of binding mode and orientations onto the nanoparticle surfaces is often invoked as an explanation for the broadening in the absorption spectrum.[189]

While the absorption of **DTBuPe-COOH** is slightly red-shifted, the spectrum of **Pe-COOH** shows a blue-shift, centered at 420 nm. This broad band is in good agreement with studies of perylene dimer in crystal[190] or perylene-doped LB films[103] and indicates the association of perylene dimers[190]. Strong coupling between the transition dipole moments of the perylene units in the dimers causes the singlet excited state of perylene to split into two exciton states.[191] A parallel alignment of transition dipole, which is also referred as H-aggregation, will allow the electronic transition from the ground state to the upper exciton state and result in a blue shift in the absorption spectra and an apparent enhancement of the higher-energy bands. On the other hand, J-aggregation, where transition dipole is in a head-to-tail alignment, allows the electronic transition from the ground state to the lower exciton state and leads to a red shift. Therefore, the absorption of bound **PeCOOH** indicated the formation of H-aggregation dimer.

Pe-COOH and **DTBuPe-COOH** were also bound to ZrO_2 films in similar conditions. Because of the wider band gap, ZrO_2 behaves as an insulator precluding electron injection from the lowest excited-state of perylene derivatives studied here (E_{bg} ~ 5 eV for ZrO_2 compared to ~ 3 eV for TiO_2). Study of the UV-vis absorption and emission spectrum of the bare ZrO_2/glass film (reference), **Pe-COOH**/ZrO_2 and **DTBuPe-COOH**/ZrO_2 are summarized in Figure C-7.

The overall binding behavior of **DTBuPe-COOH** and **Pe-COOH** to ZrO_2 surfaces is analogous to the binding measurements done on TiO_2 films. Both molecule show broadened absorption bands upon binding, and the absorption spectrum of **Pe-COOH**/ZrO2 shows a blue-shift due to aggregation. The background is due to the scattering of ZrO_2 nanoparticles, which were large in this particular sample since the absorption of ZrO_2 should occur below 250 nm.

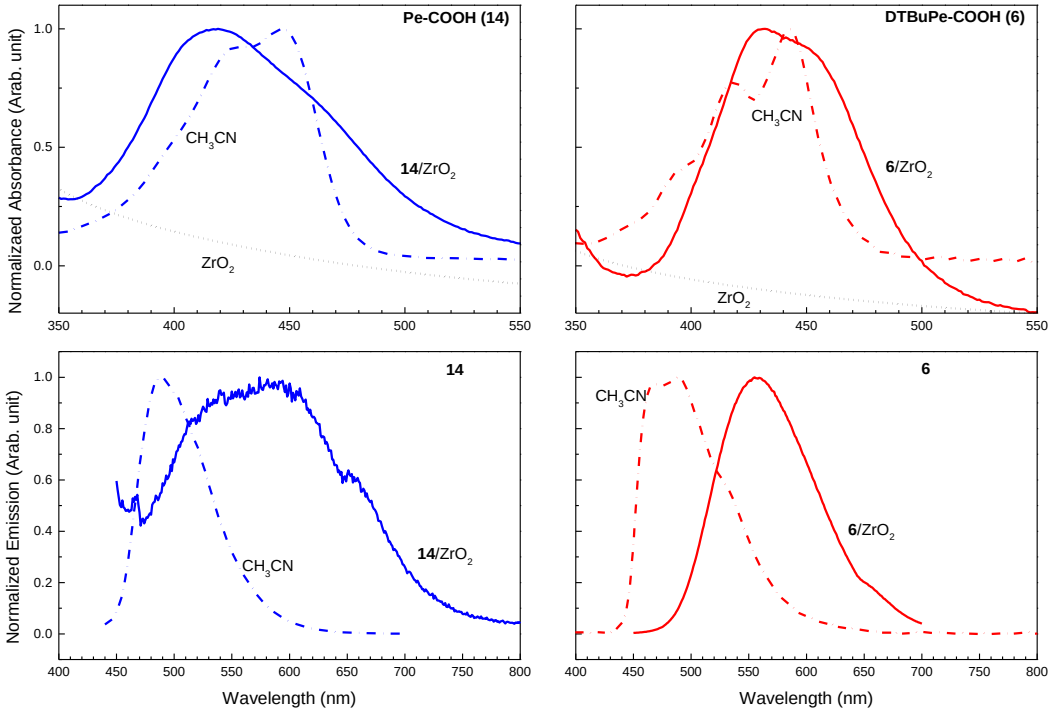

Figure C-7. Normalized difference steady-state absorption (top) and emission (bottom) spectra of **Pe-COOH**/ZrO_2 (blue solid line) and **DTBuPe-COOH**/ZrO_2 (red solid line). Non-normalized absorption spectrum of sensitized (dashed line) and pure (black dotted line) ZrO_2 film are also included. Normalized difference spectrum is shown in comparison with the normalized spectrum of **Pe-COOH** and **DTBuPe-COOH** in CH_3CN (dash-dotted line). λ_{ex} = 420 nm.

The fluorescence emission spectra of **DTBuPe-COOH**/ZrO_2 and **Pe-COOH**/ZrO_2 (Figure C-7 bottom) were significantly different from those observed in solution. The

emission spectrum of **Pe-COOH**/ZrO_2 exhibits a broad, red-shifted band that is characteristic of perylene excimer[192-193]. The fluorescence of **Pe-COOH**/ZrO_2 is also significantly quenched, when compared with **DTBuPe-COOH**/ZrO_2, as shown in Figure C-8. Both spectral changes are likely the effect of aggregation.

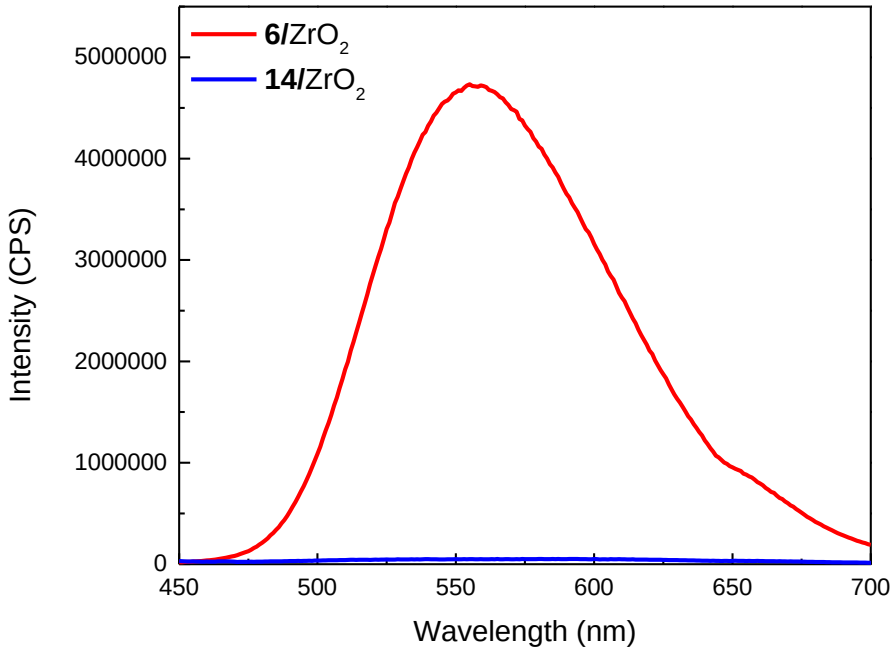

Figure C-8. Fluorescence spectra of **Pe-COOH**/ZrO_2 (blue) and **DTBuPe-COOH**/ZrO_2 (red).

The emission spectrum of **DTBuPe-COOH**/ZrO_2 is also red-shifted (555 nm) compared to the solution spectrum. However, the emission band is not significantly broadened and the fluorescence quenching is not as strong as **Pe-COOH**/ZrO_2, indicating that this red-shift is not caused by the aggregation of perylene. Similar red-shift of emission spectra have been reported for other dyes, for instance xanthene[188] and coumarin-343[187] bound to metal oxide semiconductors. Studies of Hupp et al. suggested

that binding a dye to a semiconductor surface may be accompanied by enough electronic interaction such that the locally excited (LE) state of the dye mix with the semiconductor states, resulting in a spread of the energy and a red-shift of emission spectrum. As shown in the calculation result of **DTBuPe-COOH** (Figure C-9), the LUMO wavefunction extends into the anchor group, and can result in a strong electronic coupling between the excited states of **DTBuPe-COOH** and the ZrO_2 acceptor states. Therefore, we conclude that the fluorescence behavior of **DTBuPe-COOH** on ZrO_2 film is influenced by the coupling between the molecular excited states and the semiconductor states, and that the *t*-butyl spacing groups on **DTBuPe-COOH** can efficiently prevent the aggregation of perylene on semiconductor films and quenching of the excited state.

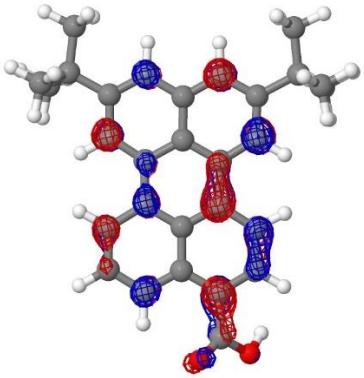

Figure C-9. LUMO of **DTBuPe-COOH**. Calculated using Gaussian 16 with B3LYP pseudopotential and 6-311+g(d) basis set.

The binding mode of **Pe-COOH** and **DTBuPe-COOH** to TiO_2 and ZrO_2 films through the COOH anchoring groups was characterized by FT-IR-ATR. IR spectra of **DTBuPe-COOH**/TiO_2 and **DTBuPe-COOH**/ZrO_2 compared to the neat compounds is shown in Figure C-10. The neat **DTBuPe-COOH** shows an intense asymmetric stretch $\nu_{(C=O)}$ at 1674 cm^{-1} that is typical of the carbonyl group in carboxylic acids. Upon binding, this

band is replaced by low-energy, broad bands from 1340 to 1600 cm^{-1} on TiO_2 and ZrO_2 films. The coordination of the COO^- group to metal cations was studied by the energy

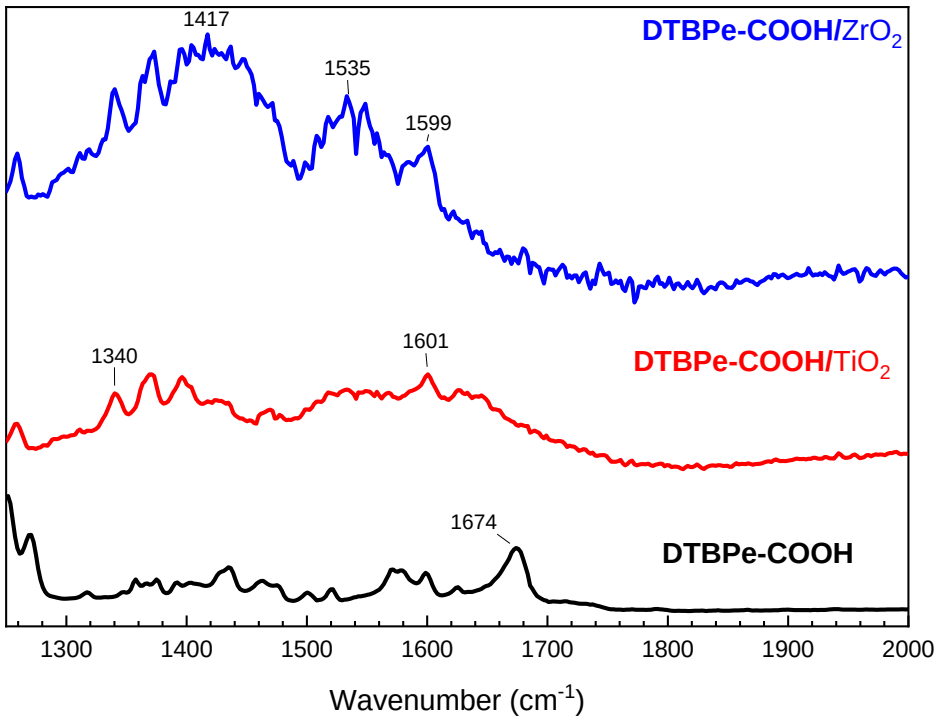

Figure C-10 FT-IR-ATR spectra of **DTBuPe-COOH** (black), **DTBuPe-COOH**/TiO_2 (red) and **DTBuPe-COOH**/ZrO_2 (blue).

splitting of antisymmetric $\upsilon_{as}(COO^-)$ and symmetric $\upsilon_s(COO^-)$ stretching vibrations.[194-195] Bauer et al. observed two peaks at 1615 cm^{-1} and 1350 cm^{-1} for the black dye bound to TiO_2, which were assigned to $\upsilon_{as}(COO^-)$ and $\upsilon_s(COO^-)$, respectively. Another study by Dobson and McQuillan measured the IR spectra of several aromatic carboxylate acid bound to TiO_2.[196] According to their results, the $\upsilon_{as}(COO^-)$ was observed at about 1550 cm^{-1} and the $\upsilon_s(COO^-)$ was assigned to bands at 1370 cm^{-1}. Therefore, the broad band between 1340 to 1600 cm^{-1} can be assigned to the presence of both $\upsilon_{as}(COO^-)$ and

$\upsilon_s(COO^-)$ stretching on **DTBuPe-COOH**/MO_n films, consistent with the bi-dentate bridging geometry (see Section **A.2.2.1**, Figure A-8).

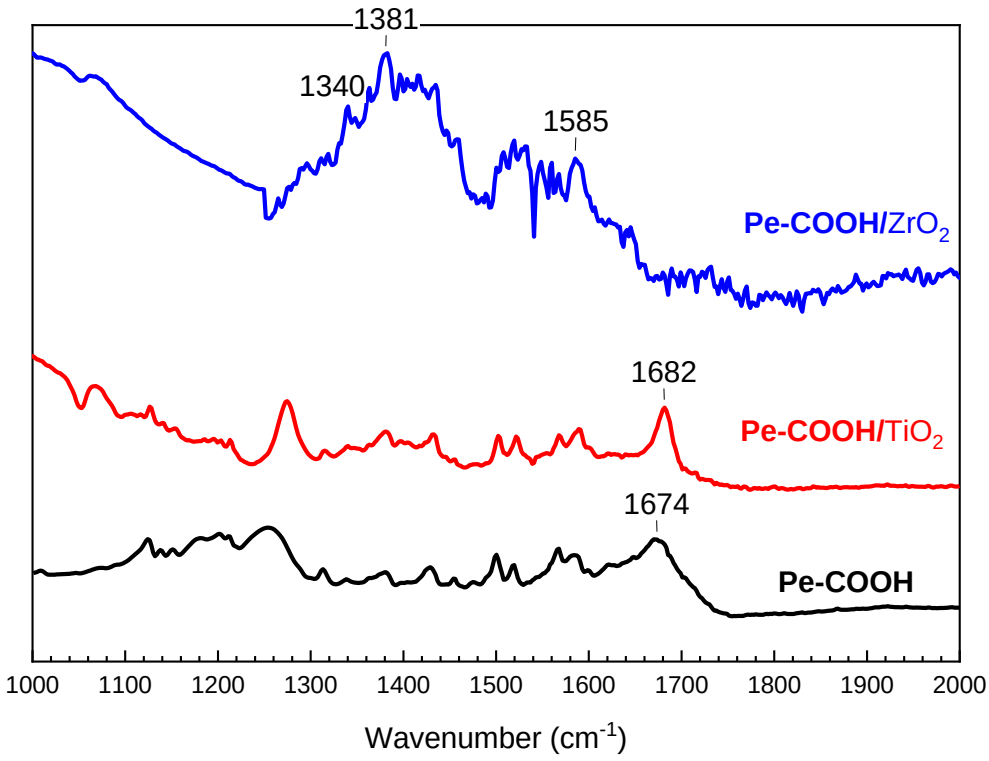

Figure C-11. FT-IR-ATR spectra of **PeCOOH** (black), **PeCOOH**/TiO_2 (red) and **PeCOOH**/ZrO_2 (blue).

FT-IR-ATR spectra of **Pe-COOH**/TiO_2 and **Pe-COOH**/ZrO_2 comparing to neat compounds in the range of 1000 to 2000 cm^{-1} is shown in Figure C-11. **Pe-COOH** shows similar IR features on ZrO_2 as **DTBuPe-COOH**: the $\nu_{(C=O)}$ asymmetric stretch at 1674 cm^{-1} disappeared, and is replaced by broad bands (1340 - 1585 cm^{-1}), consistent with a bi-dentate binding geometry. Surprisingly, **Pe-COOH**/TiO_2 showed nearly identical IR spectra as neat **Pe-COOH**, even after thoroughly rinsing the film with CH_3CN to remove any weakly physiosorbed dye on the film, or after repeating the binding on different TiO_2 films. The reason for this behavior is unclear. We suggest that it may involve the

aggregation of **Pe-COOH** on the surface: free **Pe-COOH** molecules may aggregate with bound **Pe-COOH** and then remain trapped onto the film. However, this cannot explain the binding behavior of **Pe-COOH** on ZrO_2.

In conclusion, **Pe-COOH** and **DTBuPe-COOH** were bound to nanostructured TiO_2 and ZrO_2 films and were investigated by UV-vis, fluorescence and FT-IR-ATR spectroscopy. The absorption and emission spectra of **Pe-COOH**/MO_n showed clear evidence of aggregation on the film. Spectra of **DTBuPe-COOH/**MO_n showed some difference from neat **DTBuPe-COOH**; Similar changes are often observed when dyes are bound to the surface of semiconductors. This is often related to a combination of factors, for instance electronic coupling with the surface, heterogenicity of binding modes, formation of aggregates, and other factors. These results indicate that *t*-butyl groups on **DTBuPe-COOH** can efficiently prevent the aggregation of perylene on semiconductor films and prevent quenching of the excited state. FT-IR-ATR spectra suggest that **DTBuPe-COOH** was bound to semiconductor films via a bi-dentate geometry; However, **Pe-COOH** shows different binding behavior on TiO_2 and ZrO_2 films. The reason of this phenomenon is unclear, but a possible explanation is that it is related to the aggregation of unsubstituted perylene on semiconductor films.

C.2.2.2 Influence of Bridge Units

Two **DTBuPe** bridge-anchor derivatives were bound to TiO_2 and ZrO_2 films to investigate the influence of the nature of the bridge units. We select **DTBuPe-C_2H_4-COOH** (**9)** and **DTBuPe-Ph-COOH** (**7b)** to investigate the effect of a flexible bridge and a rigid bridge, respectively. The two molecules were bound to TiO_2 using the usual procedure. Their absorption spectra, in solution and bound, are shown in Figure C-12.

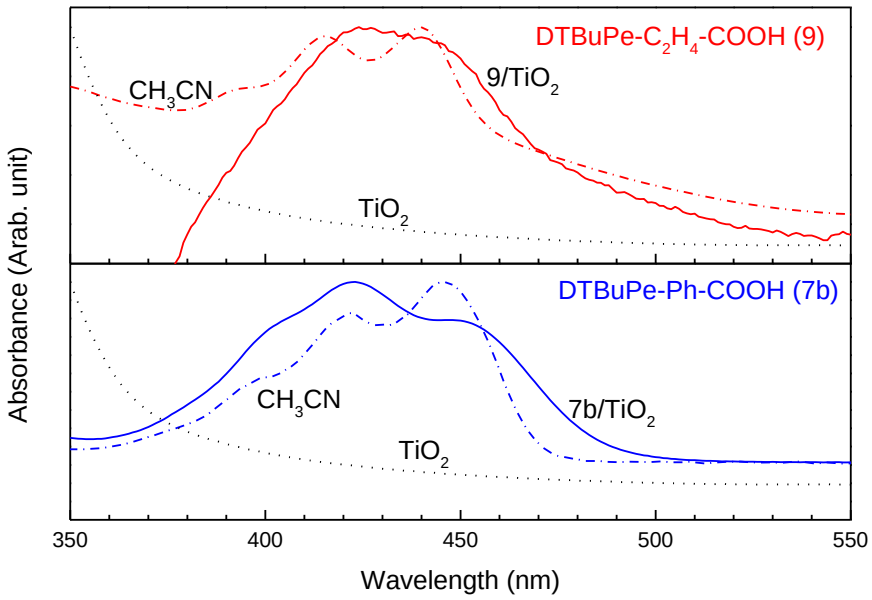

Figure C-12 Normalized absorption spectra of **DTBuPe-C_2H_4-COOH**/TiO_2 (red solid line) and **DTBuPe-Ph-COOH**/TiO_2 (blue solid line) compared to the absorption in solution (dash-dotted line, in CH_3CN), and the TiO_2 film (black dotted line).

The absorption of both **DTBuPe-C_2H_4-COOH** -sensitized TiO_2 and ZrO_2 film was much weaker compared with films sensitized with other **DTBuPe** bridge-anchor derivatives, even after extending the binding time to 16 h. It should be noted that the ethylenic bridge in **DTBuPe-C_2H_4-COOH** is flexible. Therefore, it is possible that **DTBuPe-C_2H_4-COOH** exhibits a broad distribution of binding geometries on semiconductor surfaces. In addition, *t*-butyl groups would prevent the intermolecular interaction between the dyes, which is likely to prevent the formation of a closed packed molecular layer on the surface.

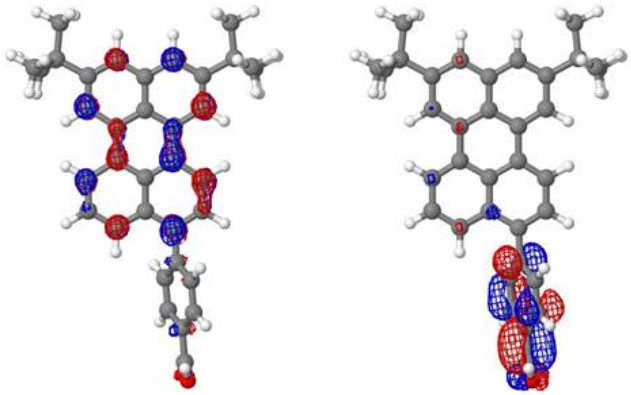

Figure C-13. LUMO (**a**) and LUMO+1 (**b**) of **DTBuPe-Ph-COOH**. Wavefunctions are calculated using Gaussian 16 with B3LYP on a B3LYP optimized geometry.

The absorption spectrum of **DTBuPe-C_2H_4-COOH**/TiO_2 shows similar features as the **DTBuPe-COOH**/TiO_2 (Figure C-6): significant broadening and a slight red-shift. Conversely, the absorption spectrum of **DTBuPe-Ph-COOH**/TiO_2 shows different features. Only a slight broadening of the band was observed, and the vibrational structure remains. It should be also noted that the S0-S2 transition becomes the dominating process in the absorption. A possible explanation is that the LUMO+1 wavefunction of **DTBuPe-Ph-COOH** has more extension to the bridge and anchor, which leads to a stronger coupling between dyes and semiconductor states. Therefore, this transition becomes more favored in the excitation process. This is visualized in Figure C-13.

DTBuPe-C_2H_4-COOH and **DTBuPe-Ph-COOH** were also bound to ZrO_2 film. The UV-vis absorption and emission spectra of the ZrO_2/glass film (reference) and **DTBuPe-Ph-COOH**/ZrO_2 are shown in Figure C-14. The absorption of **DTBuPe-C_2H_4-COOH**/ZrO_2 was very weak due to the low surface coverage, and was overwhelmed by

the scattering of ZrO_2 nanoparticles. The absorption spectrum of **DTBuPe-Ph-COOH**/ZrO_2 is qualitatively equivalent to its spectrum on TiO_2.

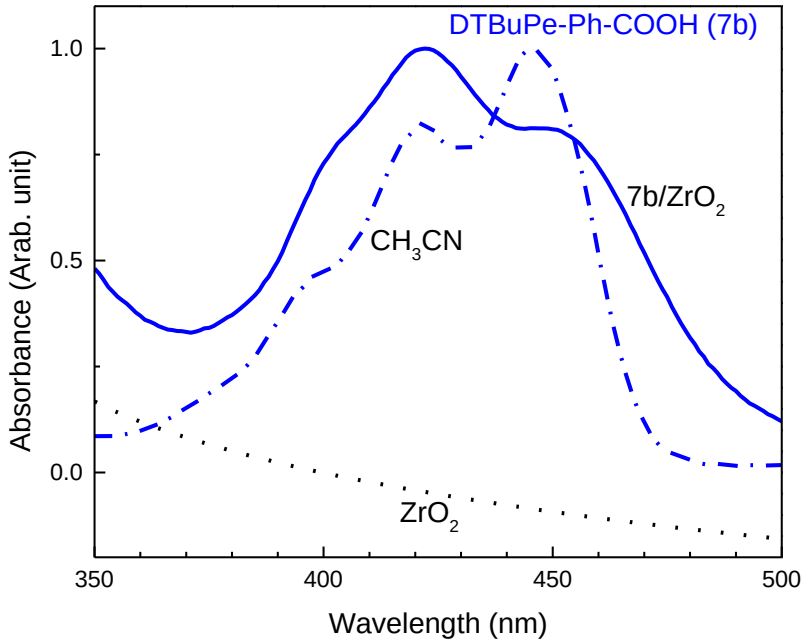

Figure C-14 Normalized absorption spectrum of **DTBuPe-Ph-COOH**/ZrO_2 (blue solid line) compared with the solution spectrum in CH_3CN (blue dash-dotted line). Absorption spectra of sensitized (blue dash line) and pure ZrO_2 film (black dotted line) are also included.

The fluorescence emission spectra of **DTBuPe-C_2H_4-COOH**/ZrO_2 and **DTBuPe-Ph-COOH**/ZrO_2 are shown in Figure C-15. Both compounds exhibit slightly red-shifted and broadened emission band. As compared with the emission spectrum of **DTBuPe-COOH**/ZrO_2 (Figure C-6), the red-shift of **DTBuPe-C_2H_4-COOH** and **DTBuPe-Ph-COOH** are much weaker. As we discussed in Section **C.2.2.1**, the red-shift of the emission spectrum of **DTBuPe-COOH**/ZrO_2 could be related to the strong electronic coupling between **DTBuPe-COOH** and ZrO_2. Therefore, this weakened red-shift can be

a clear reflection of the obvious reduction of the electronic coupling, which was introduced by the bridge units. In both cases, the emission bands of possible perylene excimers are not observed, indicating that the aggregation is prevented by the *t*-butyl groups.

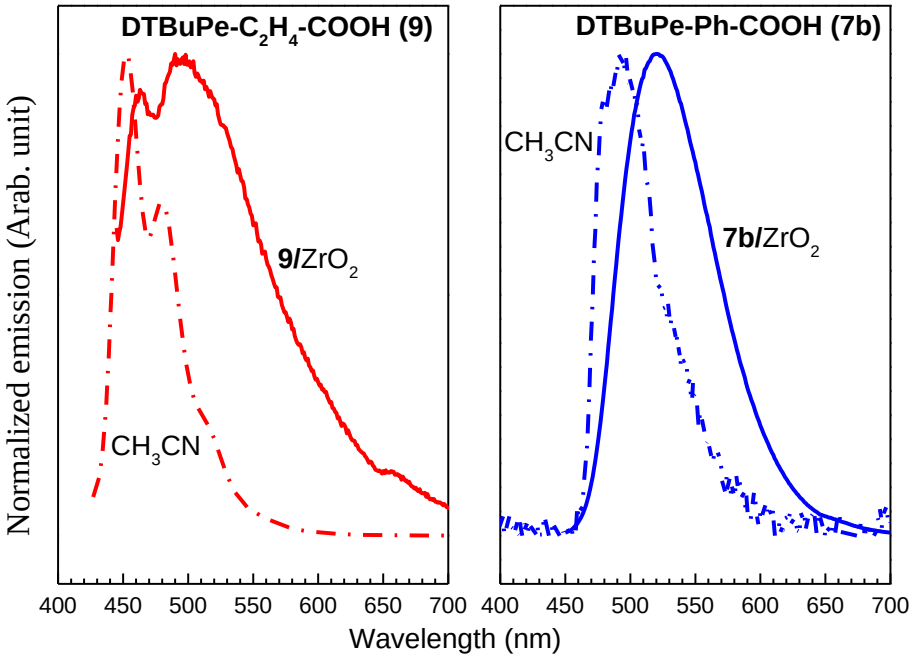

Figure C-15. Normalized emission spectra of **DTBuPe-C$_2$H$_4$-COOH**/ZrO$_2$ (red solid line) and **DTBuPe-Ph-COOH**/ZnO$_2$ (blue solid line) compared with their emission spectra in CH$_3$CN (dash-dotted line). λ_{ex} = 425 nm

FT-IR-ATR spectroscopy was also performed to investigate the binding configuration of **DTBuPe-C$_2$H$_4$-COOH** and **DTBuPe-Ph-COOH** on nanostructured semiconductor films. IR data of **DTBuPe-C$_2$H$_4$-COOH**/MO$_n$ and **DTBuPe-Ph-COOH**/MO$_n$ compared to non-bound molecules in the range of 1250 to 2000 cm^{-1} is shown in Figure C-16.

The FT-IR-ATR spectra of **DTBuPe-Ph-COOH**/MO$_n$ and **DTBuPe-C$_2$H$_4$-COOH**/MO$_n$ show similar features as the **DTBuPe-COOH**/MO$_n$ (Figure C-10):

asymmetric stretch $\nu_{(C=O)}$ of COOH at ~1680 cm^{-1} disappeared and broad bands from 1340 to 1600 cm^{-1}, assigned to $\upsilon_{as}(COO^-)$ and $\upsilon_s(COO^-)$, formed upon binding. These results indicate that both **DTBuPe-Ph-COOH** and **DTBuPe-C_2H_4-COOH** are bound to nanostructured semiconductor films via bi-dentate geometry.

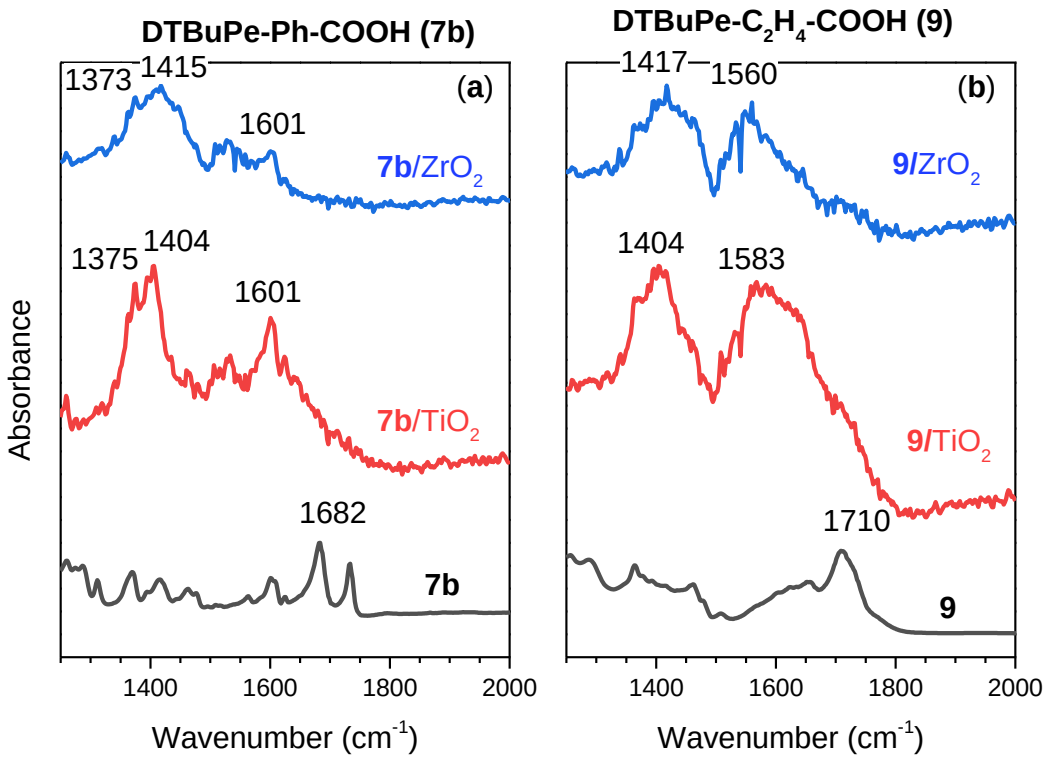

Figure C-16 FT-IR-ATR spectra of **DTBuPe-Ph-COOH**/MO_n (**a**) and **DTBuPe-C_2H_4-COOH**/MO_n (**b**).

In summary, **DTBuPe-C_2H_4-COOH** and **DTBuPe-Ph-COOH** were bound to nanostructured TiO_2 and ZrO_2 films and were investigated by UV-vis, fluorescence and FT-IR-ATR spectroscopy. Qualitatively, **DTBuPe-C_2H_4-COOH** exhibited a lower surface coverage during binding compared with other DTBuPe-bridge-anchor derivatives. We believe it is related to the flexibility of the ethylenic bridge. The emission spectra of **DTBuPe-C_2H_4-COOH**/ZnO_2 and **DTBuPe-Ph-COOH**/ZnO_2 showed a weakened red-

shift comparing with **DTBuPe-COOH**/ZrO_2. FT-IR-ATR spectra showed that both **DTBuPe-C_2H_4-COOH** and **DTBuPe-Ph-COOH** were bound to semiconductor films via bi-dentate geometry.

C.2.3 Morphology Preserving Sensitization of ZnO Nanorod Surfaces via Click-Chemistry

This work is a collaboration with Prof. Andrew. Teplyakov's research group and Prof. Lars Gundluch's research group at the University of Delaware, Department of Chemistry and Biochemistry. ZnO nanorods were prepared by Ms. Zhengxin Li and sensitized by Mr. Chuan He. Transient absorption (TA) measurements were run by Mr. Baxter Abraham.

The objective is to develop a novel pathway to functionalize highly ordered ZnO nanoparticle films without etching the morphology. Highly ordered morphologies are advantageous in many electronic applications and fundamental interfacial charge transfer studies where it is important to control the binding models and the sensitization process. However, the fact that ZnO is etched by the acidic anchor groups such as COOH greatly limits its applicability,[173-175] and leads to the formation of zincate salts during chemical modification steps that may deposit onto the surface. Therefore, carefully designed chemical modification of ZnO nanostructures can yield well-defined interfaces and interpretable measurements of HET.

C.2.3.1 Modification of ZnO Nanorod

The ZnO nanorod sample was modified via a two-step process. In the first step, the clean ZnO surface was functionalized and passivated by chemisorption of propiolic acid (HC≡C-COOH) from gas phase. This step results in a well-defined attachment of the

COOH anchor group, with only a single type of surface carboxylate, as supported by the IR spectroscopy, XPS, and solid-state NMR studies.[185] This leaves the ethyne unit ready to react via click chemistry, allowing subsequent attachment of sensitizers. More importantly, the gas phase functionalization in the first step preserves the surface morphology and protects the surface of the nanostructured ZnO material, so that the click chemistry in the second step can be performed in liquid phase. A solution vs gas phase binding comparison was made by exposing ZnO nanorod films to a propiolic acid solution (1 mM in THF).

The second step is the copper-catalyzed click reaction (CuAAC) of the alkyne functionality with the azido-substituted perylene dye, 9-(4-azidophenyl)-2,5-di-tert-butylperylene (**DTBuPe-Ph-N3**) in the presence of a Cu(I) catalyst (copper(I) acetate, 24 h, 40°C, Ar atmosphere). A comparison was made by binding a solution (1 mM solution in THF) of the expected surface click product, 1-(4-(8,11-di-*tert*-butylperylen-3-yl)-phenyl)-1H-1,2,3-triazole-4-carboxylic acid (**DTBuPe-Ph-Tz-COOH**), which was synthesized independently. (See Section B.4, Scheme B-14) The comparisons are summarized in Figure C-17.

C.2.3.1 Characterization of ZnO Nanorods

The morphology of ZnO nanorods was characterized by scanning electron microscopy (SEM) and X-ray photoelectron spectroscopy (XPS) which were also employed to detect the presence of N following the binding. Characterization of several key steps is illustrated in Figure C-18.

Figure C-18a shows the characterization of the unsubstituted ZnO nanorod film. No surface nitrogen is observed from XPS and the SEM shows a top view of the ZnO

nanowires. After the gas-phase reaction with propiolic acid, this morphology is obviously preserved, as shown in the SEM image (Figure C-18b). After that, the resulting ethyne-functionalized surface reacted with **DTBuPe-Ph-N3** in the presence of a Cu(I) catalyst

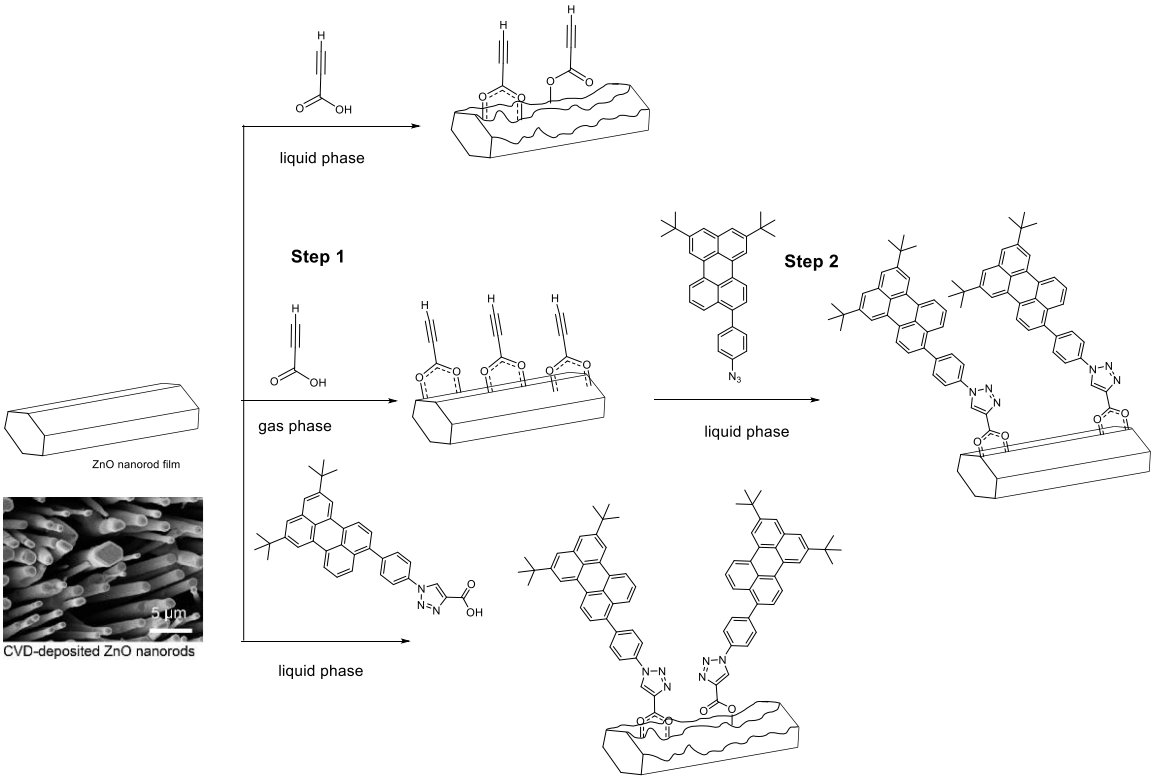

Figure C-17. Schematic representation of the reaction pathways designed to functionalize ZnO nanostructures. Reprinted with permission from ref[107]. Copyright (2018) American Chemical Society.

(copper (I) acetate, 24 h, 40°C under Ar atmosphere) in THF. Figure C-18c shows the characterization of the functionalized film and the intact morphology. In addition, XPS shows the presence of nitrogen (Figure C-18c). Consistent with triazole formation, a strong and broad peak around 401 eV can be identified, which was discerned into three peaks attributed to the triazole ring. In contrast, exposing ZnO nanorod films to propiolic

acid solution at room temperature (1 mM, THF, 30 mins) resulted in significant etching, as shown in Figure C-18d. Similarly, solution binding of **DTB-Ph-Tz-COOH** to ZnO nanorods (1 mM, THF, 30 min) leads to surface etching (Figure C-18e). The chemical attachment or physisorption of DTB-Ph-Tz-COOH to ZnO nanorods does occur, as XPS spectrum also shows a similar N 1s signature (Figure C-18e), although the intensity of the observed feature is much smaller compared to that in the spectrum in Figure C-18c.

It should be noted that solution binding conditions are widely employed in the sensitization of other metal oxides semiconductor films, for instance TiO_2 and ZrO_2. However, it is not obvious what the surface species formed in liquid phase sensitization really are, since the reaction clearly results in a nearly complete destruction of the nanorods. In order to address these concerns, a set of ultrafast measurements were performed and compared for the differently prepared samples.

It is well known that the photoexcitation of perylene dyes bound to TiO_2 or ZnO leads to interfacial electron transfer into the semiconductor conduction band. For perylene-based sensitizers with similar anchor groups, electron transfer of about 100-200 ~ fs time scales have been observed.[79, 95-96] However, strong electronic coupling between molecular donor and semiconductor acceptor state is mandatory for this ultrafast heterogeneous electron transfer, which requires in general chemisorption on the surface, rather than physisorption. To investigate such electronic coupling, pump/white-light probe transient absorption (TA) is employed to measure the population dynamics of excited state and the formation of the cation. These experiments were carried out in Prof. Lars Gundlach's lab

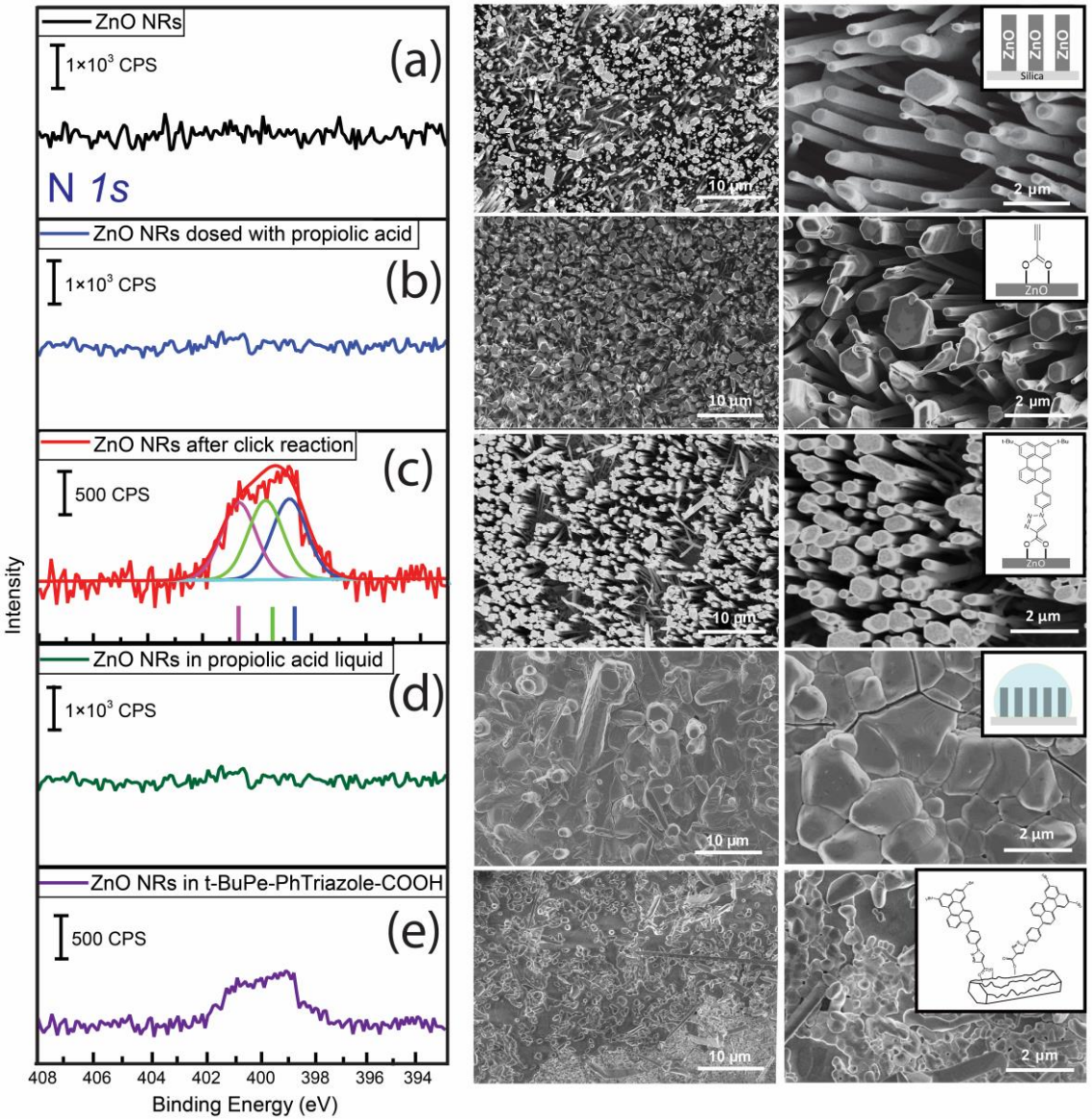

Figure C-18. XPS spectra (left column), SEM images (middle column) and enlarged SEM images (right column) of the chemical modification steps for ZnO nanorod functionalization. Reprinted with permission from ref[107]. Copyright (2018) American Chemical Society.

Kinetic traces have been extracted from TA maps at 725 nm and are compared in Figure C-19. This wavelength was referred to the absorption of the excited state of perylene, as shown in **Figure A-13**. It can be clearly seen that a long-lived contribution is present in the sensitized film, and fitted curve indicated a life-time of around 200 fs. The

spectral position agrees with that of the excited state of perylene and the lifetime (HET time) agrees well with those measured for perylene molecules with similar linker.[79] The rapid disappearance of the excited state signal indicates fast electron injection into ZnO and hence strong electronic coupling between the molecular donor state and the ZnO conduction band acceptor states. Weakly bound molecules, on the other hand, would show much slower HET. TA measurements have also been performed on the liquid phase sensitized ZnO film (Figure C-19) that resulted from direct exposure to **DTB-Ph-Tz-COOH** solution. Transients at the excited state absorption wavelength showed, as expected, slower and unclear decay pathway, and can be assigned to the weakly bound residues on the etched film.

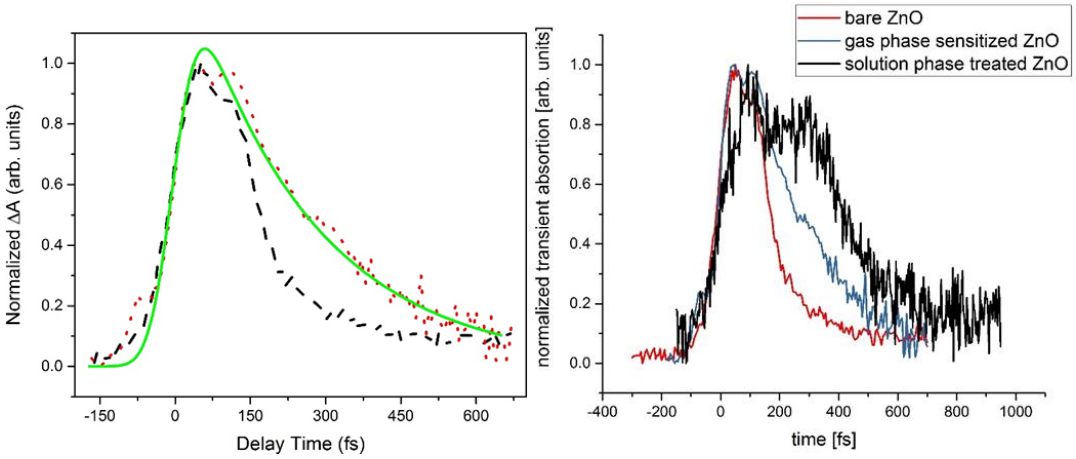

Figure C-19. Left: Comparison of excited state decay for bare ZnO (black dashed) and two-step sensitized ZnO (red dotted) together with a fit with a rate model (green solid). Right: Comparison of bare ZnO, two-step sensitized ZnO, and liquid phase sensitized ZnO. Reprinted with permission from ref[107]. Copyright (2018) American Chemical Society.

C.3 Conclusions

A series of DTBuPe bridge-anchor derivatives were studied both in solution and on nanostructured TiO_2, ZrO_2 and ZnO films. By probing their photophysical properties and comparing with neat **Pe** and **Pe-COOH**, we investigated the influence of *t*-butyl group and different bridge units. The emission spectra of sensitized ZrO_2 film indicate that *t*-butyl spacing groups on **DTBuPe** unit can efficiently prevent the aggregation of perylene on semiconductor films. A comparison of the spectra of **DTBuPe-COOH**, **DTBuPe-C_2H_4-COOH** and **DTBuPe-Ph-COOH** suggests that bridge units influence intersurface electronic coupling, binding mode and surface coverage. A low surface coverage was observed during the sensitization of **DTBuPe-C_2H_4-COOH**, suggesting that a short flexible bridge may be a drawback for the formation of a compact molecular layer on semiconductor films. FT-IR-ATR spectra of sensitized TiO_2 and ZrO_2 film show that **DTBuPe-COOH**, **DTBuPe-C_2H_4-COOH** and **DTBuPe-Ph-COOH** are all bind to semiconductor films via bi-dentate geometry. However, **Pe-COOH** showed different binding configuration on TiO_2 and we believe it is may be related to the aggregation on the surface.

Moreover, a specially designed azide substituted **DTBuPe** derivative was also employed to investigate a new two-step functionalization pathway for nanostructured ZnO. XPS and SEM characterization (Teplyakov group) confirm that large dye molecule like **DTBuPe** can be successfully immobilized to the film via click reaction without disturbing the morphology of ZnO nanoparticles. Pump/white-light probe transient absorption (Gundlach group) also proves that a strong electronic coupling was obtained using this two-step sensitization. This new functionalization pathway is especially useful

on ZnO, but it could be extended to other semiconductors (TiO_2) for reliable and useful measurements of HET process.

C.4 Experimental section

C.4.1 Materials

Isopropanol (Pharmco HPLC grade), methanol (Fisher HPLC grade), acetonitrile (Pharmco HPLC grade), titanium(IV) isopropoxide (Aldrich), zirconium(IV) isopropoxide (70% in 1-propanol, Aldrich), nitric acid (Fisher ACS grade), deionized ultra filtered (DIUF) water (Fisher) and poly(ethylene glycol) (av. Mol. Wt. 2000, Aldrich) were all used as received.

C.4.2 Synthesis of Nanostructured TiO_2

Sol-gel preparation of TiO_2 nanoparticles followed the hydrolysis and condensation of titanium(IV) isopropoxide in an aqueous nitric acid solution. A three-necked round bottom flask was set up with a thermometer, addition funnel in the middle neck and Dean-Stark apparatus, Figure C-20. The round bottom flask contained a solution of 100 ml water containing 0.69 mL of concentrated nitric acid (68 – 70 %). The addition funnel contained titanium(IV) isopropoxide (20 mL in isopropanol, 80mL). Both the aqueous and the alkoxide solution were deaerated with nitrogen for at least 10min prior to the addition. The acidic solution was rigorously stirred using a magnetic stirrer and in the meantime the alkoxide solution was added through the dropping funnel at a rate not faster than one drop per second. The additions lead to an immediate formation of a white precipitate in the round bottom flask, indicating the hydrolysis to TiO_2.

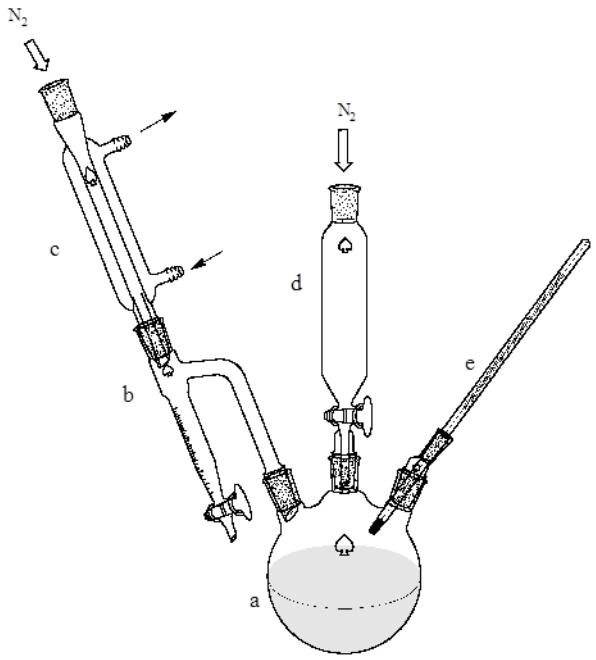

Figure C-20. Setup for the hydrolysis and condensation of titanium(IV) isopropoxide.

After all the titanium(IV) isopropoxide solution was consumed and the hydrolysis was complete, changes in the setup have to be made: the addition funnel is removed, and the Dean-Stark apparatus and the flask should be covered by aluminum foil or glass wool. The insulation is necessary during the following distillation. The isopropanol needs to be removed from the aqueous solution and can be collected as isopropanol/water mixture of approximately 130 mL at a temperature range of 86-95 °C. The distillation has to be terminated as soon as the distillate reaches 100 °C, indicating that only water remains in the solution. At this point the apparatus is reduced to the three-neck round bottom flask with a condenser in the middle. The reaction mixture remains overnight to reflux. Following the reflux also the condenser is removed and the reaction volume is reduced to 45 mL by allowing the water to evaporate. The reaction mixture was allowed to cool down, and sonicated for 5 min, and transferred to the glass beaker with a magnetic

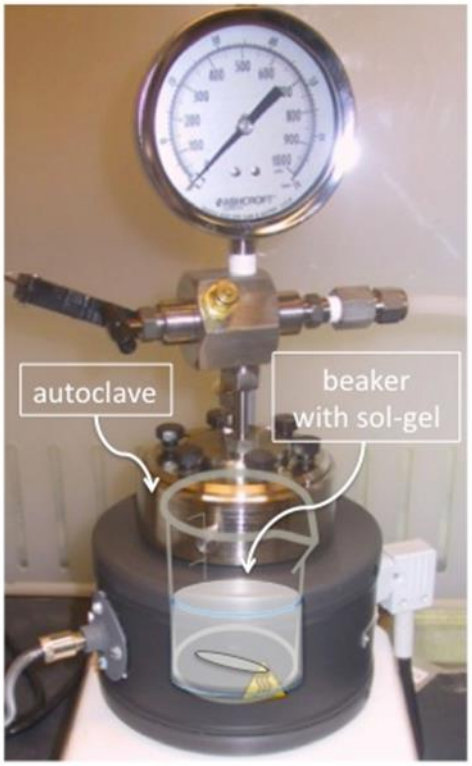

Figure C-21. Setup for the titanium autoclave

stirring rod belonging to the titanium autoclave (Figure C-21). The titanium autoclave (Model 4760, Parr) is programmed to heat the sol gel at 200 °C for 12 hours at a pressure reaching 17-18 bar. The white sol-gel was cooled to room temperature, sonicated (5 min), and transferred from the autoclave beaker to a graduated beaker. At this point the TiO_2 concentration in the gel was determined by the 'glass dies' method. The method involves weighing a small amount of sol-gel on a glass slide before and after drying the gel at 100 °C to remove the containing water. The difference determines the wt. % of TiO_2 in the sol-gel. The concentration should be in a range of 13-17 wt % in order to be processed. Poly(ethylene glycol) (PEG 2,000; amount: 6 g/L) was added to the colloid to

yield a white viscous paste and the mixture was stirred for at least 72 h to reach a good homogeneity for the casting of TiO_2 paste on a substrate.

C.4.3 Synthesis of Nanostructured ZrO_2

Sol-gel synthesis of ZrO_2 nanoparticles is very similar to the TiO_2 nanoparticles synthesis. A three-necked round bottom flask was set up with a thermometer, dropping funnel and Dean-Stark apparatus. To the round bottom flask containing 100 mL solution of water containing 0.69 ml conc. HNO_3 (68 – 70 %) a 20 mL solution of 70 % zirconium(IV) isopropoxide and 80 mL of isopropanol was added drop wise through a dropping funnel under nitrogen atmosphere and stirred vigorously. The slow mixing of the two solutions leads to a fast formation of white precipitate of the zirconia dioxide nanoparticles. After the addition step, the reaction mixture was brought to reflux and ca. 140 ml of isopropanol-water mixture were collected by distillation. Unnecessary equipment, Dean-Stark apparatus and the dropping funnel were removed from the set up and the condenser was moved to the middle neck of the flask. The reaction was allowed to reflux overnight. Following reflux, the water was evaporated from the flask until a final volume of ca. 30 mL was reached and allowed to cool down to RT. The resulting white sol was sonicated for 2 min, transferred to a glass beaker belonging to the autoclave. The sol was allowed to stir in the titanium autoclave with heating at 200 ºC for 12 h, reaching atypical pressure of 17-18 bar. After the sintering procedure, the content of ZrO_2 was determined by the ‘glass dies’ method. To the sol gel poly(ethyleneglycol) (avg. Mol. Wt. 2,000) was added (ca. 1.5 g PEG per 25 cm3 sol-gel) to improve the viscosity for better casting on a substrate. The PEG/ZrO_2 mixture was stirred for at least 4 days to ensure homogeneity. The prepared white paste was directly used to be casted on glass

substrate before sintering and removing the polymer at 450 °C for 30 min. The prepared ZrO_2 films were directly used or stored in desiccator.

C.4.4 Metal Oxide Film Preparation

The TiO_2 and ZrO_2 films were casted on glass films. Briefly, the metal oxide paste was spread using a glass test tube on the precut glass films, followed by sintering at 450 °C for 30 min under oxygen flow. The films were allowed to cool down before immediate use or were stored in a dark desiccator. No difference was observed when using films stored for weeks as indicated.

C.4.5 Sensitization of Metal Oxide Films

Sensitization of **Pe-COOH**, **DTBuPe-COOH**, **DTBuPe-C_2H_4-COOH** and **DTBuPe-Ph-COOH** was done by immersing the films in CH_3CN solutions of the dyes (0.5 mM) for 3 h. Afterwards, the films were rinsed with MeCN and dried with N_2 flow. Sensitized films were stored in desiccator and kept from ambient light.

C.4.6 DFT and TD-DFT Calculations

Geometry optimization and molecular orbital calculations were done using the Gaussian 16 package. The DFT geometry optimization of the S0 ground state was performed using the B3LYP pseudopotential and 6-311+g(d) basis set. Optimization of the S1 state, as well as the calculation of the S0-S1 transition energies in the equilibrium geometry of the S0 and S1 states utilized the same 6-311+g(d) basis set.

C.4.7 Spectroscopic Measurements

FT-IR-ATR spectra were acquired on a Thermo Electron Nicolet 6700 FT-IR spectrometer equipped with a Smart iTR ATR accessory with ZnSe HATR. UV-VIS absorbance spectra were collected at room temperature on a Cary 500 UV-Vis-IR

Spectrophotometer, or on an Edmund Optics BDS130 UV/Vis/NIR Light Source. Steady-state fluorescence spectra were acquired and recorded at room temperature on a VARIAN Cary-Eclipse fluorescence spectrophotometer calibrated with a standard NIST tungsten-halogen lamp.

Chapter D Summary

2,5-di-*tert*-Butylperylene (**DTBuPe**) and a series of **DTBuPe**-bridge-anchor derivatives compounds were synthesized, and their steady state photochemical properties in solutions as well as on nanostructured metal oxide semiconductor films were studied. The **DTBuPe** framework was shown to be a succeful improvement to perylene as the *t*-butyl groups efficiently prevented perylene aggregation both in solution and on nanostructured semiconductor films.

The **DTBuPe** framwork was synthesized via a practical North-South approach. *t*-Butyl group was first introduced through Friedel-Crafts alkylation of naphthalene, and the mixture of 2,6-di-*tert*-butylnaphthalene and 2,7-di-*tert*-butylnaphthalene was separated via a thiourea-adduct formation method to yield pure 2,7-di-*tert*-butylnaphthalene. Following by bromination and palladium-catalyzed Suzuki cross coupling, 2,7-di-*tert*-butylnaphthalene was coupled with another naphthalene moiety, forming 3,6-di-*tert*-butyl-1,1'-binaphthyl. After screening several aromatic coupling reactions, we selected anionic cyclization, for its higher yield and less side reactions. By utilizing stabilized lithium metal powder, the anionic cyclization of 3,6-di-*tert*-butyl-1,1'-binaphthyl consistently yielded **DTBuPe** with ~ 50% yield.

Functional group addition in the 9-position of **DTBuPe** was carried out via two simple pathways. The first approach involved formylation of **DTBuPe** via Friedel-Crafts with dichloromethyl methyl ether to form **DTBuPe-CHO**, in a 1-C homologation. The resulting **DTBuPe-CHO** was oxidized using $KMnO_4$ at room temperature to afford 8,11-di-*tert*-Butylperylene-3-carboxylic acid **(DTBuPe-COOH)**. The second path involves the formation of bromo-derivative **DTBuPe-Br** via *N*-bromosuccinimide (NBS) bromination, leading to as an easy entry to Pd-catalyzed cross coupling reactions. Followed by various

palladium-catalyzed cross-coupling reactions, a series of DTBuPe-bridge-anchor derivatives were obtained, indicating an expanded functionalization potential of **DTBuPe** framework. Moreover, for the first time, perylene was successfully functionalized with an azide group, and copper-catalyzed click reaction (CuAAC) was performed with **DTBuPe-Ph-N3** in high yield. This could lead to promising applications of perylene in a variety of field, as the CuAAC reaction is widely employed in surface modification.

The photophysical properties of **DTBuPe** derivatives were first investigated in solution. Absorption and emission spectra of **DTBuPe** showed that *t*-butyl groups only slightly influence the electronic properties of the perylene core. All DTBuPe-bridge-anchor derivatives showed red-shifted and broadened absorption and emission spectra. This was mainly due to the electronic coupling between the linker units (bridge-anchor) and perylene. Derivative **8b** with the conjugated ethylene bridge showed a significant red-shift and the vibrational structure was almost absent, suggesting that the unsaturated double bond is strongly coupled with the perylene core. Derivatives **DTBuPe-Ph-COOH** and **DTBuPe-Ph-Tz-COOH**, which had an unsaturated phenyl ring connected to the perylene, showed similar spectra as **DTBuPe-COOH**, indicating that the π system of the phenyl ring is not strongly coupled with the π system of perylene. This observation is also in good qualitative agreement with calculated results.

Pe-COOH and **DTBuPe-COOH** were bound to nanostructured TiO_2 and ZrO_2 films, and the influence of *t*-butyl groups were investigated by UV-vis, fluorescence and FT-IR-ATR spectroscopy. The absorption and emission spectra of **Pe-COOH**/MO_n showed clear evidence of aggregation on the film. Spectra of **DTBuPe-COOH**/MO_n showed some difference from neat **DTBuPe-COOH**; however, we believe these changes are due

to the electronic coupling between the molecule and the semiconductor films. These results indicate that *t*-butyl groups on **DTBuPe-COOH** can efficiently prevent the aggregation of perylene on semiconductor films and quenching of the excited state. FT-IR-ATR spectra showed that **DTBuPe-COOH** binds to semiconductor films via a bi-dentate geometry; However, **Pe-COOH** shows different binding behavior on TiO_2 and ZrO_2 films. The reason of this phenomenon is unclear, but we believe it is related to aggregation.

DTBuPe-C_2H_4-COOH and **DTBuPe-Ph-COOH** were bound to nanostructured TiO_2 and ZrO_2 films, and the influence of bridge units structure were investigated by UV-vis, fluorescence and FT-IR-ATR spectroscopy. **DTBuPe-C_2H_4-COOH** exhibited a lower surface coverage during binding compared with other DTBuPe-bridge-anchor derivatives. We believe it is related to the flexibility of the ethylenic bridge. The emission spectra of **DTBuPe-C_2H_4-COOH**/ZrO_2 and **DTBuPe-Ph-COOH**/ZrO_2 showed a weakened red-shift comparing with **DTBuPe-COOH/**ZrO_2, indicating that the electronic coupling between chromophore and semiconductor surfaces was weakened by the bridge units. FT-IR-ATR spectra showed that both **DTBuPe-C_2H_4-COOH** and **DTBuPe-Ph-COOH** were bound to semiconductor films via bi-dentate geometry.

By collaborating with Prof. Andrew. Teplyakov's research group and Prof. Lars Gundluch's research group at the University of Delaware, a novel pathway to functionalize highly ordered ZnO nanoparticle films without etching the morphology was developed. The ZnO nanorod surface was first functionalized, and passivated, by chemisorption of propiolic acid from gas phase, followed by solution phase CuAAC reaction with azido-derivative **DTBuPe-Ph-N3**. XPS and SEM characterization

confirmed that large dye molecule like **DTBuPe** can be successfully immobilized to the film via click reaction without etching the morphology of ZnO nanoparticles. Pump/white-light probe transient absorption also proved that a strong electronic coupling was obtained using this two-step sensitization. This new functionalization pathway could be ideal for reliable and useful measurements of HET process.

This thesis provides practical pathways to utilize perylene framework without the influence of aggregation. Investigations on **DTBuPe**-bridge-anchor derivatives are ongoing in the group of Prof. Lars Gundlach to probe the effect of coherence in HET process. Our group is also working on attaching **DTBuPe** core to other functional linkers, for instance peptides, to tune and control the HET process. Azido-derivative **DTBuPe-Ph-N3** can also be employed in various surface modification investigations involving click chemistry.

APPENDIX

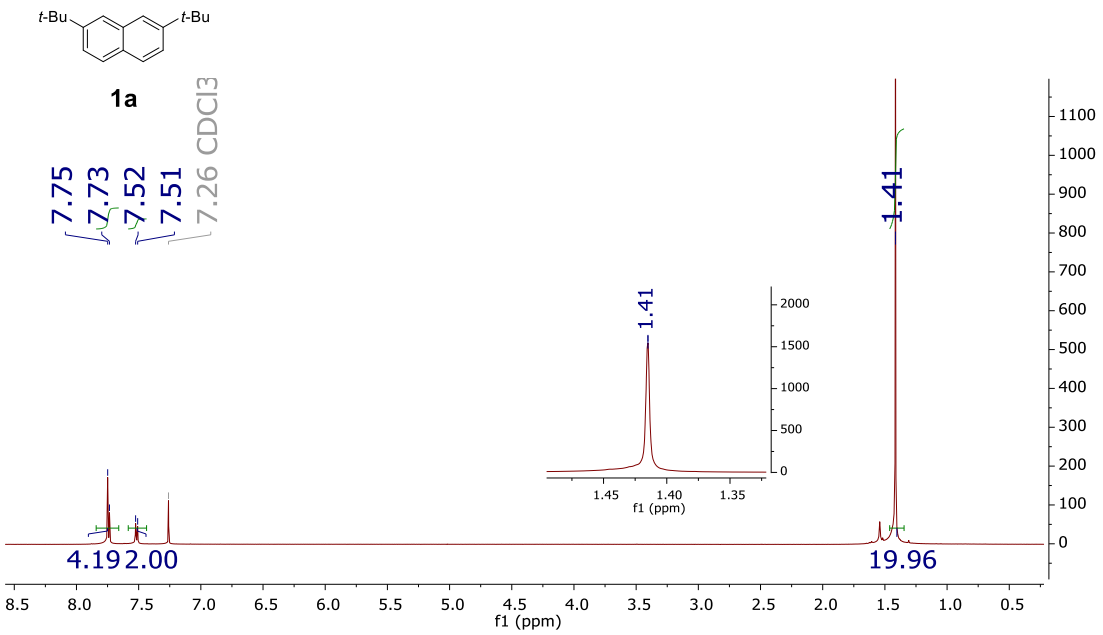

Figure 0-1. ^{1}H NMR of compound **1a** in $CDCl_3$

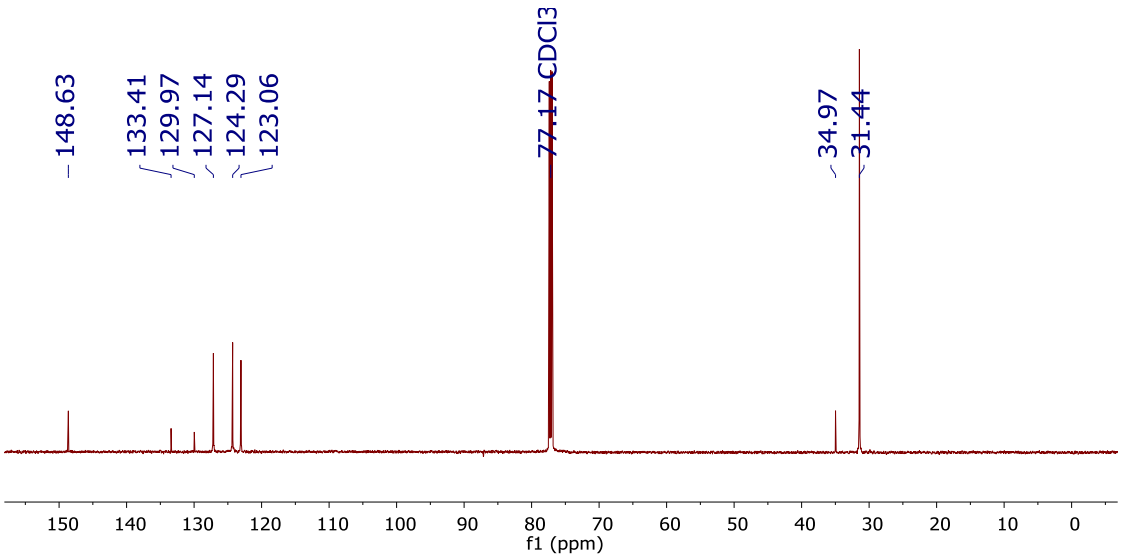

Figure 0-2. ^{13}C NMR of compound **1a** in $CDCl_3$

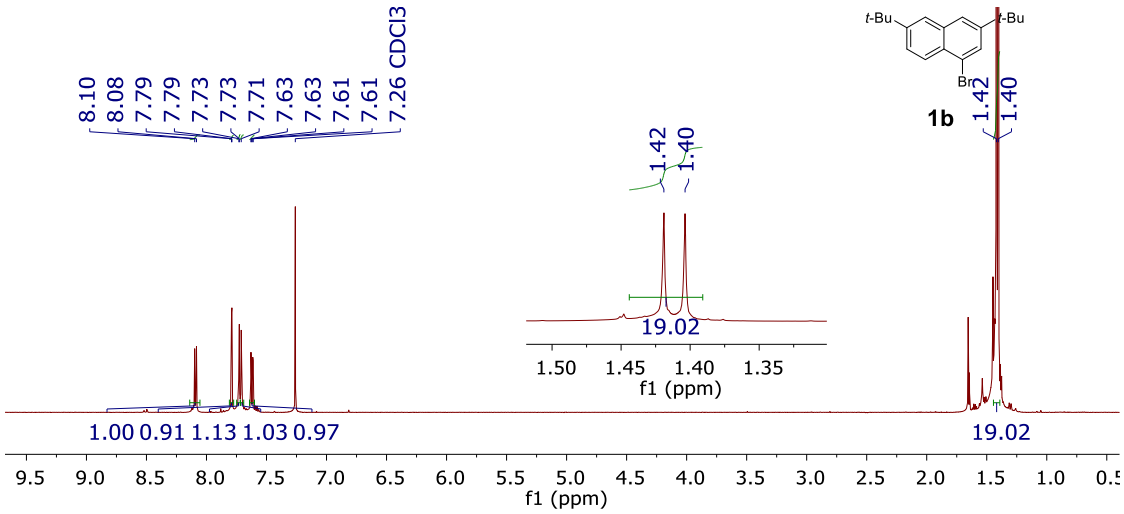

Figure 0-3. ^{1}H NMR of compound **1b** in $CDCl_3$

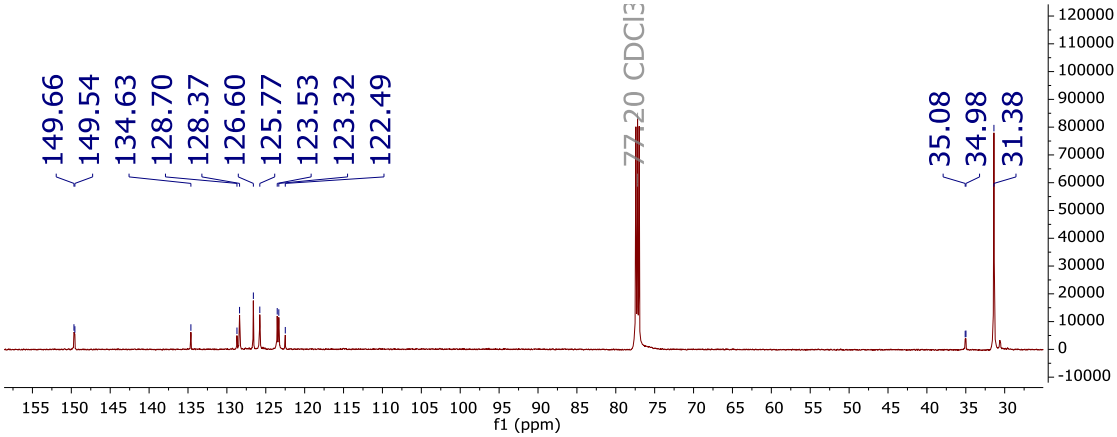

Figure 0-4. ^{13}C NMR of compound **1b** in $CDCl_3$

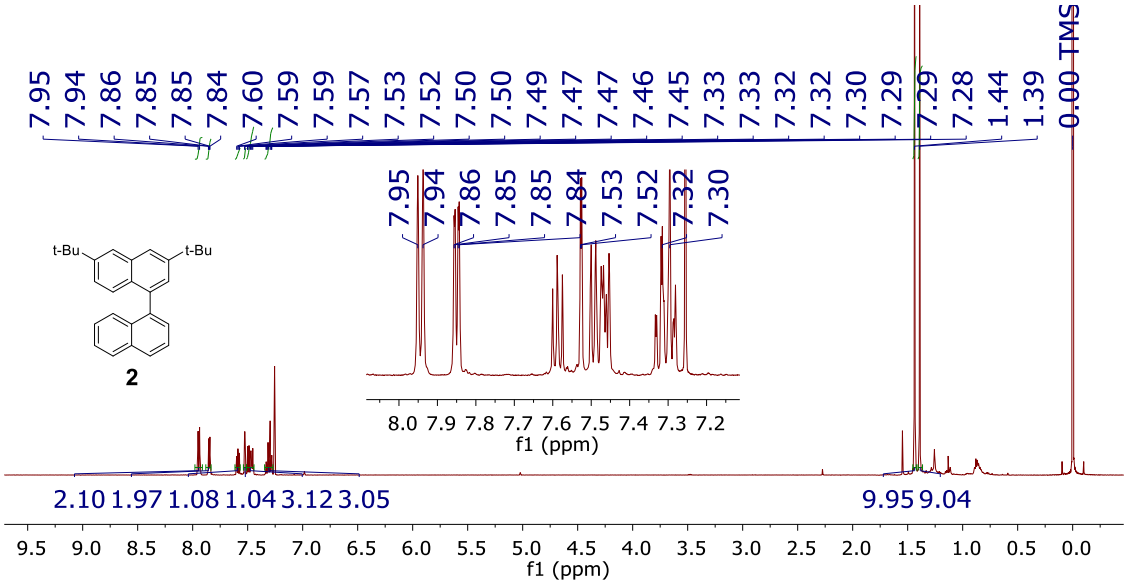

Figure 0-5. ^{1}H NMR of compound **2** in $CDCl_3$

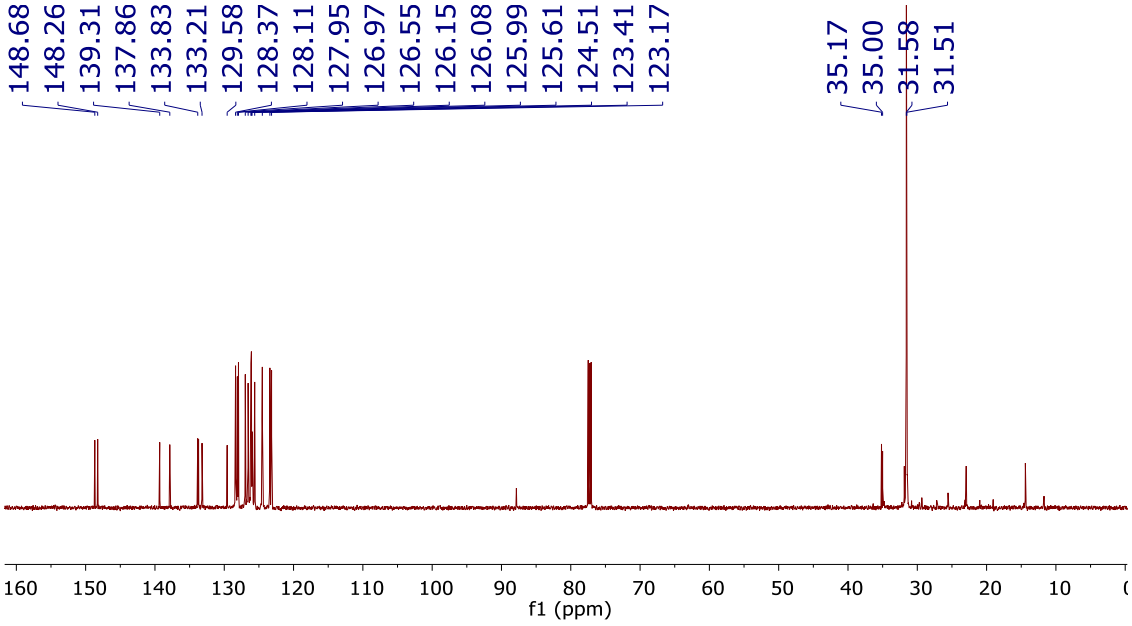

Figure 0-6. ^{13}C NMR of compound **2** in $CDCl_3$

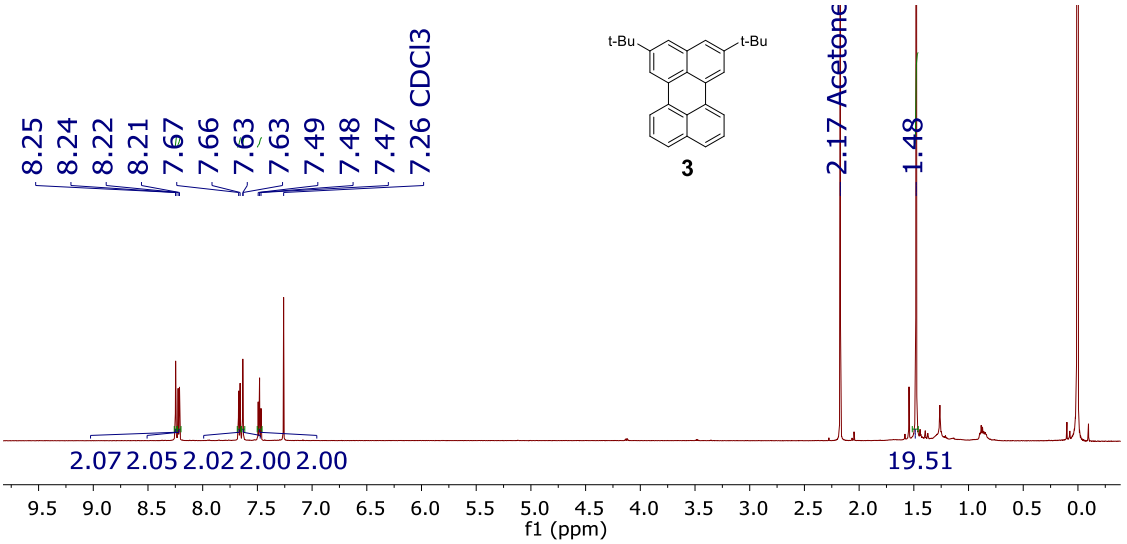

Figure 0-7. ^{1}H NMR of compound **3** in $CDCl_3$

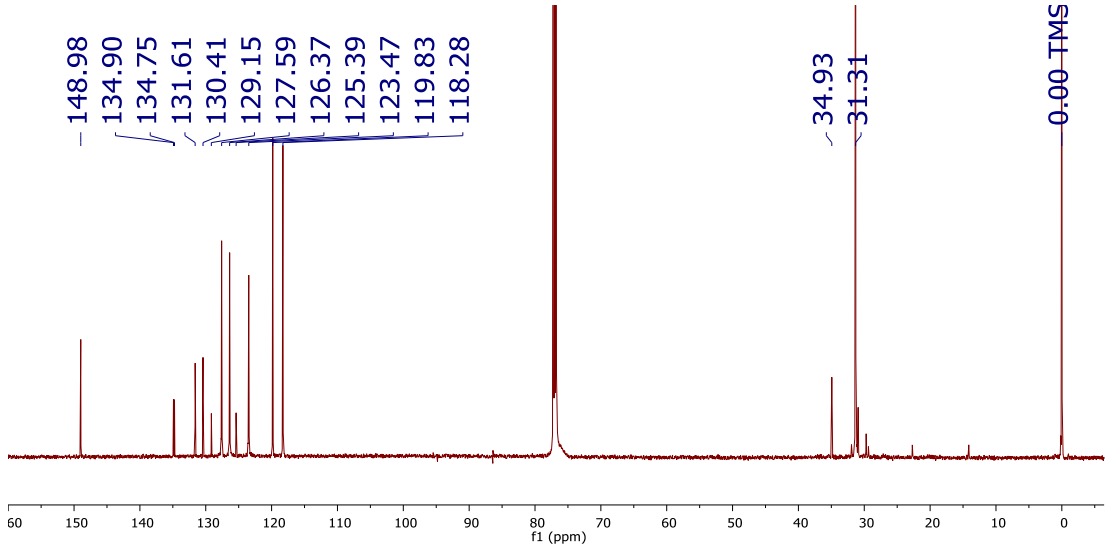

Figure 0-8. ^{13}C NMR of compound **3** in $CDCl_3$

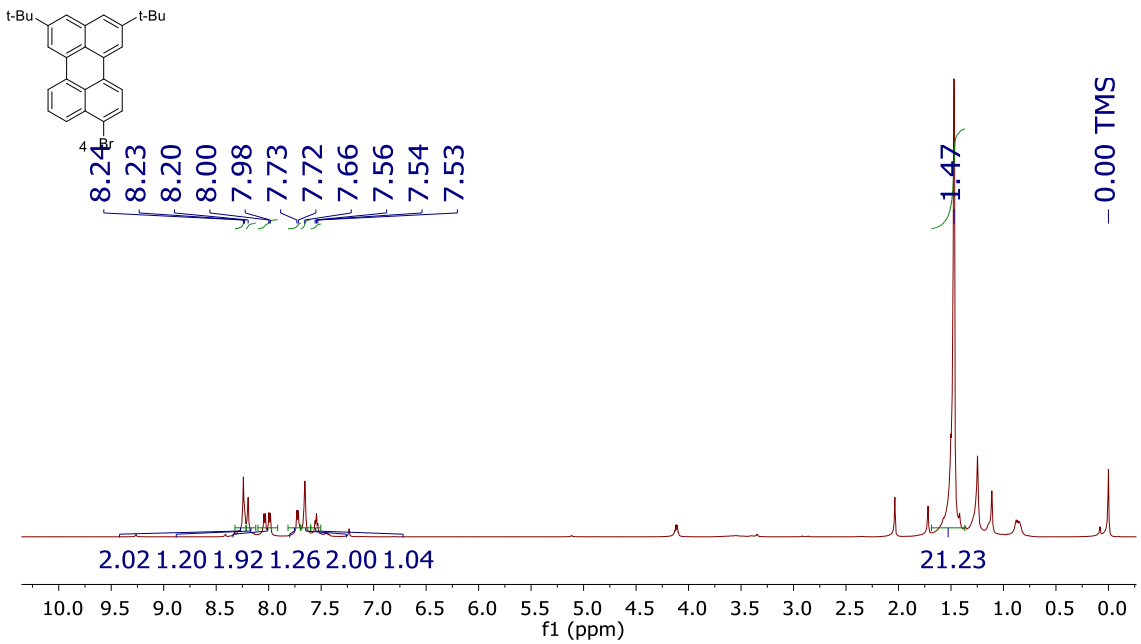

Figure 0-9. ^{1}H NMR of compound **4** in $CDCl_3$

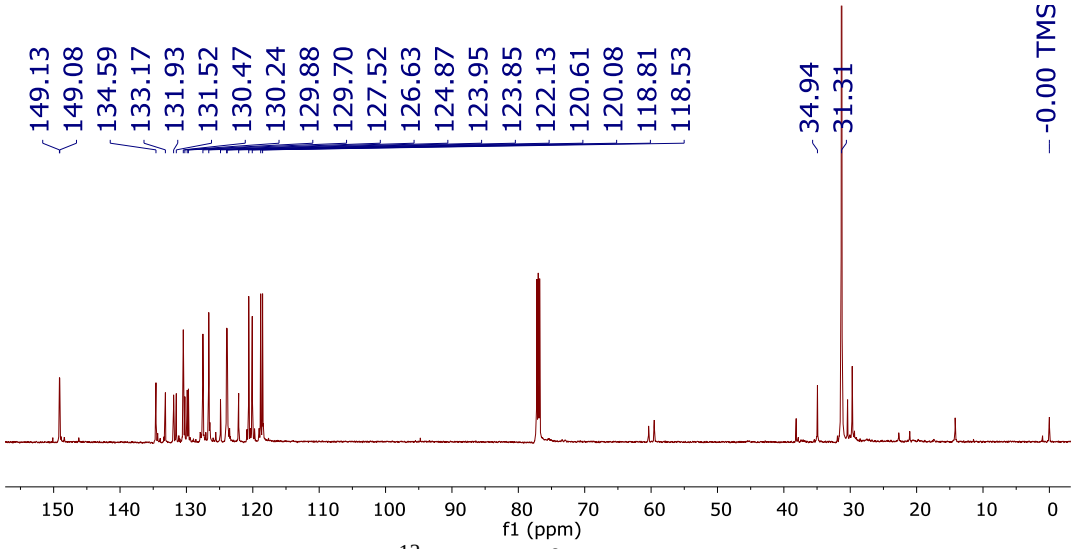

Figure 0-10 . ^{13}C NMR of compound **4** in $CDCl_3$

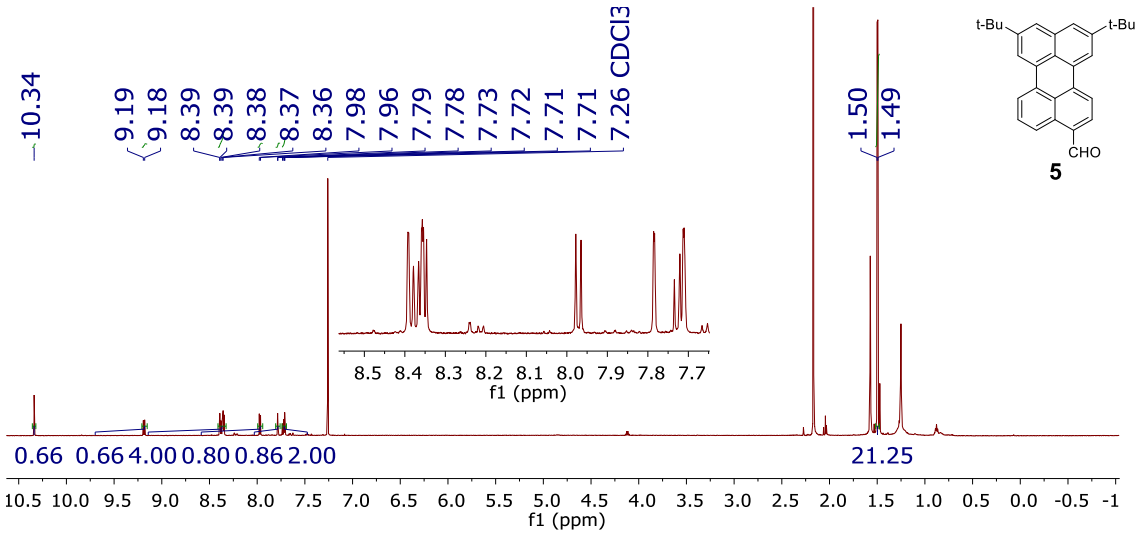

Figure 0-11 ^{1}H NMR of compound **5** in $CDCl_3$

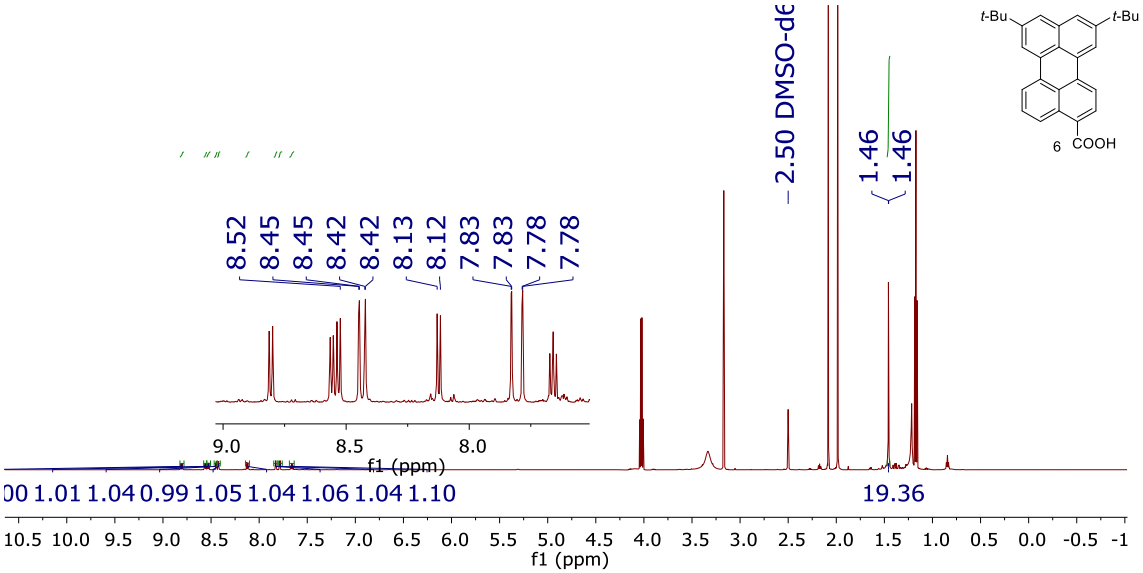

Figure 0-12. ^{1}H NMR of **6** in DMSO.

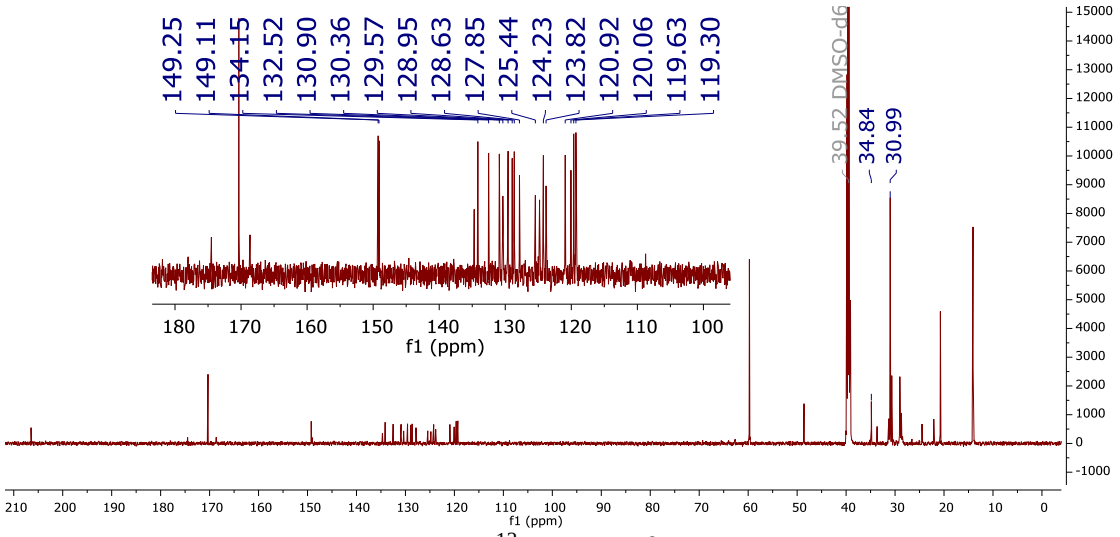

Figure 0-13. ^{13}C NMR of **6** in DMSO.

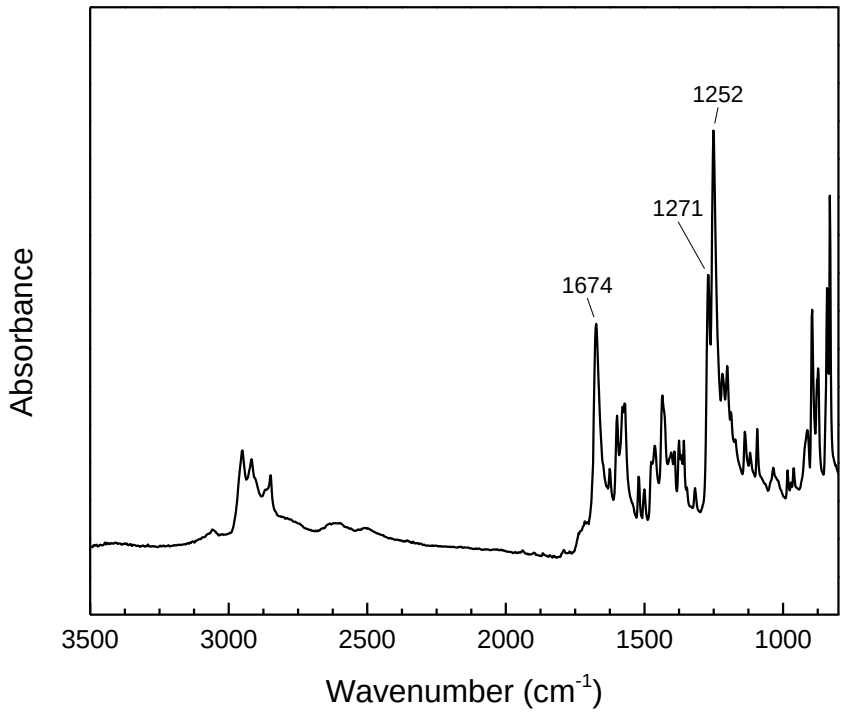

Figure 0-14. FT-IR spectrum of **6**.

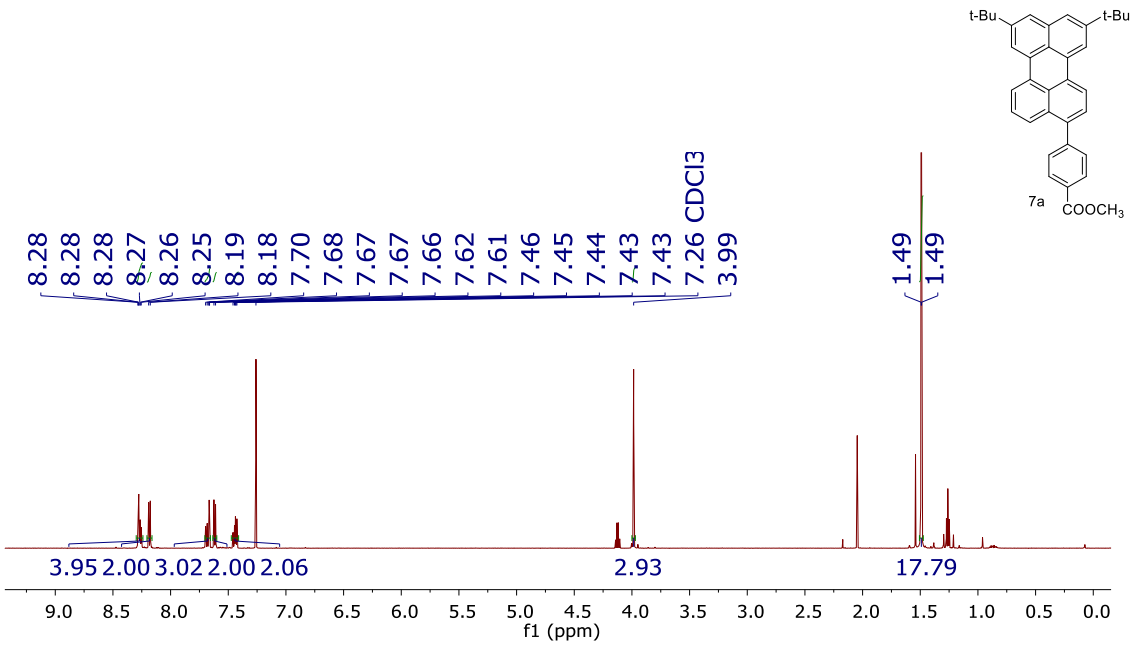

Figure 0-15. ^{1}H NMR of **7a** in $CDCl_3$.

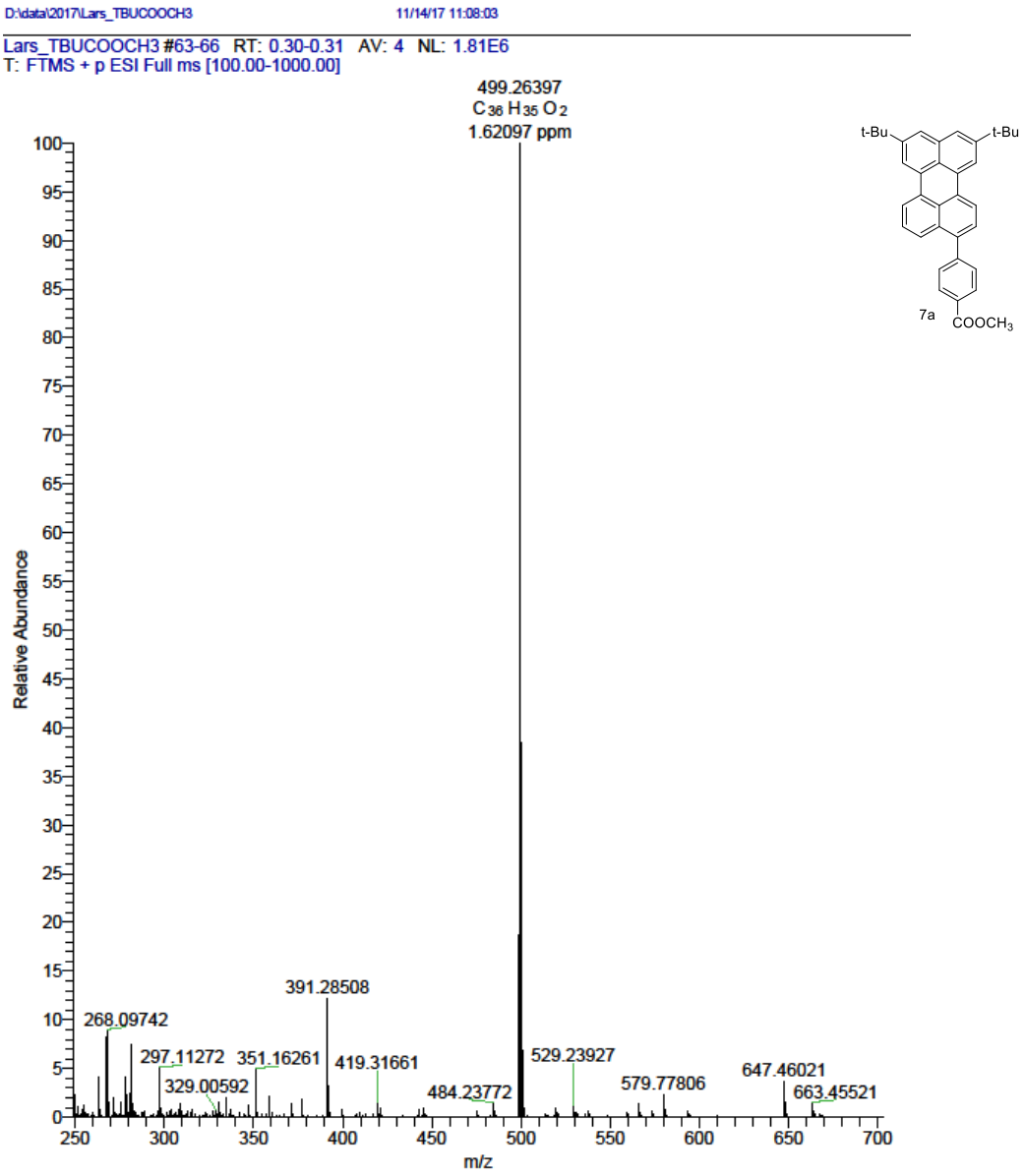

Figure 0-16. ESI-MS spectra of **7a**.

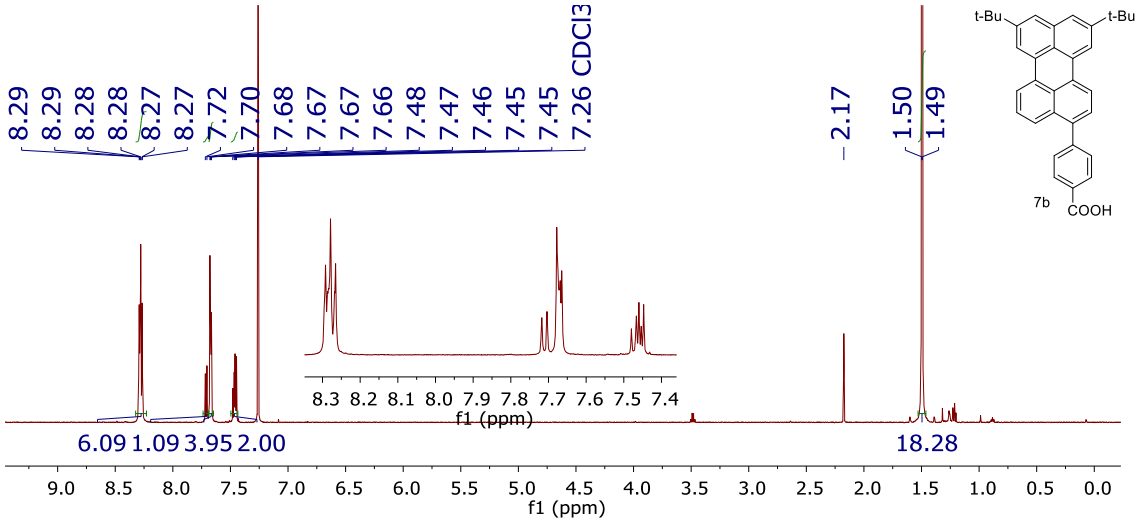

Figure 0-17. ^{1}H NMR of **7b** in DMSO.

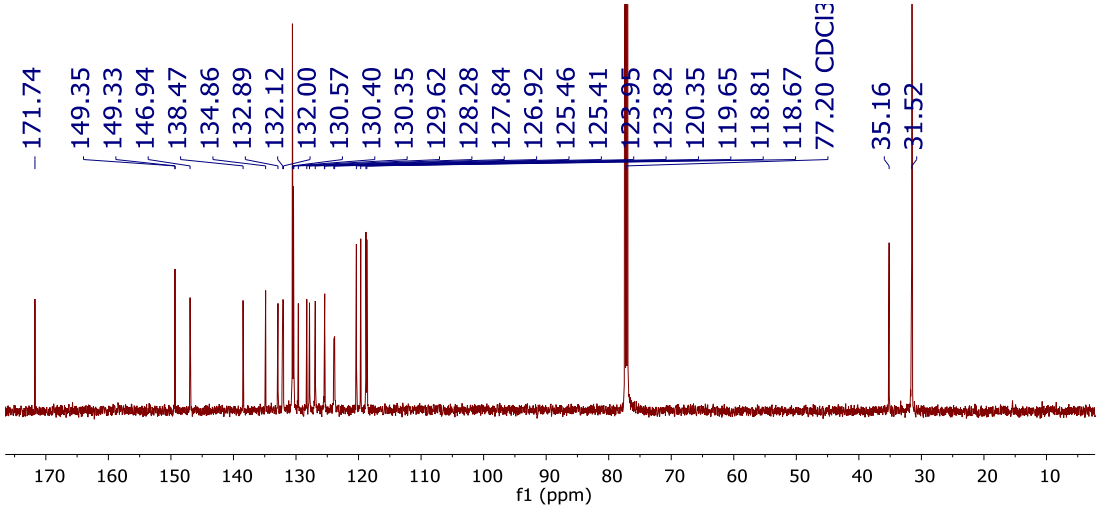

Figure 0-18. ^{13}C NMR of **7b** in DMSO.

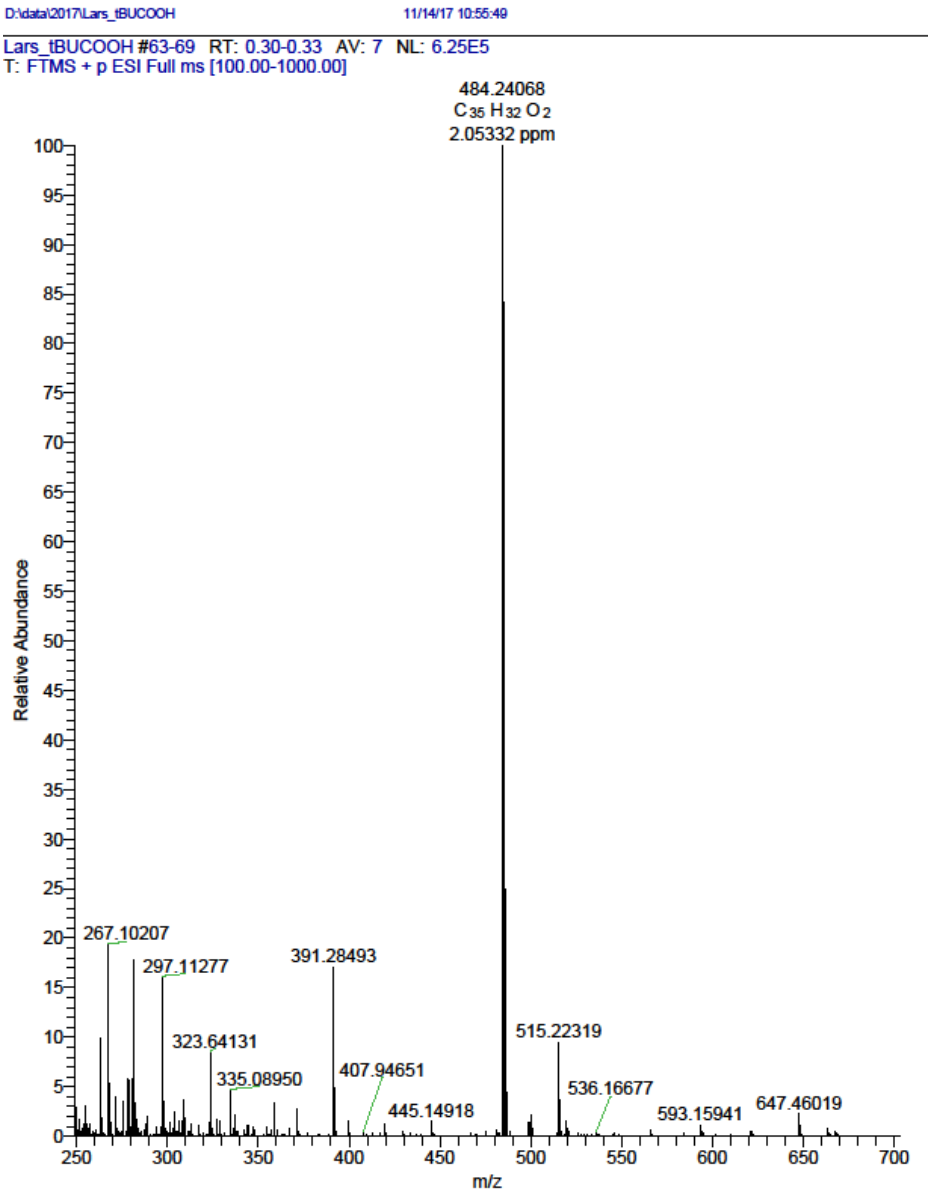

Figure 0-19. ESI-MS spectra of **7b**.

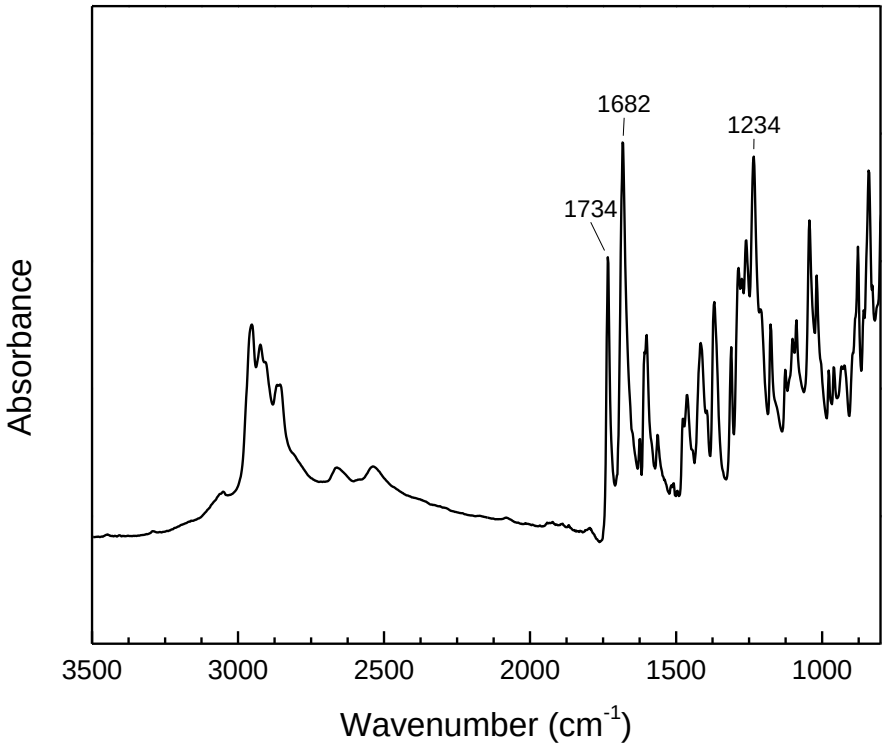

Figure 0-20. FT-IR spectrum of **7b**.

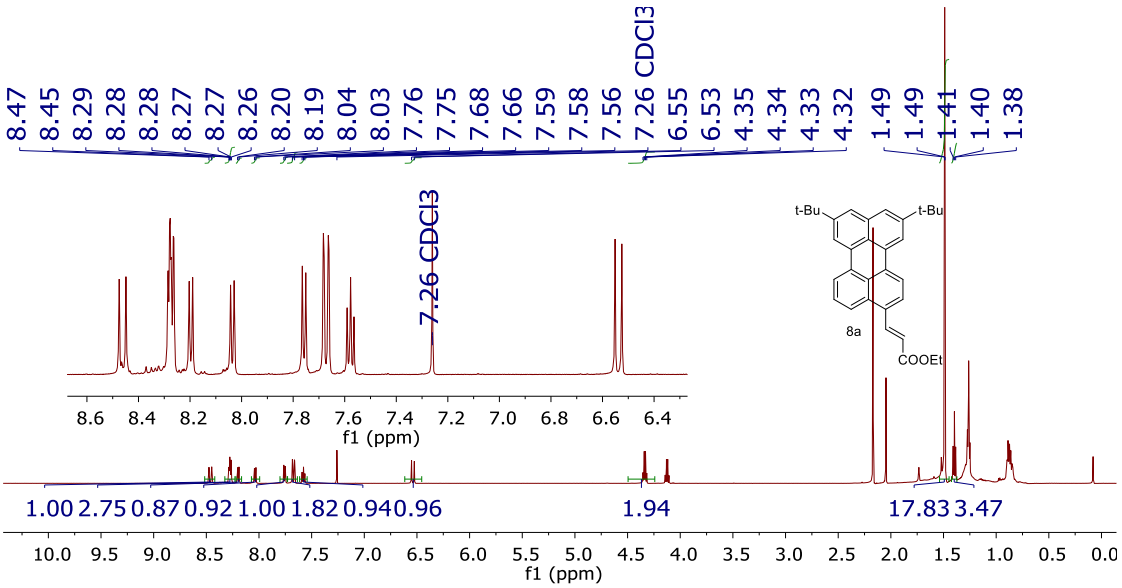

Figure 0-21 ^{1}H NMR of **8a** in $CDCl_3$

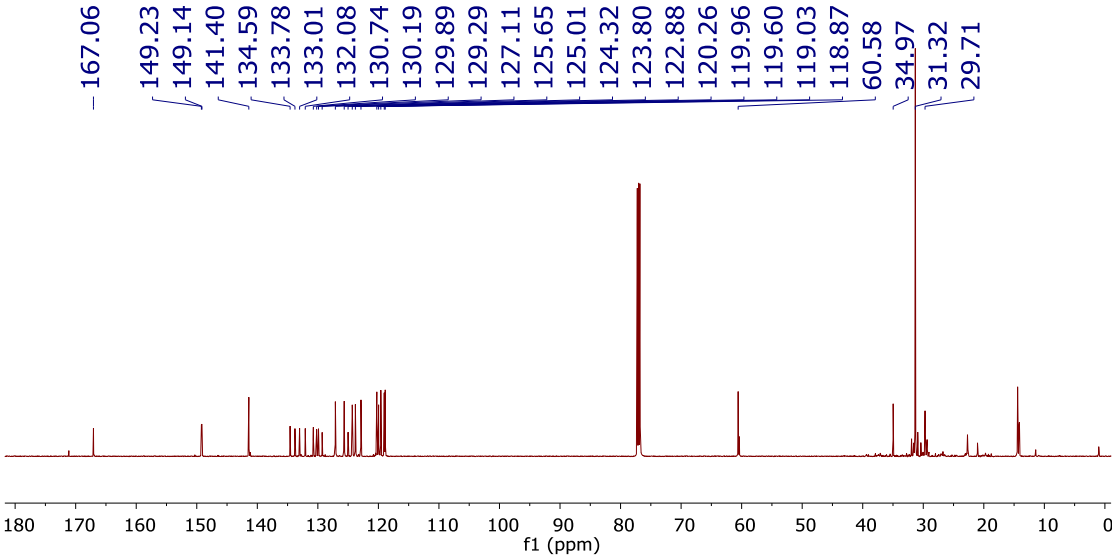

Figure 0-22 ^{13}C NMR of **8a** in $CDCl_3$

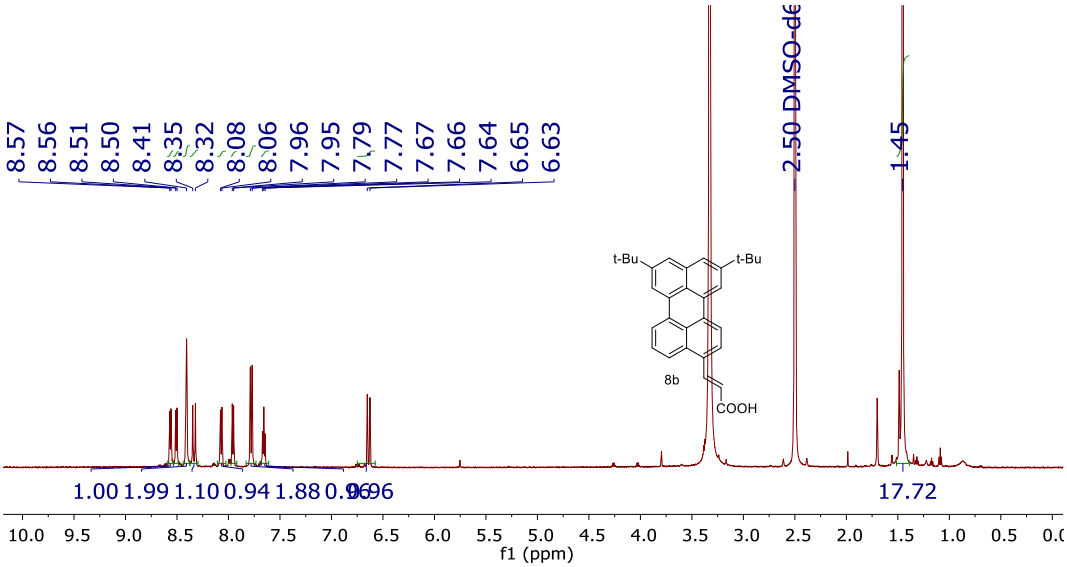

Figure 0-23. ^{1}H NMR of **8b** in DMSO

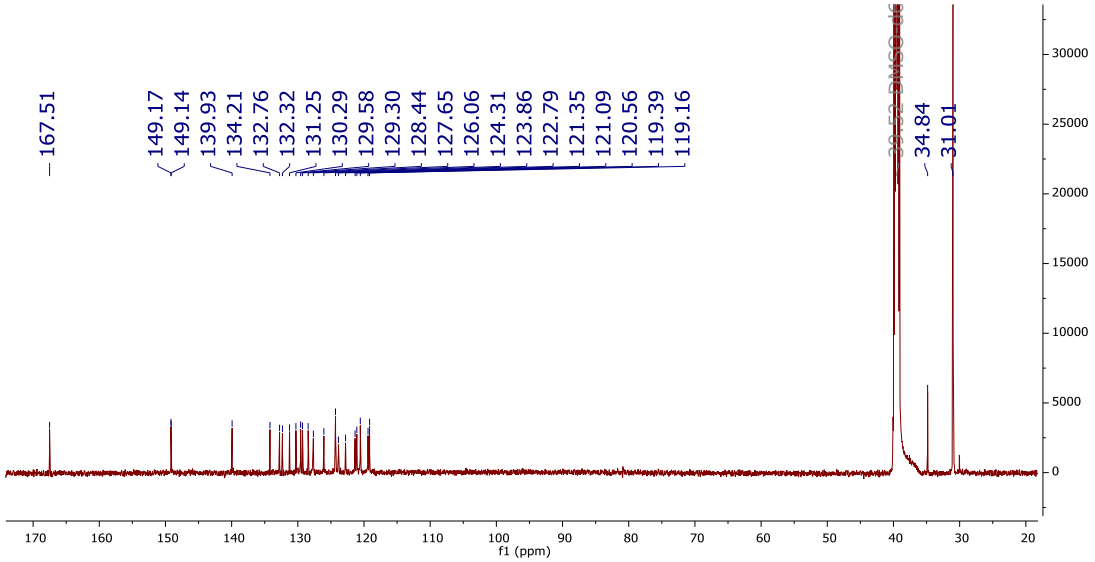

Figure 0-24. ^{13}C NMR of **8b** in DMSO.

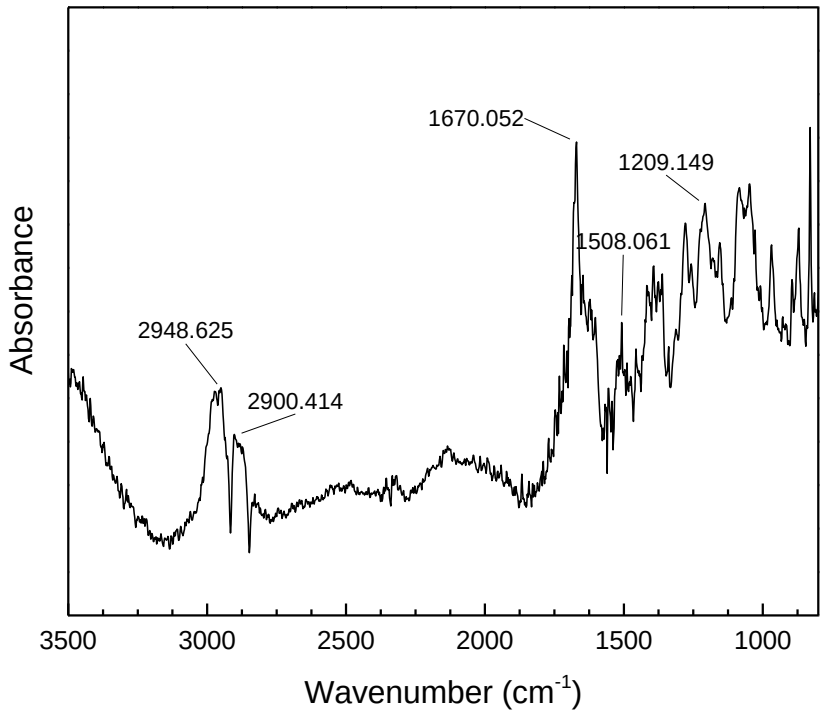

Figure 0-25 FT-IR spectrum of **8b**.

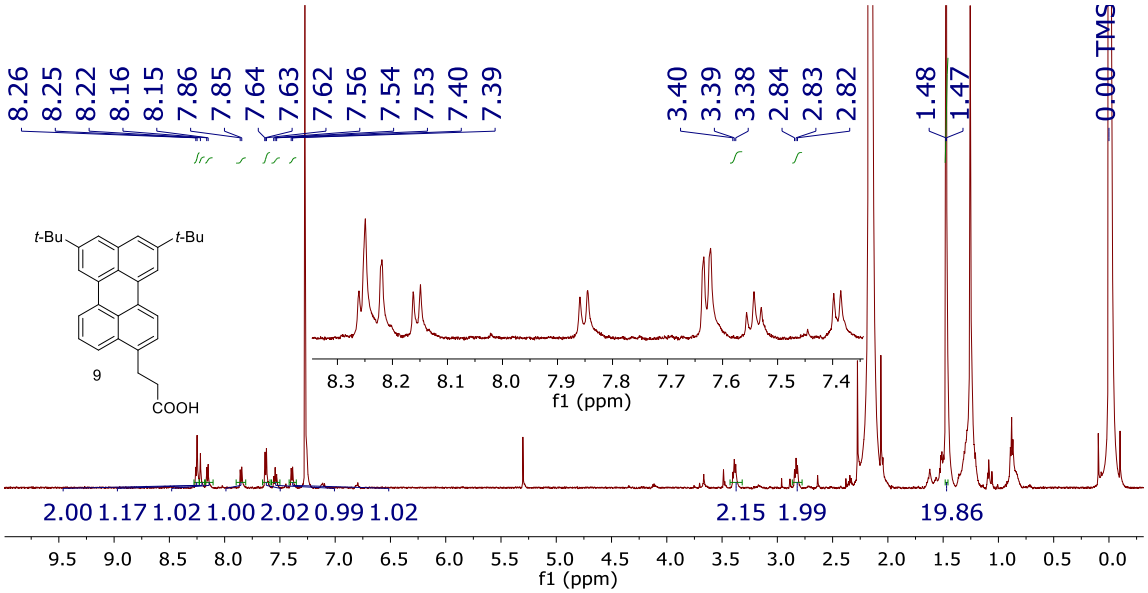

Figure 0-26. ^{1}H NMR of **9** in $CDCl_3$

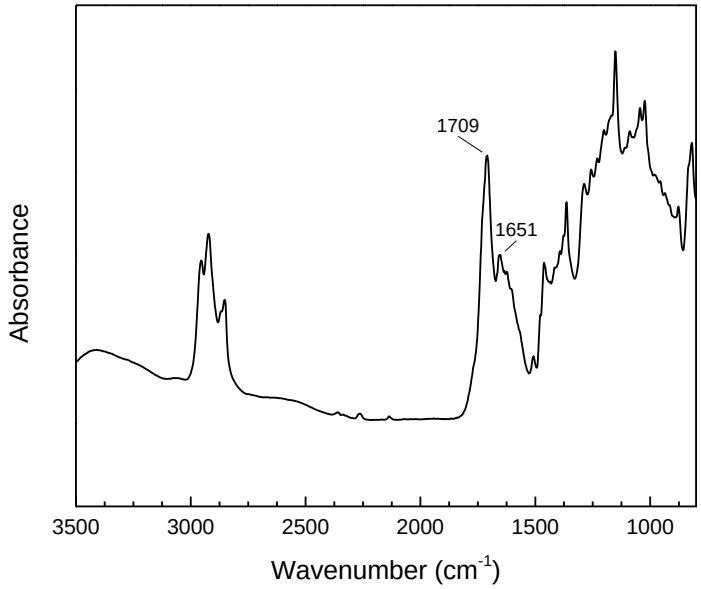

Figure 0-27 FT-IR spectrum of **9**.

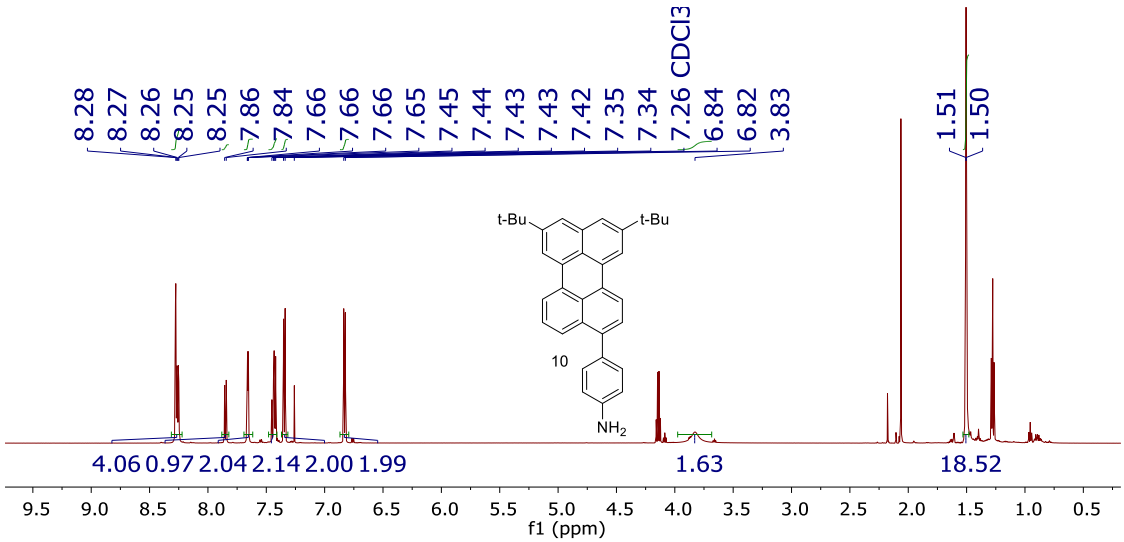

Figure 0-28. ^{1}H NMR of **10** in $CDCl_3$

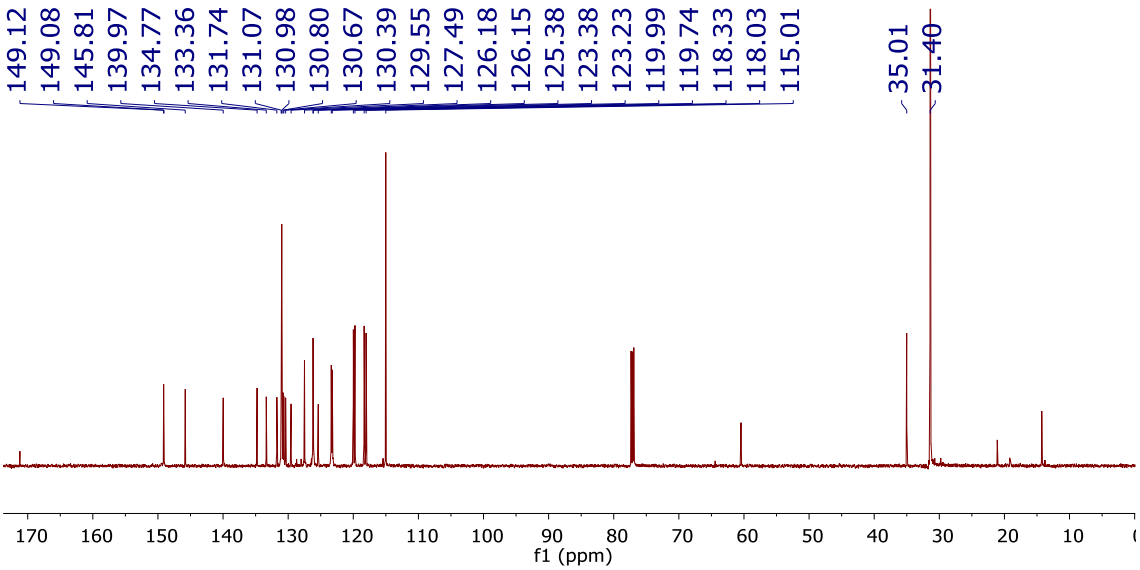

Figure 0-29. ^{13}C NMR of **10** in $CDCl_3$

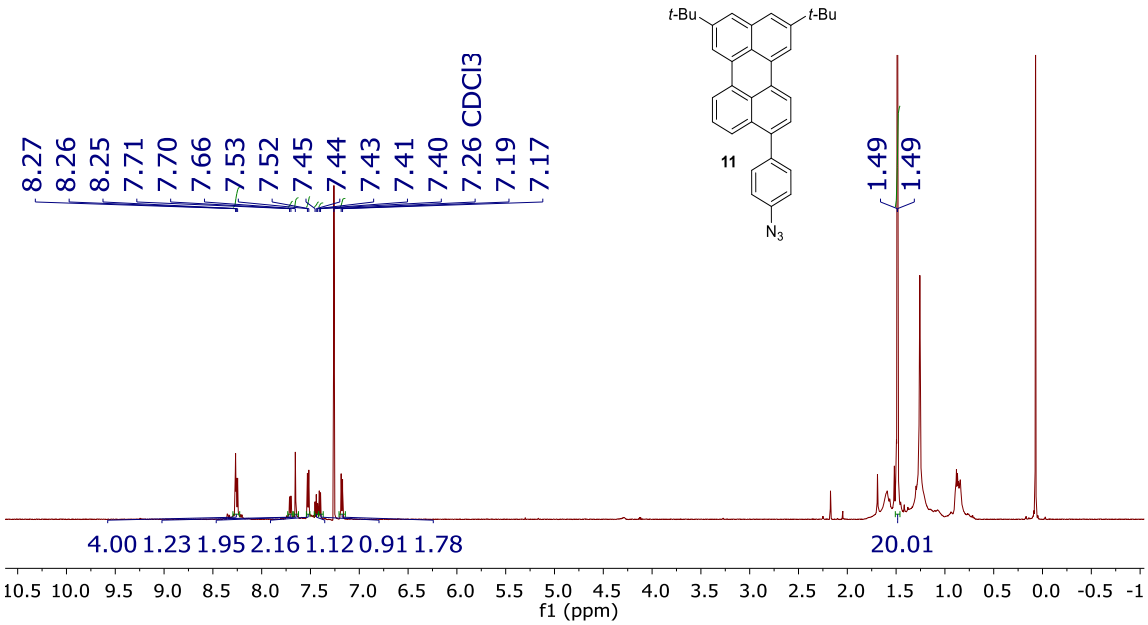

Figure 0-30. ^{1}H NMR of **11** in $CDCl_3$

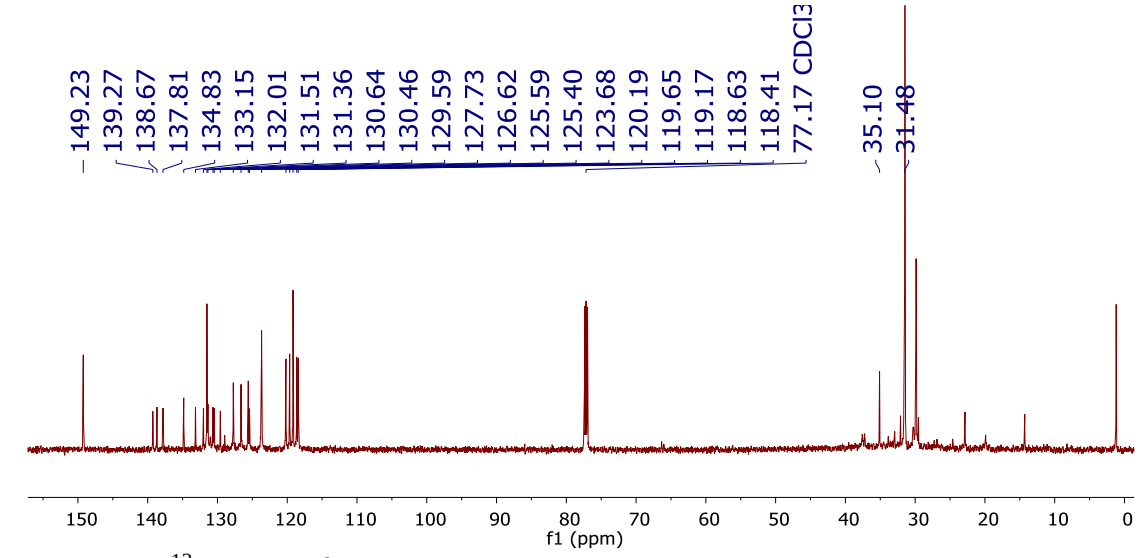

Figure 0-31. ^{13}C NMR of **11** in $CDCl_3$

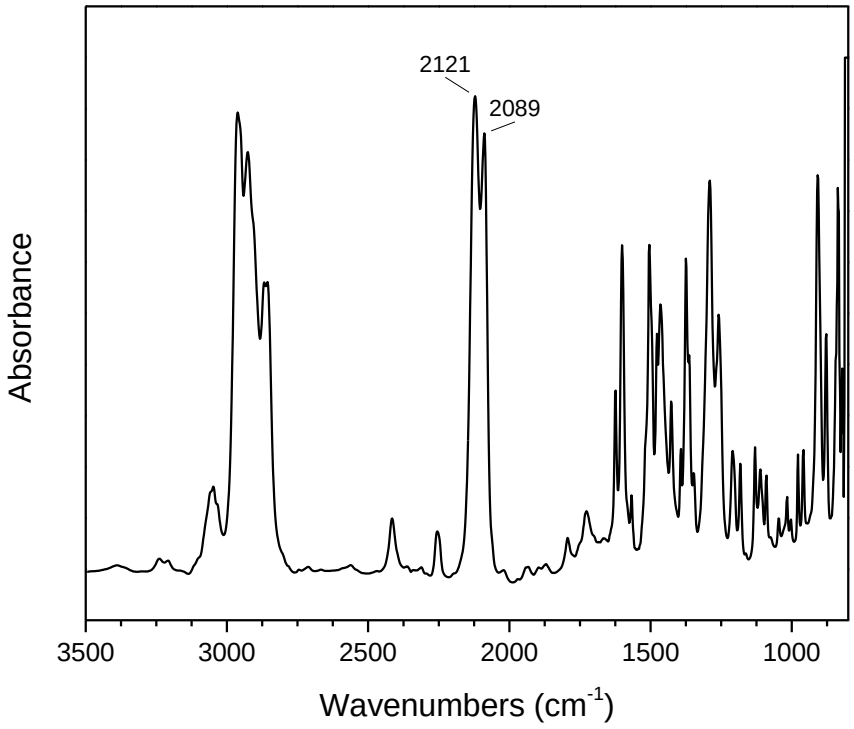

Figure 0-32. FT-IR spectra of **11.**

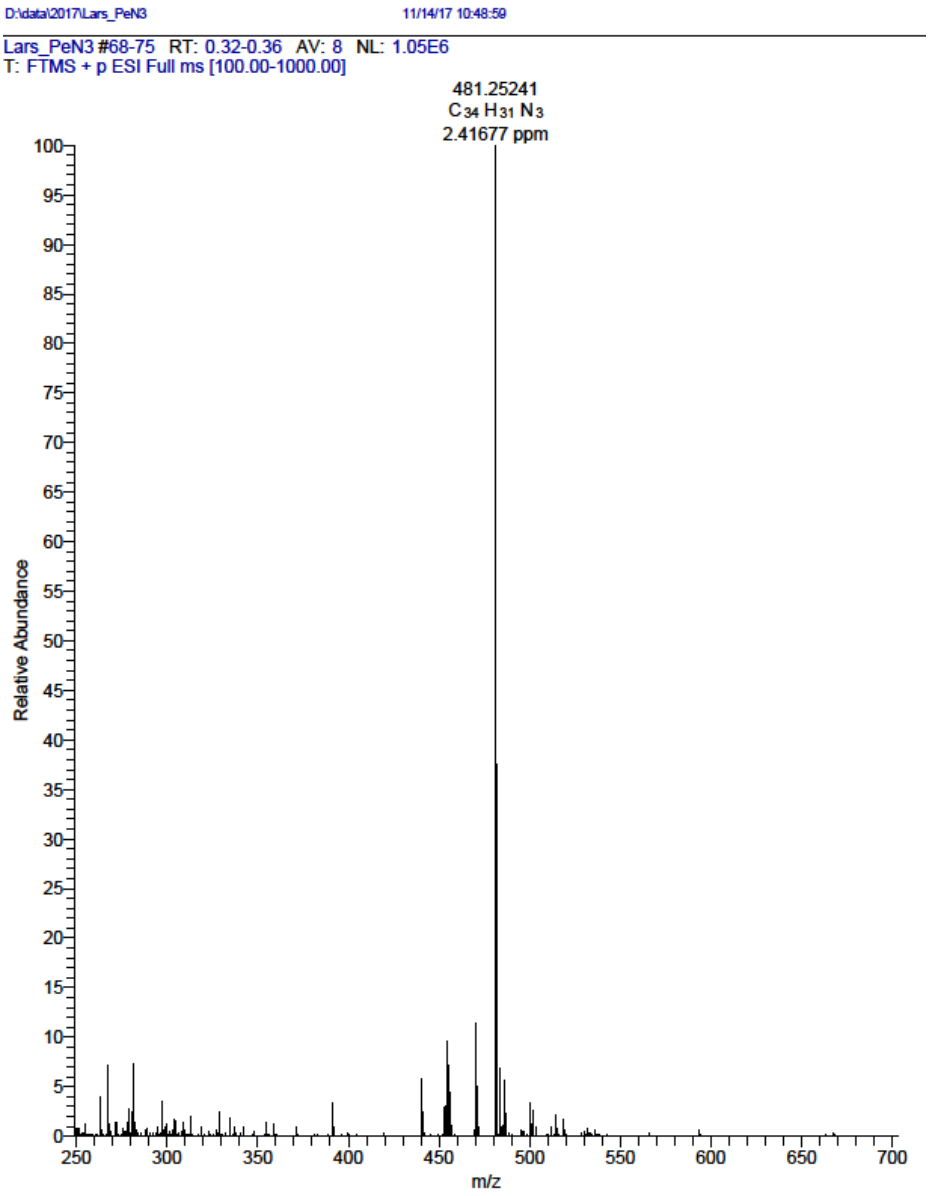

Figure 0-33. ESI-MS of **11**.

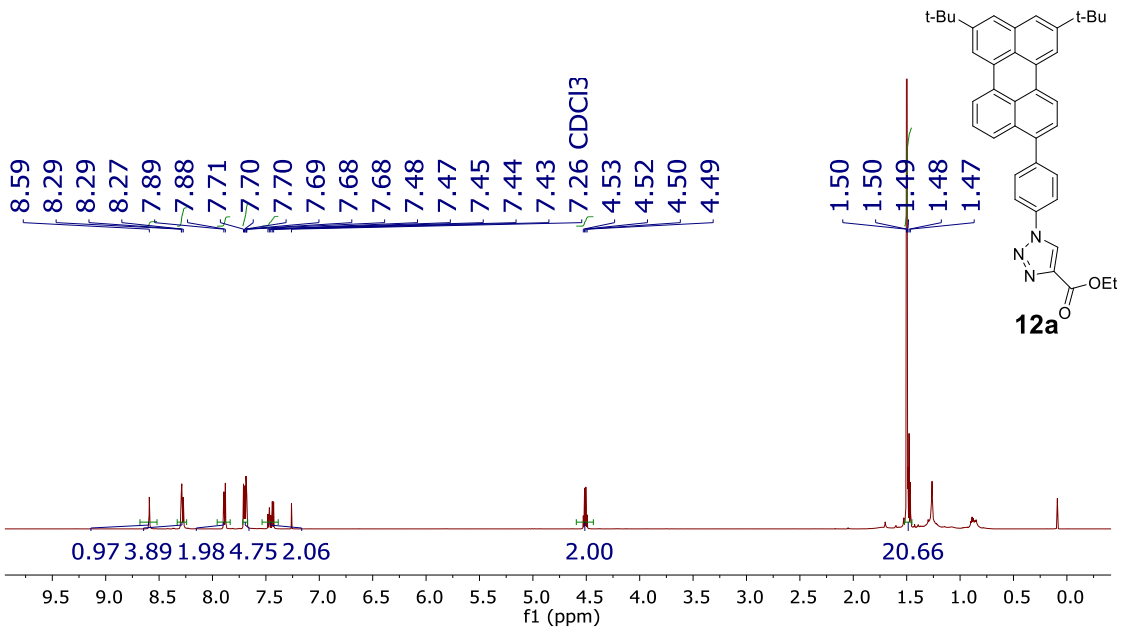

Figure 0-34. ^{1}H NMR of **12a** in $CDCl_3$

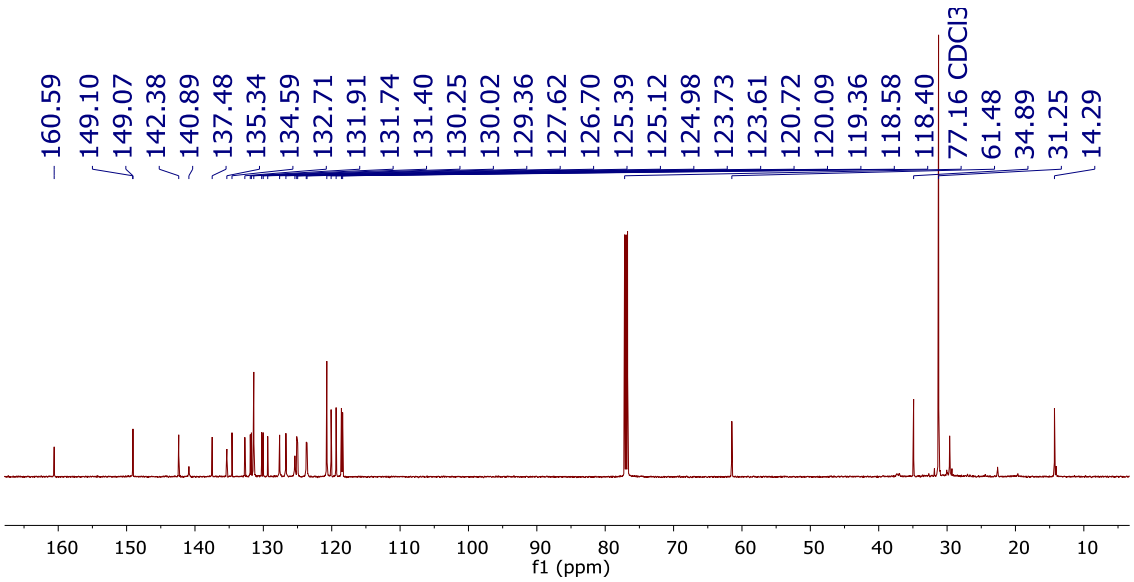

Figure 0-35. ^{13}C NMR of compound **12a** in $CDCl_3$

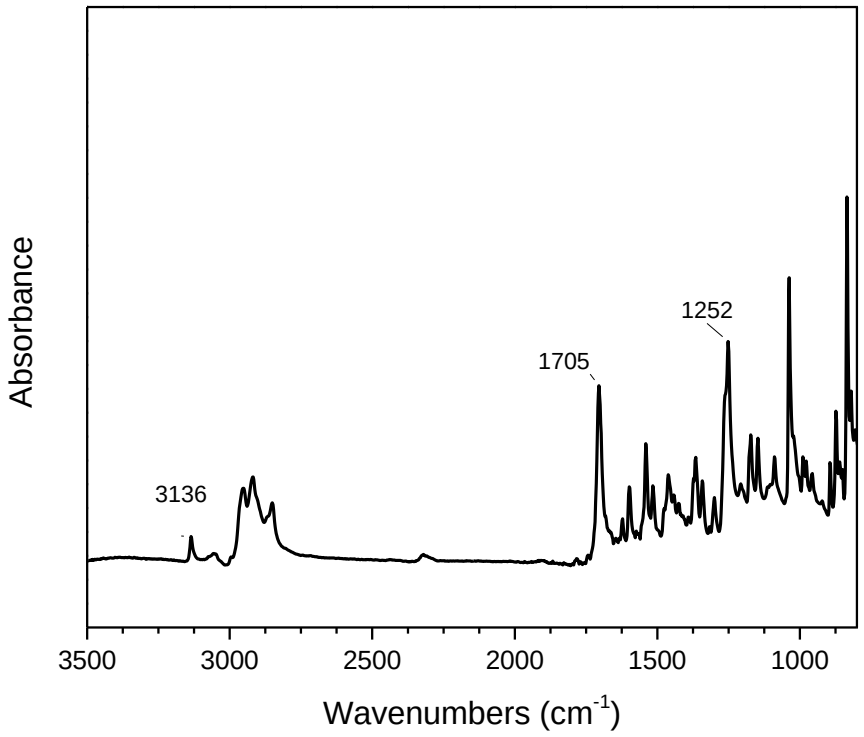

Figure 0-36. FT-IR spectra of **12a**

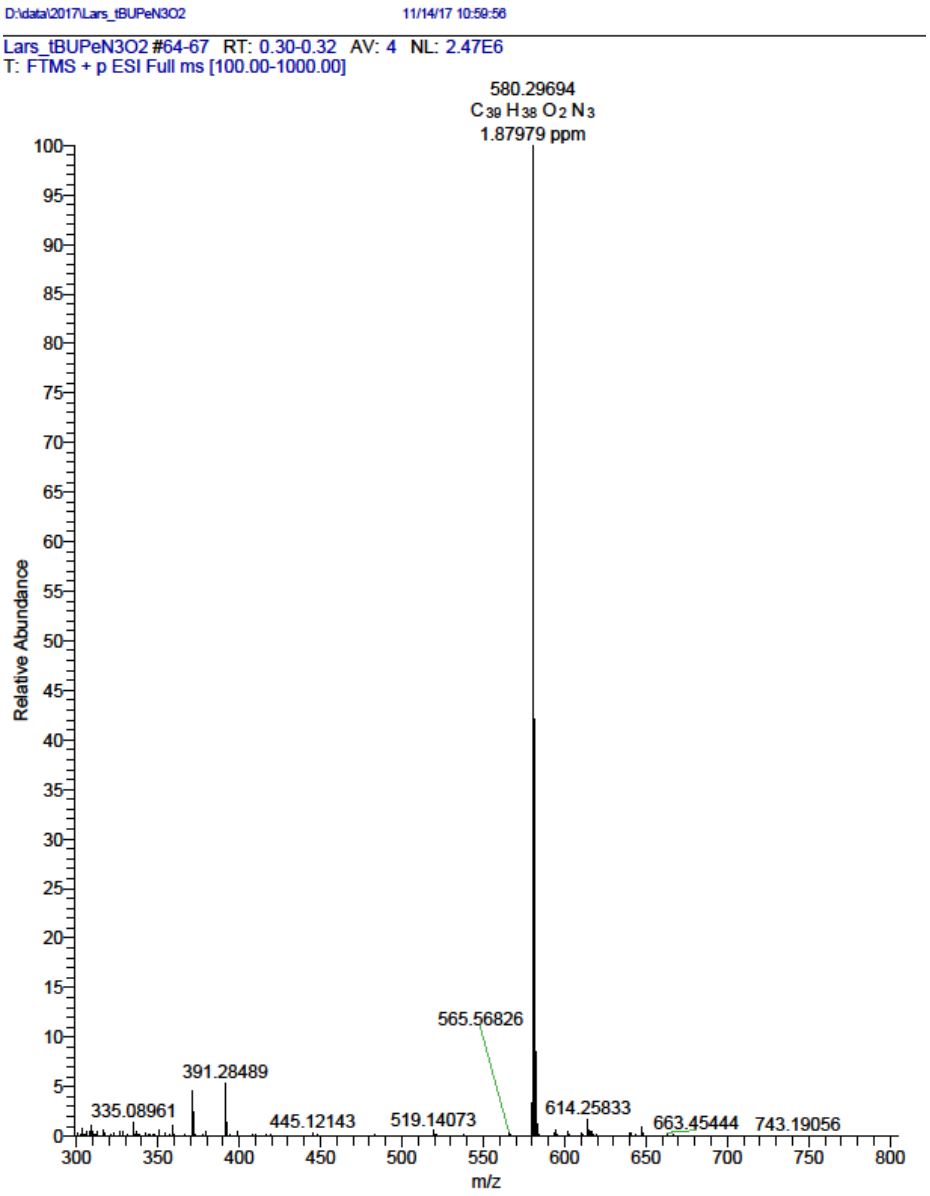

Figure 0-37. ESI-MS of **12a**.

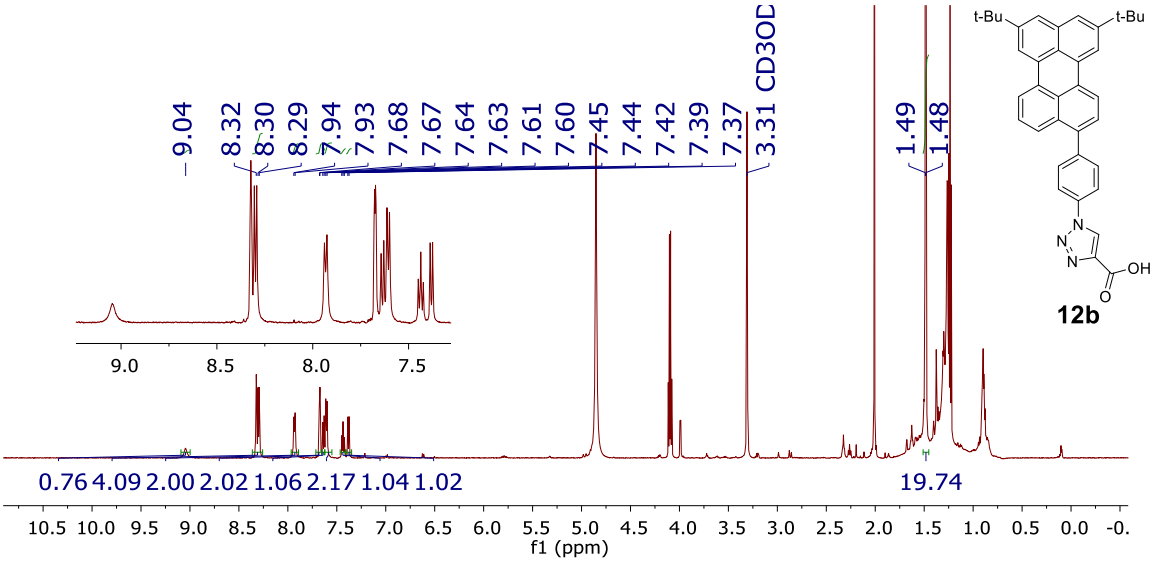

Figure 0-38. ^{1}H NMR of **12b** in CD_3OD

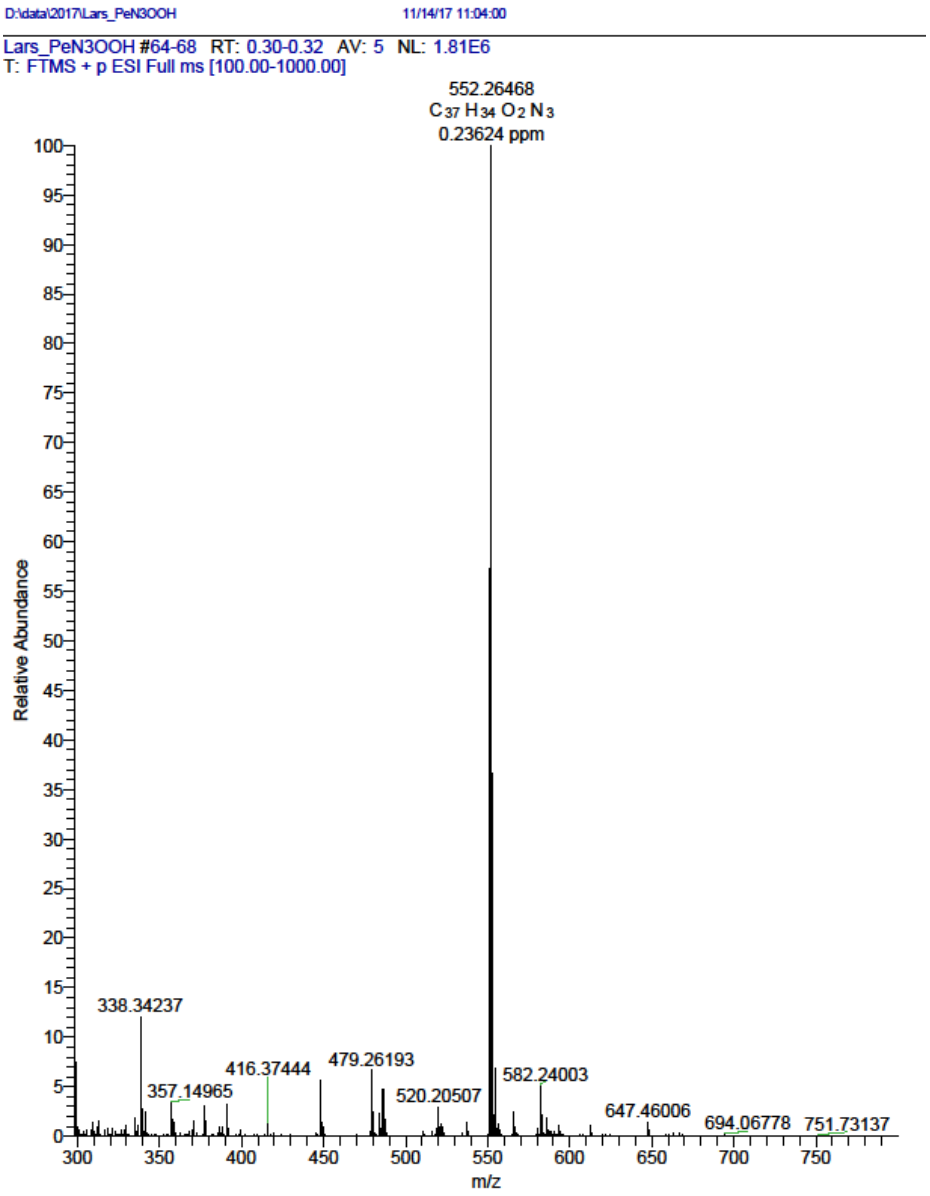

Figure 0-39. ESI-MS of **12b**.

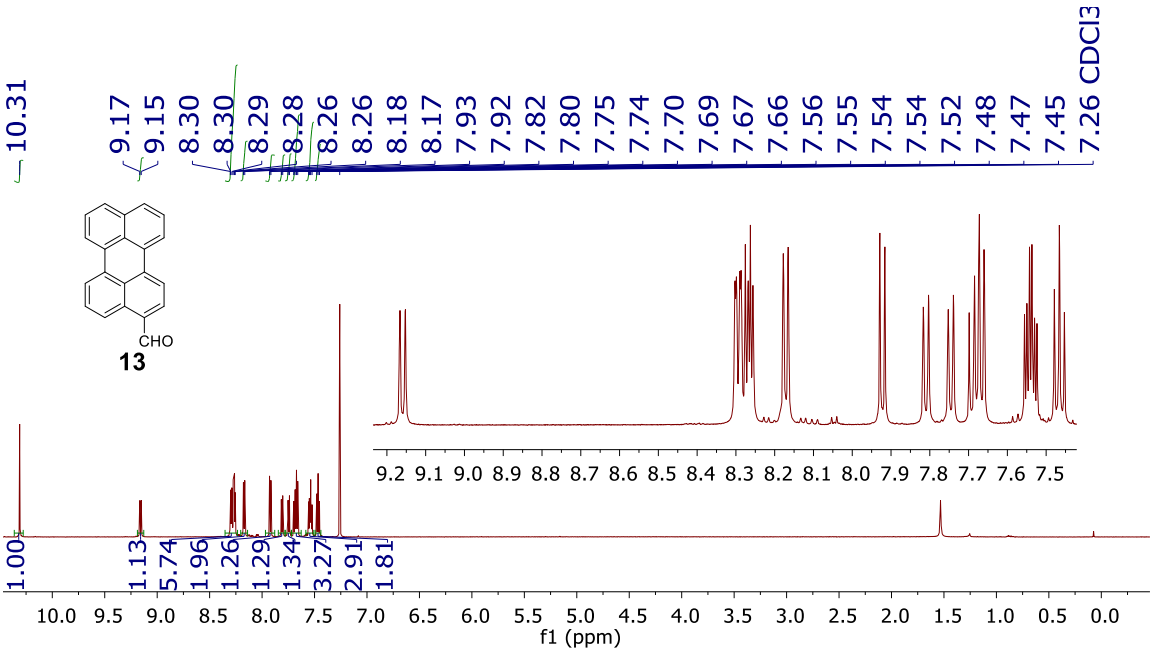

Figure 0-40 ^{1}H NMR of **13** in $CDCl_3$

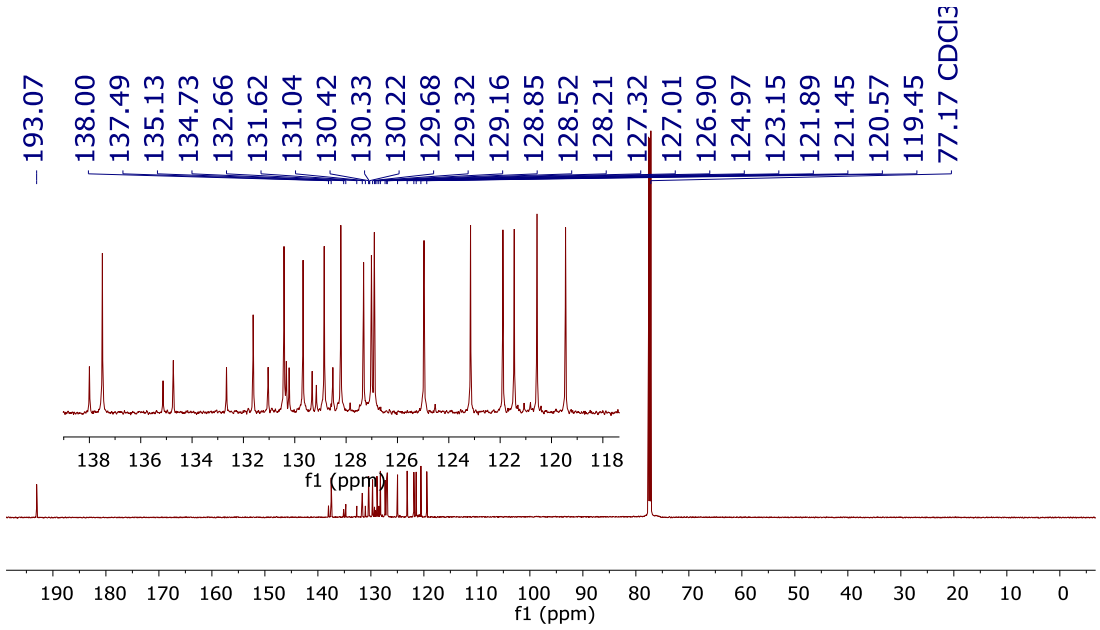

Figure 0-41^{13}C NMR of **13** in $CDCl_3$

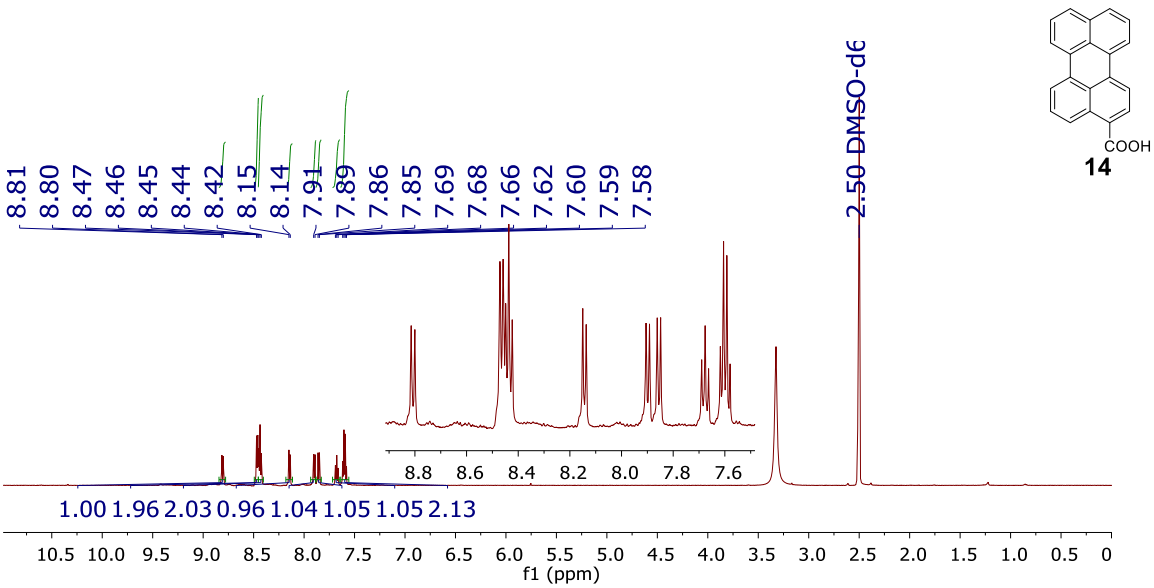

Figure 0-42 ^{1}H NMR of **14** in DMSO

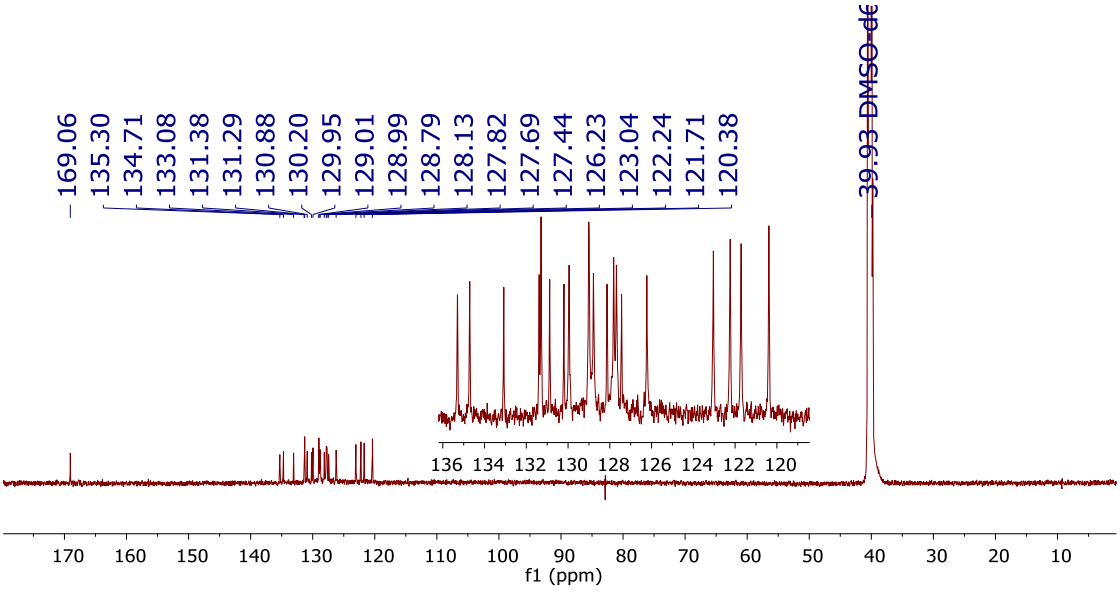

Figure 0-43 ^{13}C NMR of **14** in DMSO

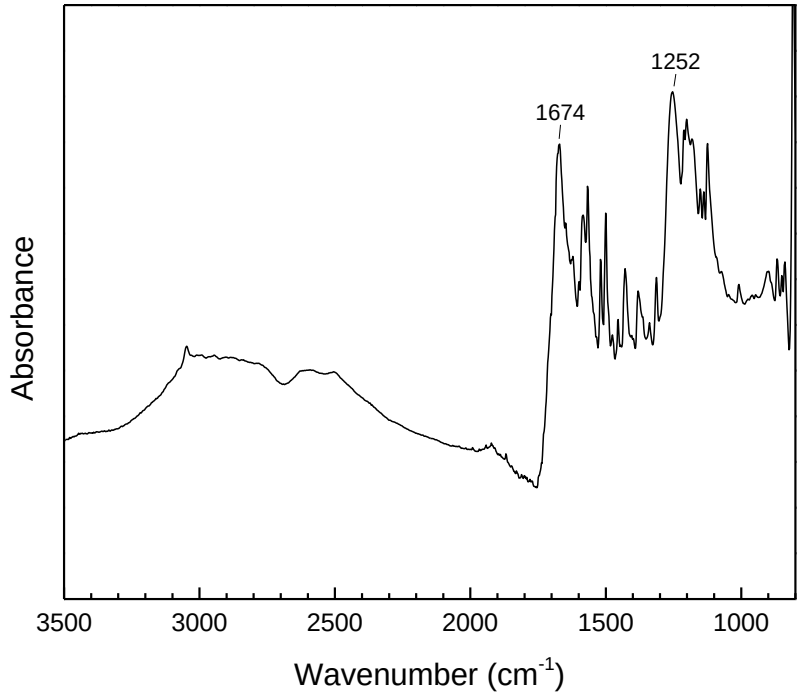

Figure 0-44 FT-IR-ATR of **14**

Bibliography

1. Sherman, B. D.; Pillai, S.; Kodis, G.; Bergkamp, J.; Mallouk, T. E.; Gust, D.; Moore, T. A.; Moore, A. L., A porphyrin-stabilized iridium oxide water oxidation catalyst. *Canadian Journal of Chemistry* **2011,** *89* (2), 152-157.
2. Osterloh, F. E., Inorganic nanostructures for photoelectrochemical and photocatalytic water splitting. *Chem. Soc. Rev.* **2013,** *42* (6), 2294-2320.
3. Ashford, D. L.; Gish, M. K.; Vannucci, A. K.; Brennaman, M. K.; Templeton, J. L.; Papanikolas, J. M.; Meyer, T. J., Molecular Chromophore–Catalyst Assemblies for Solar Fuel Applications. *Chemical Reviews* **2015,** *115* (23), 13006-13049.
4. Pho, T. V.; Sheridan, M. V.; Morseth, Z. A.; Sherman, B. D.; Meyer, T. J.; Papanikolas, J. M.; Schanze, K. S.; Reynolds, J. R., Efficient Light-Driven Oxidation of Alcohols Using an Organic Chromophore–Catalyst Assembly Anchored to TiO2. *Acs Appl Mater Inter* **2016,** *8* (14), 9125-9133.
5. Sheridan, M. V.; Sherman, B. D.; Coppo, R. L.; Wang, D.; Marquard, S. L.; Wee, K.-R.; Murakami Iha, N. Y.; Meyer, T. J., Evaluation of Chromophore and Assembly Design in Light-Driven Water Splitting with a Molecular Water Oxidation Catalyst. *ACS Energy Letters* **2016,** *1* (1), 231-236.
6. Youngblood, W. J.; Lee, S.-H. A.; Maeda, K.; Mallouk, T. E., Visible Light Water Splitting Using Dye-Sensitized Oxide Semiconductors. *Accounts Chem Res* **2009,** *42* (12), 1966-1973.
7. Sugathan, V.; John, E.; Sudhakar, K., Recent improvements in dye sensitized solar cells: A review. *Renewable and Sustainable Energy Reviews* **2015,** *52*, 54-64.
8. Meyer, G. J., The 2010 Millennium Technology Grand Prize: Dye-Sensitized Solar Cells. *Acs Nano* **2010,** *4* (8), 4337-4343.
9. Martinson, A. B. F.; Hamann, T. W.; Pellin, M. J.; Hupp, J. T., New Architectures for Dye-Sensitized Solar Cells. *Chemistry - A European Journal* **2008,** *14* (15), 4458-4467.
10. Hagfeldt, A.; Boschloo, G.; Sun, L.; Kloo, L.; Pettersson, H., Dye-Sensitized Solar Cells. *Chemical Reviews* **2010,** *110* (11), 6595-6663.
11. Ardo, S.; Meyer, G. J., Photodriven heterogeneous charge transfer with transition-metal compounds anchored to TiO2 semiconductor surfaces. *Chemical Society Reviews* **2009,** *38* (1), 115-164.
12. Weng, Z.; Guo, H.; Liu, X.; Wu, S.; Yeung, K. W. K.; Chu, P. K., Nanostructured TiO2 for energy conversion and storage. *RSC Advances* **2013,** *3* (47), 24758.
13. Tachibana, Y.; Vayssieres, L.; Durrant, J. R., Artificial photosynthesis for solar water-splitting. *Nature Photonics* **2012,** *6* (8), 511-518.
14. Su, J.; Vayssieres, L., A Place in the Sun for Artificial Photosynthesis? *ACS Energy Letters* **2016,** *1* (1), 121-135.
15. Nocera, D. G., The Artificial Leaf. *Accounts Chem Res* **2012,** *45* (5), 767-776.
16. Moore, G. F.; Konezny, S. J.; Song, H.-e.; Milot, R. L.; Blakemore, J. D.; Lee, M. L.; Batista, V. S.; Schmuttenmaer, C. A.; Crabtree, R. H.; Brudvig, G. W., Bioinspired

High-Potential Porphyrin Photoanodes. *The Journal of Physical Chemistry C* **2012,** *116* (7), 4892-4902.
17. Moore, G. F.; Hambourger, M.; Gervaldo, M.; Poluektov, O. G.; Rajh, T.; Gust, D.; Moore, T. A.; Moore, A. L., A Bioinspired Construct That Mimics the Proton Coupled Electron Transfer between P680•+and the TyrZ-His190 Pair of Photosystem II. *J Am Chem Soc* **2008,** *130* (32), 10466-10467.
18. Moore, G. F.; Brudvig, G. W., Energy Conversion in Photosynthesis: A Paradigm for Solar Fuel Production. *Annual Review of Condensed Matter Physics* **2011,** *2* (1), 303-327.
19. Karlsson, S.; Boixel, J.; Pellegrin, Y.; Blart, E.; Becker, H.-C.; Odobel, F.; Hammarström, L., Accumulative Charge Separation Inspired by Photosynthesis. *J Am Chem Soc* **2010,** *132* (51), 17977-17979.
20. Gust, D.; Moore, T. A.; Moore, A. L., Solar Fuels via Artificial Photosynthesis. *Accounts Chem Res* **2009,** *42* (12), 1890-1898.
21. Gratzel, M., Photoelectrochemical cells. *Nature* **2001,** *414* (6861), 338-344.
22. F., M. A. B.; W., H. T.; J., P. M.; T., H. J., New Architectures for Dye‐Sensitized Solar Cells. *Chemistry – A European Journal* **2008,** *14* (15), 4458-4467.
23. Gueymard, C. A.; Myers, D.; Emery, K., Proposed reference irradiance spectra for solar energy systems testing. *Sol Energy* **2002,** *73* (6), 443-467.
24. Zhang, L.; Cole, J. M., Dye aggregation in dye-sensitized solar cells. *J Mater Chem A* **2017,** *5* (37), 19541-19559.
25. Oregan, B.; Gratzel, M., A Low-Cost, High-Efficiency Solar-Cell Based on Dye-Sensitized Colloidal Tio2 Films. *Nature* **1991,** *353* (6346), 737-740.
26. Burschka, J.; Pellet, N.; Moon, S. J.; Humphry-Baker, R.; Gao, P.; Nazeeruddin, M. K.; Gratzel, M., Sequential deposition as a route to high-performance perovskite-sensitized solar cells. *Nature* **2013,** *499* (7458), 316-+.
27. Kay, A.; Gratzel, M., Artificial Photosynthesis .1. Photosensitization of Tio2 Solar-Cells with Chlorophyll Derivatives and Related Natural Porphyrins. *J Phys Chem-Us* **1993,** *97* (23), 6272-6277.
28. Nazeeruddin, M. K.; Humphry-Baker, R.; Gratzel, M.; Wohrle, D.; Schnurpfeil, G.; Schneider, G.; Hirth, A.; Trombach, N., Efficient near-IR sensitization of nanocrystalline TiO2 films by zinc and aluminum phthalocyanines. *J Porphyr Phthalocya* **1999,** *3* (3), 230-237.
29. Nazeeruddin, M. K.; Humphry-Baker, R.; Gratzel, M.; Murrer, B. A., Efficient near IR sensitization of nanocrystalline TiO2 films by ruthenium phthalocyanines. *Chem Commun* **1998,** (6), 719-720.
30. Nazeeruddin, M. K.; Kay, A.; Rodicio, I.; Humphrybaker, R.; Muller, E.; Liska, P.; Vlachopoulos, N.; Gratzel, M., Conversion of Light to Electricity by Cis-X2bis(2,2'-Bipyridyl-4,4'-Dicarboxylate)Ruthenium(Ii) Charge-Transfer Sensitizers (X = Cl-, Br-, I-, Cn-, and Scn-) on Nanocrystalline Tio2 Electrodes. *J Am Chem Soc* **1993,** *115* (14), 6382-6390.
31. Gawelda, W.; Cannizzo, A.; Pham, V. T.; van Mourik, F.; Bressler, C.; Chergui, M., Ultrafast nonadiabatic dynamics of [Fe-II(bpy)(3)](2+) in solution. *J Am Chem Soc* **2007,** *129* (26), 8199-8206.

32. Creutz, C.; Chou, M.; Netzel, T. L.; Okumura, M.; Sutin, N., Lifetimes, Spectra, and Quenching of the Excited-States of Polypyridine Complexes of Iron(Ii), Ruthenium(Ii), and Osmium(Ii). *J Am Chem Soc* **1980,** *102* (4), 1309-1319.
33. Monat, J. E.; McCusker, J. K., Femtosecond excited-state dynamics of an iron(II) polypyridyl solar cell sensitizer model. *J Am Chem Soc* **2000,** *122* (17), 4092-4097.
34. Liu, Y. Z.; Persson, P.; Sundstrom, V.; Warnmark, K., Fe N-Heterocyclic Carbene Complexes as Promising Photosensitizers. *Accounts Chem Res* **2016,** *49* (8), 1477-1485.
35. Liu, Y. Z.; Harlang, T.; Canton, S. E.; Chabera, P.; Suarez-Alcantara, K.; Fleckhaus, A.; Vithanage, D. A.; Goransson, E.; Corani, A.; Lomoth, R.; Sundstrom, V.; Warnmark, K., Towards longer-lived metal-to-ligand charge transfer states of iron(II) complexes: an N-heterocyclic carbene approach. *Chem Commun* **2013,** *49* (57), 6412-6414.
36. Harlang, T. C. B.; Liu, Y. Z.; Gordivska, O.; Fredin, L. A.; Ponseca, C. S.; Huang, P.; Chabera, P.; Kjaer, K. S.; Mateos, H.; Uhlig, J.; Lomoth, R.; Wallenberg, R.; Styring, S.; Persson, P.; Sundstrom, V.; Warnmark, K., Iron sensitizer converts light to electrons with 92% yield. *Nat Chem* **2015,** *7* (11), 883-889.
37. Liu, Y. Z.; Kjaer, K. S.; Fredin, L. A.; Chabera, P.; Harlang, T.; Canton, S. E.; Lidin, S.; Zhang, J. X.; Lomoth, R.; Bergquist, K. E.; Persson, P.; Warnmark, K.; Sundstrom, V., A Heteroleptic Ferrous Complex with Mesoionic Bis(1,2,3-triazol-5-ylidene) Ligands: Taming the MLCT Excited State of Iron(II). *Chem-Eur J* **2015,** *21* (9), 3628-3639.
38. Chabera, P.; Liu, Y. Z.; Prakash, O.; Thyrhaug, E.; El Nahhas, A.; Honarfar, A.; Essen, S.; Fredin, L. A.; Harlang, T. C. B.; Kjaer, K. S.; Handrup, K.; Ericson, F.; Tatsuno, H.; Morgan, K.; Schnadt, J.; Haggstrom, L.; Ericsson, T.; Sobkowiak, A.; Lidin, S.; Huang, P.; Styring, S.; Uhlig, J.; Bendix, J.; Lomoth, R.; Sundstrom, V.; Persson, P.; Warnmark, K., A low-spin Fe(III) complex with 100-ps ligand-to-metal charge transfer photoluminescence. *Nature* **2017,** *543* (7647), 695-+.
39. Bessho, T.; Constable, E. C.; Graetzel, M.; Redondo, A. H.; Housecroft, C. E.; Kylberg, W.; Nazeeruddin, M. K.; Neuburger, M.; Schaffner, S., An element of surprise - efficient copper-functionalized dye-sensitized solar cells. *Chem Commun* **2008,** (32), 3717-3719.
40. Alonsovante, N.; Nierengarten, J. F.; Sauvage, J. P., Spectral Sensitization of Large-Band-Gap Semiconductors (Thin-Films and Ceramics) by a Carboxylated Bis(1,10-Phenanthroline)Copper(I) Complex. *J Chem Soc Dalton* **1994,** (11), 1649-1654.
41. Sakaki, S.; Kuroki, T.; Hamada, T., Synthesis of a new copper(I) complex, [Cu(tmdcbpy)(2)](+) (tmdcbpy=4,4 ',6,6 '-tetramethyl-2,2 '-bipyridine-5,5 '-dicarboxylic acid), and its application to solar cells. *J Chem Soc Dalton* **2002,** (6), 840-842.
42. Baheti, A.; Lee, C. P.; Thomas, K. R. J.; Ho, K. C., Pyrene-based organic dyes with thiophene containing pi-linkers for dye-sensitized solar cells: optical, electrochemical and theoretical investigations. *Phys Chem Chem Phys* **2011,** *13* (38), 17210-17221.
43. Ferrere, S.; Zaban, A.; Gregg, B. A., Dye sensitization of nanocrystalline tin oxide by perylene derivatives. *J Phys Chem B* **1997,** *101* (23), 4490-4493.
44. Srinivas, K.; Yesudas, K.; Bhanuprakash, K.; Rao, V. J.; Giribabu, L., A Combined Experimental and Computational Investigation of Anthracene Based

Sensitizers for DSSC: Comparison of Cyanoacrylic and Malonic Acid Electron Withdrawing Groups Binding onto the TiO2 Anatase (101) Surface. *J Phys Chem C* **2009,** *113* (46), 20117-20126.

45. Rehm, J. M.; McLendon, G. L.; Nagasawa, Y.; Yoshihara, K.; Moser, J.; Gratzel, M., Femtosecond electron-transfer dynamics at a sensitizing dye-semiconductor (TiO2) interface. *J Phys Chem-Us* **1996,** *100* (23), 9577-9578.

46. Wang, Z. S.; Cui, Y.; Dan-Oh, Y.; Kasada, C.; Shinpo, A.; Hara, K., Molecular Design of Coumarin Dyes for Stable and Efficient Organic Dye-Sensitized Solar Cells. *J Phys Chem C* **2008,** *112* (43), 17011-17017.

47. Hara, K.; Sato, T.; Katoh, R.; Furube, A.; Ohga, Y.; Shinpo, A.; Suga, S.; Sayama, K.; Sugihara, H.; Arakawa, H., Molecular design of coumarin dyes for efficient dye-sensitized solar cells. *J Phys Chem B* **2003,** *107* (2), 597-606.

48. Feldt, S. M.; Gibson, E. A.; Gabrielsson, E.; Sun, L.; Boschloo, G.; Hagfeldt, A., Design of Organic Dyes and Cobalt Polypyridine Redox Mediators for High-Efficiency Dye-Sensitized Solar Cells. *J Am Chem Soc* **2010,** *132* (46), 16714-16724.

49. Zhang, X. Y.; Xu, Y. Y.; Giordano, F.; Schreier, M.; Pellet, N.; Hu, Y.; Yi, C. Y.; Robertson, N.; Hua, J. L.; Zakeeruddin, S. M.; Tian, H.; Gratzel, M., Molecular Engineering of Potent Sensitizers for Very Efficient Light Harvesting in Thin-Film Solid-State Dye-Sensitized Solar Cells. *J Am Chem Soc* **2016,** *138* (34), 10742-10745.

50. Wang, J.; Liu, K.; Ma, L.; Zhan, X., Triarylamine: Versatile Platform for Organic, Dye-Sensitized, and Perovskite Solar Cells. *Chem. Rev. (Washington, DC, U. S.)* **2016,** *116* (23), 14675-14725.

51. Wu, D.; Chen, L.; Lee, W.; Ko, G.; Yin, J.; Yoon, J., Recent progress in the development of organic dye based near-infrared fluorescence probes for metal ions. *Coord. Chem. Rev.* **2018,** *354*, 74-97.

52. Yuan, L.; Lin, W.; Zheng, K.; He, L.; Huang, W., Far-red to near infrared analyte-responsive fluorescent probes based on organic fluorophore platforms for fluorescence imaging. *Chem Soc Rev* **2013,** *42* (2), 622-61.

53. Wang, L. X.; Ernstorfer, R.; Willig, F.; May, V., Absorption spectra related to heterogeneous electron transfer reactions: The perylene TiO2 system. *J Phys Chem B* **2005,** *109* (19), 9589-9595.

54. Freitag, M.; Giordano, F.; Yang, W. X.; Pazoki, M.; Hao, Y.; Zietz, B.; Gratzel, M.; Hagfeldt, A.; Boschloo, G., Copper Phenanthroline as a Fast and High-Performance Redox Mediator for Dye-Sensitized Solar Cells. *J Phys Chem C* **2016,** *120* (18), 9595-9603.

55. Freitag, M.; Daniel, Q.; Pazoki, M.; Sveinbjornsson, K.; Zhang, J. B.; Sun, L. C.; Hagfeldt, A.; Boschloo, G., High-efficiency dye-sensitized solar cells with molecular copper phenanthroline as solid hole conductor. *Energ Environ Sci* **2015,** *8* (9), 2634-2637.

56. Freitag, M.; Teuscher, J.; Saygili, Y.; Zhang, X. Y.; Giordano, F.; Liska, P.; Hua, J. L.; Zakeeruddin, S. M.; Moser, J. E.; Gratzel, M.; Hagfeldt, A., Dye-sensitized solar cells for efficient power generation under ambient lighting (vol 11, pg 370, 2017). *Nature Photonics* **2017,** *11* (6).

57. Yan, S. G.; Hupp, J. T., Semiconductor-based interfacial electron-transfer reactivity: Decoupling kinetics from pH-dependent band energetics in a dye-sensitized titanium dioxide aqueous solution system. *J Phys Chem-Us* **1996,** *100* (17), 6867-6870.

58. Nakhle, B. M.; Trammell, S. A.; Sigel, K. M.; Meyer, T. J.; Erickson, B. W., Synthesis of 3,5-bis(phosphonomethyl)benzoic acid and its application as a metal oxide surface bivalent anchor. *Tetrahedron* **1999,** *55* (10), 2835-2846.
59. Ghosh, P. K.; Spiro, T. G., Photoelectrochemistry of Tris(Bipyridyl)Ruthenium(Ii) Covalently Attached to Normal-Type Sno2. *J Am Chem Soc* **1980,** *102* (17), 5543-5549.
60. Lin, J.; Siddiqui, J. A.; Ottenbrite, R. M., Surface modification of inorganic oxide particles with silane coupling agent and organic dyes. *Polym Advan Technol* **2001,** *12* (5), 285-292.
61. Argazzi, R.; Bignozzi, C. A.; Heimer, T. A.; Castellano, F. N.; Meyer, G. J., Enhanced Spectral Sensitivity from Ruthenium(Ii) Polypyridyl Based Photovoltaic Devices. *Inorg Chem* **1994,** *33* (25), 5741-5749.
62. Vittadini, A.; Selloni, A.; Rotzinger, F. P.; Gratzel, M., Formic acid adsorption on dry and hydrated TiO2 anatase (101) surfaces by DFT calculations. *J Phys Chem B* **2000,** *104* (6), 1300-1306.
63. Galoppini, E., Linkers for anchoring sensitizers to semiconductor nanoparticles. *Coordin Chem Rev* **2004,** *248* (13-14), 1283-1297.
64. Kilsa, K.; Mayo, E. I.; Kuciauskas, D.; Villahermosa, R.; Lewis, N. S.; Winkler, J. R.; Gray, H. B., Effects of Bridging ligands on the current-potential behavior and interfacial kinetics of ruthenium-sensitized nanocrystalline TiO2 photoelectrodes. *J Phys Chem A* **2003,** *107* (18), 3379-3383.
65. Lundqvist, M. J.; Galoppini, E.; Meyer, G. J.; Persson, P., Calculated optoelectronic properties of ruthenium tris-bipyridine dyes containing oligophenyleneethynylene rigid rod linkers in different chemical environments. *J Phys Chem A* **2007,** *111* (8), 1487-1497.
66. Wei, Q.; Galoppini, E., Tripodal Ru(II) complexes with conjugated and non-conjugated rigid-rod bridges for semiconductor nanoparticles sensitization. *Tetrahedron* **2004,** *60* (38), 8497-8508.
67. Thyagarajan, S.; Galoppini, E.; Persson, P.; Giaimuccio, J. M.; Meyer, G. J., Large Footprint Pyrene Chromophores Anchored to Planar and Colloidal Metal Oxide Thin Films. *Langmuir* **2009,** *25* (16), 9219-9226.
68. Lee, C. H.; Zhang, Y. Y.; Romayanantakit, A.; Galoppini, E., Modular synthesis of ruthenium tripodal system with variable anchoring groups positions for semiconductor sensitization. *Tetrahedron* **2010,** *66* (22), 3897-3903.
69. Persson, P.; Knitter, M.; Galoppini, E., Light-harvesting and electronic contacting capabilities of Ru(II) Ipa rod and star complexes-first principles predictions. *Rsc Advances* **2012,** *2* (20), 7868-7874.
70. Chitre, K. P.; Guillen, E.; Yoon, A. S.; Galoppini, E., Synthesis of Homoleptic Ruthenium "Star" Complexes by Click Reaction for TiO2 Sensitization. *Eur J Inorg Chem* **2012,** (33), 5461-5464.
71. Zhang, Y. Y.; Galoppini, E.; Johansson, P. G.; Meyer, G. J., Homoleptic star-shaped Ru(II) complexes. *Pure Appl Chem* **2011,** *83* (4), 861-868.
72. Urbani, M.; Barea, E. M.; Trevisan, R.; Aljarilla, A.; de la Cruz, P.; Bisquert, J.; Langa, F., A star-shaped sensitizer based on thienylenevinylene for dye-sensitized solar cells. *Tetrahedron Lett* **2013,** *54* (5), 431-435.

73. Anderson, N. A.; Ai, X.; Chen, D. T.; Mohler, D. L.; Lian, T. Q., Bridge-assisted ultrafast interfacial electron transfer to nanocrystalline SnO2 thin films. *J Phys Chem B* **2003,** *107* (51), 14231-14239.
74. Cao, Y.; Galoppini, E.; Reyes, P. I.; Lu, Y. C., Functionalization of Nanostructured ZnO Films by Copper-Free Click Reaction. *Langmuir* **2013,** *29* (25), 7768-7775.
75. Imahori, H.; Kang, S.; Hayashi, H.; Haruta, M.; Kurata, H.; Isoda, S.; Canton, S. E.; Infahsaeng, Y.; Kathiravan, A.; Pascher, T.; Chabera, P.; Yartsev, A. P.; Sundstrom, V., Photoinduced Charge Carrier Dynamics of Zn-Porphyrin-TiO2 Electrodes: The Key Role of Charge Recombination for Solar Cell Performance. *J Phys Chem A* **2011,** *115* (16), 3679-3690.
76. Nieto-Pescador, J.; Abraham, B.; Li, J. J.; Batarseh, A.; Bartynski, R. A.; Galoppini, E.; Gundlach, L., Heterogeneous Electron-Transfer Dynamics through Dipole-Bridge Groups. *J Phys Chem C* **2016,** *120* (1), 48-55.
77. Rangan, S.; Batarseh, A.; Chitre, K. P.; Kopecky, A.; Galoppini, E.; Bartynski, R. A., Tuning Energy Level Alignment At Organic/Semiconductor Interfaces Using a Built-In Dipole in Chromophore-Bridge-Anchor Compounds. *J Phys Chem C* **2014,** *118* (24), 12923-12928.
78. Hu, K.; Blair, A. D.; Piechota, E. J.; Schauer, P. A.; Sampaio, R. N.; Parlane, F. G. L.; Meyer, G. J.; Berlinguette, C. P., Kinetic pathway for interfacial electron transfer from a semiconductor to a molecule. *Nat Chem* **2016,** *8* (9), 853-859.
79. Gundlach, L.; Ernstorfer, R.; Willig, F., Pathway-dependent electron transfer for rod-shaped perylene-derived molecules adsorbed in nanometer-size TiO2 cavities. *J Phys Chem C* **2007,** *111* (36), 13586-13594.
80. Mishra, A.; Fischer, M. K. R.; Bauerle, P., Metal-Free Organic Dyes for Dye-Sensitized Solar Cells: From Structure: Property Relationships to Design Rules. *Angew Chem Int Edit* **2009,** *48* (14), 2474-2499.
81. Hara, K.; Sayama, K.; Ohga, Y.; Shinpo, A.; Suga, S.; Arakawa, H., A coumarin-derivative dye sensitized nanocrystalline TiO2 solar cell having a high solar-energy conversion efficiency up to 5.6%. *Chem Commun* **2001,** (6), 569-570.
82. Wang, Z. S.; Cui, Y.; Dan-Oh, Y.; Kasada, C.; Shinpo, A.; Hara, K., Thiophene-functionalized coumarin dye for efficient dye-sensitized solar cells: Electron lifetime improved by coadsorption of deoxycholic acid. *J Phys Chem C* **2007,** *111* (19), 7224-7230.
83. Seo, K. D.; Song, H. M.; Lee, M. J.; Pastore, M.; Anselmi, C.; De Angelis, F.; Nazeeruddin, M. K.; Graetzel, M.; Kim, H. K., Coumarin dyes containing low-band-gap chromophores for dye-sensitised solar cells. *Dyes Pigments* **2011,** *90* (3), 304-310.
84. Scholl, R. a. M., J, meso-Benzdianthron (Helianthron), meso-Naphthodianthron, und ein neuer Weg zum Flavanthren. *Ber. Dtsch. Chem. Ges.* **1910,** *43*, 1734.
85. Berlman, I. B., 6 - GRAPHS. In *Handbook of Fluorescence Spectra of Aromatic Molecules (Second Edition)*, Academic Press: 1971; pp 107-415.
86. Zhan, X. W.; Tan, Z. A.; Domercq, B.; An, Z. S.; Zhang, X.; Barlow, S.; Li, Y. F.; Zhu, D. B.; Kippelen, B.; Marder, S. R., A high-mobility electron-transport polymer with broad absorption and its use in field-effect transistors and all-polymer solar cells. *J Am Chem Soc* **2007,** *129* (23), 7246-+.

87. Mansour, A. F.; El-Shaarawy, M. G.; El-Bashir, S. M.; El-Mansy, M. K.; Hammam, M., Optical study of perylene dye doped poly(methyl methacrylate) as fluorescent solar collector. *Polym Int* **2002,** *51* (5), 393-397.
88. Lemaur, V.; Steel, M.; Beljonne, D.; Bredas, J. L.; Cornil, J., Photoinduced charge generation and recombination dynamics in model donor/acceptor pairs for organic solar cell applications: A full quantum-chemical treatment. *J Am Chem Soc* **2005,** *127* (16), 6077-6086.
89. Edvinsson, T.; Li, C.; Pschirer, N.; Schoneboom, J.; Eickemeyer, F.; Sens, R.; Boschloo, G.; Herrmann, A.; Mullen, K.; Hagfeldt, A., Intramolecular charge-transfer tuning of perylenes: Spectroscopic features and performance in Dye-sensitized solar cells. *J Phys Chem C* **2007,** *111* (42), 15137-15140.
90. Yagai, S.; Hamamura, S.; Wang, H.; Stepanenko, V.; Seki, T.; Unoike, K.; Kikkawa, Y.; Karatsu, T.; Kitamura, A.; Wurthner, F., Unconventional hydrogen-bond-directed hierarchical co-assembly between perylene bisimide and azobenzene-functionalized melamine. *Org Biomol Chem* **2009,** *7* (19), 3926-3929.
91. Feng, Y. Y.; Feng, W., Photo-responsive perylene diimid-azobenzene dyad: Photochemistry and its morphology control by self-assembly. *Opt Mater* **2008,** *30* (6), 876-880.
92. Bachman, J. C.; Kavian, R.; Graham, D. J.; Kim, D. Y.; Noda, S.; Nocera, D. G.; Shao-Horn, Y.; Lee, S. W., Electrochemical polymerization of pyrene derivatives on functionalized carbon nanotubes for pseudocapacitive electrodes. *Nat Commun* **2015,** *6*.
93. Ernstorfer, R. Spectroscopic investigation of photoinduced heterogeneous electron transfer. PhD thesis, Freie Universität Berlin, 2004.
94. Burfeindt, B.; Hannappel, T.; Storck, W.; Willig, F., Measurement of temperature-independent femtosecond interfacial electron transfer from an anchored molecular electron donor to a semiconductor as acceptor. *J Phys Chem-Us* **1996,** *100* (41), 16463-16465.
95. Ernstorfer, R.; Gundlach, L.; Felber, S.; Storck, W.; Eichberger, R.; Willig, F., Role of molecular anchor groups in molecule-to-semiconductor electron transfer. *J Phys Chem B* **2006,** *110* (50), 25383-25391.
96. Zimmermann, C.; Willig, F.; Ramakrishna, S.; Burfeindt, B.; Pettinger, B.; Eichberger, R.; Storck, W., Experimental fingerprints of vibrational wave-packet motion during ultrafast heterogeneous electron transfer. *J Phys Chem B* **2001,** *105* (38), 9245-9253.
97. 'Excimer' fluorescence. IV. Solution spectra of polycyclic hydrocarbons. *Proceedings of the Royal Society of London. Series A. Mathematical and Physical Sciences* **1964,** *277* (1371), 571.
98. Tanaka, J., The Electronic Spectra of Aromatic Molecular Crystals. II. The Crystal Structure and Spectra of Perylene. *Bulletin of the Chemical Society of Japan* **1963,** *36* (10), 1237-1249.
99. Walker, B.; Port, H.; Wolf, H. C., The two-step excimer formation in perylene crystals. *Chemical Physics* **1985,** *92* (2), 177-185.
100. Ma, L.; Tan, K. J.; Jiang, H.; Kloc, C.; Michel-Beyerle, M. E.; Gurzadyan, G. G., Excited-State Dynamics in an alpha-Perylene Single Crystal: Two-Photon- and Consecutive Two-Quantum-Induced Singlet Fission. *J Phys Chem A* **2014,** *118* (5), 838-843.

101. Tachikawa, H.; Faulkner, L. R., Anomalous luminescence from perylene in thin polymer films. *Chemical Physics Letters* **1976,** *39* (3), 436-441.
102. Mahrt, J.; Willig, F.; Storck, W.; Weiss, D.; Kietzmann, R.; Schwarzburg, K.; Tufts, B.; Trosken, B., Luminescence and Configurations of Perylene Dimers in a Langmuir-Blodgett-Film. *J Phys Chem-Us* **1994,** *98* (7), 1888-1894.
103. Akimoto, S.; Ohmori, A.; Yamazaki, I., Dimer formation and excitation relaxation of perylene in Langmuir-Blodgett films. *J Phys Chem B* **1997,** *101* (19), 3753-3758.
104. Vitukhnovsky, A. G.; Sluch, M. I.; Warren, J. G.; Petty, M. C., The Fluorescence of Perylene-Doped Langmuir-Blodgett-Films. *Chem Phys Lett* **1990,** *173* (5-6), 425-429.
105. Weiss, D.; Kietzmann, R.; Mahrt, J.; Tufts, B.; Storck, W.; Willig, F., E-Excimer and Y-Type Luminescence of Perylene Dimers in a Langmuir-Blodgett-Film at 1.5-K. *J Phys Chem-Us* **1992,** *96* (13), 5320-5325.
106. Cook, R. E.; Phelan, B. T.; Kamire, R. J.; Majewski, M. B.; Young, R. M.; Wasielewski, M. R., Excimer Formation and Symmetry-Breaking Charge Transfer in Cofacial Perylene Dimers. *J Phys Chem A* **2017,** *121* (8), 1608-1616.
107. He, C.; Abraham, B.; Fan, H.; Harmer, R.; Li, Z. X.; Galoppini, E.; Gundlach, L.; Teplyakov, A. V., Morphology-Preserving Sensitization of ZnO Nanorod Surfaces via Click-Chemistry. *J Phys Chem Lett* **2018,** *9* (4), 768-772.
108. Brown, K. E.; Veldkamp, B. S.; Co, D. T.; Wasielewski, M. R., Vibrational Dynamics of a Perylene-Perylenediimide Donor-Acceptor Dyad Probed with Femtosecond Stimulated Raman Spectroscopy. *J Phys Chem Lett* **2012,** *3* (17), 2362-2366.
109. Scholl, R.; Meyer, K., Die aromatischen Grundkohlenwasserstoffe des Anth - anthrons, Anth - dianthrons (2.3,4.5 - Dibenz - coronenchinons - (1.6)), Pyranthrons bzw. amphi - Isopyranthrons, Violanthrons, Iso - violanthrons, 1.2.3,7.8.9 - Dinaphthocoronenchinons - (4.10) und das Dibenz - rubicen. *Berichte der deutschen chemischen Gesellschaft (A and B Series)* **1934,** *67* (7), 1229-1235.
110. Avlasevich, Y.; Kohl, C.; Mullen, K., Facile synthesis of terrylene and its isomer benzoindenoperylene. *J Mater Chem* **2006,** *16* (11), 1053-1057.
111. Pieters, G.; Gaucher, A.; Prim, D.; Besson, T.; Planas, J. G.; Teixidor, F.; Vinas, C.; Light, M. E.; Hursthouse, M. B., Binaphthyl platform as starting materials for the preparation of electron rich benzo[g,h,i]perylenes. Application to molecular architectures based on amino benzo[g,h,i]perylenes and carborane combinations. *Chem Commun* **2011,** *47* (27), 7725-7727.
112. Luo, J.; Xu, X. M.; Mao, R. X.; Miao, Q., Curved Polycyclic Aromatic Molecules That Are pi-Isoelectronic to Hexabenzocoronene. *J Am Chem Soc* **2012,** *134* (33), 13796-13803.
113. Jones, D. J.; Purushothaman, B.; Ji, S. M.; Holmes, A. B.; Wong, W. W. H., Synthesis of electron-poor hexa-peri-hexabenzocoronenes. *Chem Commun* **2012,** *48* (65), 8066-8068.
114. Dou, X.; Yang, X. Y.; Bodwell, G. J.; Wagner, M.; Enkelmann, V.; Mullen, K., Unexpected phenyl group rearrangement during an intramolecular Scholl reaction leading to an alkoxy-substituted hexa-peri-hexabenzocoronene. *Org Lett* **2007,** *9* (13), 2485-2488.
115. Kramer, B.; Averhoff, A.; Waldvogel, S. R., Highly selective formation of eight-membered-ring systems by oxidative cyclization with molybdenum pentachloride - An

environmentally friendly and inexpensive access to 2,2 '-cyclolignans. *Angew Chem Int Edit* **2002,** *41* (16), 2981-2982.
116. Lowe, J., *Z. Chemie* **1868,** *4*.
117. R., S.; Chr., S.; R., W., Perylen, ein hoch kondensierter aromatischer Kohlenwasserstoff C20H12. *Berichte der deutschen chemischen Gesellschaft* **1910,** *43* (2), 2202-2209.
118. Kovacic, P.; Kyriakis, A., Polymerization of benzene to p-polyphenyl. *Tetrahedron Lett* **1962,** *3* (11), 467-469.
119. Grzybowski, M.; Skonieczny, K.; Butenschon, H.; Gryko, D. T., Comparison of Oxidative Aromatic Coupling and the Scholl Reaction. *Angew Chem Int Edit* **2013,** *52* (38), 9900-9930.
120. Watson, M. D.; Fechtenkotter, A.; Mullen, K., Big is beautiful - "Aromaticity" revisited from the viewpoint of macromolecular and supramolecular benzene chemistry. *Chemical Reviews* **2001,** *101* (5), 1267-1300.
121. Wu, J. S.; Pisula, W.; Mullen, K., Graphenes as potential material for electronics. *Chemical Reviews* **2007,** *107* (3), 718-747.
122. Zhi, L. J.; Mullen, K., A bottom-up approach from molecular nanographenes to unconventional carbon materials. *J Mater Chem* **2008,** *18* (13), 1472-1484.
123. Feng, X. L.; Pisula, W.; Mullen, K., Large polycyclic aromatic hydrocarbons: Synthesis and discotic organization. *Pure Appl Chem* **2009,** *81* (12), 2203-2224.
124. Rempala, P.; Kroulik, J.; King, B. T., A slippery slope: Mechanistic analysis of the intramolecular Scholl reaction of hexaphenylbenzene. *J Am Chem Soc* **2004,** *126* (46), 15002-15003.
125. Baddeley, G., 205. Hydrogen chloride–aluminium chloride as an agent of isomerisation. *Journal of the Chemical Society (Resumed)* **1950**, 994-997.
126. Nenitzescu Costin, D.; Balaban, A., Zum Chemismus der Hydridübertragung bei der Schollschen Reaktion. *Chemische Berichte* **1958,** *91* (10), 2109-2116.
127. Rooney, J. J.; Pink, R. C., The interaction between aluminum chloride and aromatic hydrocarbons. *Proc. Chem. Soc., London* **1961**, 142-3.
128. Clowes, G. A., Studies of the Scholl reaction: oxidative dehydrogenation involving 1-ethoxynaphthalene and related compounds. *Journal of the Chemical Society C: Organic* **1968,** (0), 2519-2526.
129. Zhai, L.; Shukla, R.; Wadumethrige, S. H.; Rathore, R., Probing the arenium-ion (protontransfer) versus the cation-radical (electron transfer) mechanism of Scholl reaction using DDQ as oxidant. *J Org Chem* **2010,** *75* (14), 4748-60.
130. Wadumethrige, S. H.; Rathore, R., A Facile Synthesis of Elusive Alkoxy-Substituted Hexa-peri-hexabenzocoronene. *Org. Lett.* **2008,** *10* (22), 5139-5142.
131. Zhai, L.; Shukla, R.; Rathore, R., Oxidative C-C Bond Formation (Scholl Reaction) with DDQ as an Efficient and Easily Recyclable Oxidant. *Org. Lett.* **2009,** *11* (15), 3474-3477.
132. Copeland, P. G.; Dean, R. E.; McNeil, D., Some cyclodehydrogenation and isomerization reactions of the binaphthyls. *J. Chem. Soc.* **1960**, 1689-91.
133. Olah, G. A.; Meyer, M. W., Friedel-Crafts isomerization. V. Aluminum-chloride catalyzed isomerization of terphenyls. *J. Org. Chem.* **1962,** *27*, 3682-3.

134. Skraba-Joiner, S. L.; McLaughlin, E. C.; Ajaz, A.; Thamatam, R.; Johnson, R. P., Scholl Cyclizations of Aryl Naphthalenes: Rearrangement Precedes Cyclization. *Journal of Organic Chemistry* **2015,** *80* (19), 9578-9583.
135. Photocyclization of Stilbenes and Related Molecules. In *Organic Reactions*.
136. Mallory, F. B.; Butler, K. E.; Evans, A. C.; Brondyke, E. J.; Mallory, C. W.; Yang, C. Q.; Ellenstein, A., Phenacenes: A family of graphite ribbons .2. Syntheses of some [7]phenacenes and an [11]phenacene by stilbene-like photocyclizations. *J Am Chem Soc* **1997,** *119* (9), 2119-2124.
137. Mallory, F. B.; Butler, K. E.; Berube, A.; Luzik, E. D.; Mallory, C. W.; Brondyke, E. J.; Hiremath, R.; Ngo, P.; Carroll, P. J., Phenacenes: a family of graphite ribbons. Part 3: Iterative strategies for the synthesis of large phenacenes. *Tetrahedron* **2001,** *57* (17), 3715-3724.
138. Scott, L. T.; Bratcher, M. S.; Hagen, S., Synthesis and characterization of a C36H12 fullerene subunit. *J Am Chem Soc* **1996,** *118* (36), 8743-8744.
139. Hagen, S.; Bratcher, M. S.; Erickson, M. S.; Zimmermann, G.; Scott, L. T., Novel syntheses of three C30H12 bowl-shaped polycyclic aromatic hydrocarbons. *Angewandte Chemie-International Edition in English* **1997,** *36* (4), 406-408.
140. Boorum, M. M.; Vasil'ev, Y. V.; Drewello, T.; Scott, L. T., Groundwork for a rational synthesis of C-60: Cyclodehydrogenation of a C60H30 polyarene. *Science* **2001,** *294* (5543), 828-831.
141. Scott, L. T.; Boorum, M. M.; McMahon, B. J.; Hagen, S.; Mack, J.; Blank, J.; Wegner, H.; de Meijere, A., A rational chemical synthesis of C-60. *Science* **2002,** *295* (5559), 1500-1503.
142. Solodovnikov, S. P. Z., Y. B.; Ioffe, S. T.; Kabachnik, M. I., *Radiospektrosk. Kvantovokhim. Metody Strukt. Issled.* **1967**, 106.
143. Koch, K. H.; Mullen, K., Polyarylenes and Poly(Arylenevinylene)S .5. Synthesis of Tetraalkyl-Substituted Oligo(1,4-Naphthylene)S and Cyclization to Soluble Oligo(Peri-Naphthylene)S. *Chemische Berichte* **1991,** *124* (9), 2091-2100.
144. Rickhaus, M.; Belanger, A. P.; Wegner, H. A.; Scott, L. T., An Oxidation Induced by Potassium Metal. Studies on the Anionic Cyclodehydrogenation of 1,1 '-Binaphthyl to Perylene. *Journal of Organic Chemistry* **2010,** *75* (21), 7358-7364.
145. Bank, S.; Lois, T. A.; Prislopski, M. C., Reactions of aromatic radical anions. IV. Evidence for an addition mechanism in the reaction of sodium naphthalene and hydrogen. *J Am Chem Soc* **1969,** *91* (19), 5407-5408.
146. Shindo, T.; Shindo, M.; Ohnuma, H.; Kabuto, C., Crystal-Structure of the Adduct of Thiourea with 2,6-Diethylnaphthalene. *Bulletin of the Chemical Society of Japan* **1993,** *66* (7), 1914-1918.
147. Shindo, T.; Ojima, R.; Hoshino, M.; Kitabayashi, S.; Ozawa, S., Equilibrium constants for formation of thiourea adduct of diisopropylnaphthalene isomers and di-t-butylnaphthalene isomers. *Sekiyu Gakkaishi* **1999,** *42* (6), 392-398.
148. Kodomari, M.; Satoh, H.; Yoshitomi, S., Selective Halogenation of Aromatic-Hydrocarbons with Alumina-Supported Copper(Ii) Halides. *Journal of Organic Chemistry* **1988,** *53* (9), 2093-2094.
149. Flockhart, B. D.; Sesay, I. M.; Pink, R. C., Perylene Cation-Radicals on the Surface of Catalytic Aluminas. *J Chem Soc Chem Comm* **1980,** (10), 439-440.

150. Michel, P.; Moradpour, A., A Convenient Access to Polyalkylperylenes. *Synthesis-Stuttgart* **1988,** (11), 894-896.
151. Li, Y. X.; Fitch, B., Effective enhancement of lithium-ion battery performance using SLMP. *Electrochem Commun* **2011,** *13* (7), 664-667.
152. Burglova, K.; Okorochenkov, S.; Budesinsky, M.; Hlavac, J., Efficient Method for Aromatic-Aldehyde Oxidation by Cleavage of Their Hydrazones Catalysed by Trimethylsilanolate. *Eur J Org Chem* **2017,** (2), 389-396.
153. Zeng, W. D.; Qi, Q. B.; Wu, J. S., Cyclopenta-fused perylene: a new soluble, stable and functionalizable rylene building block. *Sci Bull* **2015,** *60* (14), 1266-1271.
154. Schrock, A. K.; Schuster, G. B., Photochemistry of Naphthyl and Pyrenyl Azides - Chemical-Properties of the Transient Intermediates Probed by Laser Spectroscopy. *J Am Chem Soc* **1984,** *106* (18), 5234-5240.
155. Fulmer, G. R.; Miller, A. J. M.; Sherden, N. H.; Gottlieb, H. E.; Nudelman, A.; Stoltz, B. M.; Bercaw, J. E.; Goldberg, K. I., NMR Chemical Shifts of Trace Impurities: Common Laboratory Solvents, Organics, and Gases in Deuterated Solvents Relevant to the Organometallic Chemist. *Organometallics* **2010,** *29* (9), 2176-2179.
156. Skorobogatyi, M. V.; Pchelintseva, A. A.; Petrunina, A. L.; Stepanova, I. A.; Andronova, V. L.; Galegov, G. A.; Malakhov, A. D.; Korshun, V. A., 5-Alkynyl-2 '-deoxyuridines, containing bulky aryl groups: evaluation of structure-anti-HSV-1 activity relationship. *Tetrahedron* **2006,** *62* (6), 1279-1287.
157. Rajakumar, P.; Visalakshi, K.; Ganesan, S.; Maruthamuthu, P.; Suthanthiraraj, S. A., Synthesis of Pyrene-Based Ester Dendrimers for Applications in Dye-Sensitized Solar Cells. *Bulletin of the Chemical Society of Japan* **2012,** *85* (8), 902-911.
158. Shipway, A. N.; Katz, E.; Willner, I., Nanoparticle arrays on surfaces for electronic, optical, and sensor applications. *Chemphyschem* **2000,** *1* (1), 18-52.
159. Oskam, G., Metal oxide nanoparticles: synthesis, characterization and application. *J Sol-Gel Sci Techn* **2006,** *37* (3), 161-164.
160. Murphy, C. F.; Kenig, G. A.; Allen, D. T.; Laurent, J. P.; Dyer, D. E., Development of parametric material, energy, and emission inventories for wafer fabrication in the semiconductor industry. *Environ Sci Technol* **2003,** *37* (23), 5373-5382.
161. Henderson, M. A., A surface science perspective on TiO2 photocatalysis. *Surf Sci Rep* **2011,** *66* (6-7), 185-297.
162. Chen, X.; Mao, S. S., Titanium dioxide nanomaterials: Synthesis, properties, modifications, and applications. *Chemical Reviews* **2007,** *107* (7), 2891-2959.
163. Kim, H. J.; Lee, J. H., Highly sensitive and selective gas sensors using p-type oxide semiconductors: Overview. *Sensor Actuat B-Chem* **2014,** *192*, 607-627.
164. Murakami, M.; Matsumoto, Y.; Nakajima, K.; Makino, T.; Segawa, Y.; Chikyow, T.; Ahmet, P.; Kawasaki, M.; Koinuma, H., Anatase TiO2 thin films grown on lattice-matched LaAlO3 substrate by laser molecular-beam epitaxy. *Appl Phys Lett* **2001,** *78* (18), 2664-2666.
165. Kavan, L.; Gratzel, M.; Gilbert, S. E.; Klemenz, C.; Scheel, H. J., Electrochemical and photoelectrochemical investigation of single-crystal anatase. *J Am Chem Soc* **1996,** *118* (28), 6716-6723.
166. Kalyanasundaram, K.; Gratzel, M., Applications of functionalized transition metal complexes in photonic and optoelectronic devices. *Coordin Chem Rev* **1998,** *177*, 347-414.

167. Gonzalez-Valls, I.; Lira-Cantu, M., Vertically-aligned nanostructures of ZnO for excitonic solar cells: a review. *Energ Environ Sci* **2009,** *2* (1), 19-34.
168. Huss, A. S.; Bierbaum, A.; Chitta, R.; Ceckanowicz, D. J.; Mann, K. R.; Gladfelter, W. L.; Blank, D. A., Tuning Electron Transfer Rates via Systematic Shifts in the Acceptor State Density Using Size-Selected ZnO Colloids. *J Am Chem Soc* **2010,** *132* (40), 13963-13965.
169. Klabunde, K. J., *Nanoscale materials in chemistry*. Wiley-Interscience: 2001.
170. Thyagarajan, S.; Galoppini*, E.; Persson, P.; Giaimuccio, J. M.; Meyer, G. J., Large Footprint Pyrene Chromophores Anchored to Planar and Colloidal Metal Oxide Thin Films. *Langmuir* **2009,** *25* (16), 9219-9226.
171. Fan, Z. Y.; Lu, J. G., Zinc oxide nanostructures: Synthesis and properties. *J Nanosci Nanotechno* **2005,** *5* (10), 1561-1573.
172. Devan, R. S.; Patil, R. A.; Lin, J. H.; Ma, Y. R., One-Dimensional Metal-Oxide Nanostructures: Recent Developments in Synthesis, Characterization, and Applications. *Adv Funct Mater* **2012,** *22* (16), 3326-3370.
173. Yang, J. Y.; Lin, Y.; Meng, Y. M., Effects of dye etching on the morphology and performance of ZnO nanorod dye-sensitized solar cells. *Korean J Chem Eng* **2013,** *30* (11), 2026-2029.
174. Yan, F. P.; Huang, L. H.; Zheng, J. S.; Huang, J.; Lin, Z.; Huang, F.; Wei, M. D., Effect of Surface Etching on the Efficiency of ZnO-Based Dye-Sensitized Solar Cells. *Langmuir* **2010,** *26* (10), 7153-7156.
175. Bishop, L. M.; Yeager, J. C.; Chen, X.; Wheeler, J. N.; Torelli, M. D.; Benson, M. C.; Burke, S. D.; Pedersen, J. A.; Hamers, R. J., A Citric Acid-Derived Ligand for Modular Functionalization of Metal Oxide Surfaces via "Click" Chemistry. *Langmuir* **2012,** *28* (2), 1322-1329.
176. Brenner, T. M.; Flores, T. A.; Ndione, P. F.; Meinig, E. P.; Chen, G.; Olson, D. C.; Furtak, T. E.; Collins, R. T., Etch-Resistant Zn1-xMgxO Alloys: An Alternative to ZnO for Carboxylic Acid Surface Modification. *J Phys Chem C* **2014,** *118* (24), 12599-12607.
177. Torbrugge, S.; Ostendorf, F.; Reichling, M., Stabilization of Zinc-Terminated ZnO(0001) by a Modified Surface Stoichiometry. *J Phys Chem C* **2009,** *113* (12), 4909-4914.
178. Law, M.; Greene, L. E.; Radenovic, A.; Kuykendall, T.; Liphardt, J.; Yang, P. D., ZnO-Al2O3 and ZnO-TiO2 core-shell nanowire dye-sensitized solar cells. *J Phys Chem B* **2006,** *110* (45), 22652-22663.
179. Luo, B.; Rossini, J. E.; Gladfelter, W. L., Zinc Oxide Nanocrystals Stabilized by Alkylammonium Alkylcarbamates. *Langmuir* **2009,** *25* (22), 13133-13141.
180. Cardiel, A. C.; Benson, M. C.; Bishop, L. M.; Louis, K.; Yeager, J.; Tan, Y. Z.; Hamers, R. J., Chemically directed assembly of photoactive metal oxide nanoparticle heterojunctions via the copper-catalyzed azide-alkyne cycloaddition "click" reaction. *Abstr Pap Am Chem S* **2012,** *243*.
181. Rostovtsev, V. V.; Green, L. G.; Fokin, V. V.; Sharpless, K. B., A stepwise Huisgen cycloaddition process: Copper(I)-catalyzed regioselective "ligation" of azides and terminal alkynes. *Angew Chem Int Edit* **2002,** *41* (14), 2596-+.
182. Meldal, M.; Tornoe, C. W., Cu-catalyzed azide-alkyne cycloaddition. *Chemical Reviews* **2008,** *108* (8), 2952-3015.

183. Xi, W. X.; Scott, T. F.; Kloxin, C. J.; Bowman, C. N., Click Chemistry in Materials Science. *Adv Funct Mater* **2014,** *24* (18), 2572-2590.
184. Wong, C. H.; Zimmerman, S. C., Orthogonality in organic, polymer, and supramolecular chemistry: from Merrifield to click chemistry. *Chem Commun* **2013,** *49* (17), 1679-1695.
185. Gao, F.; Aminane, S.; Bai, S.; Teplyakov, A. V., Chemical Protection of Material Morphology: Robust and Gentle Gas-Phase Surface Functionalization of ZnO with Propiolic Acid. *Chem Mater* **2017,** *29* (9), 4063-4071.
186. Hara, K.; Dan-Oh, Y.; Kasada, C.; Ohga, Y.; Shinpo, A.; Suga, S.; Sayama, K.; Arakawa, H., Effect of additives on the photovoltaic performance of coumarin-dye-sensitized nanocrystalline TiO2 solar cells. *Langmuir* **2004,** *20* (10), 4205-4210.
187. Walters, K. A.; Gaal, D. A.; Hupp, J. T., Interfacial charge transfer and colloidal semiconductor dye-sensitization: Mechanism assessment via stark emission spectroscopy. *J Phys Chem B* **2002,** *106* (20), 5139-5142.
188. Ramakrishna, G.; Ghosh, H. N., Emission from the charge transfer state of xanthene dye-sensitized TiO2 nanoparticles: A new approach to determining back electron transfer rate and verifying the marcus inverted regime. *J Phys Chem B* **2001,** *105* (29), 7000-7008.
189. Linsebigler, A. L.; Lu, G. Q.; Yates, J. T., Photocatalysis on Tio2 Surfaces - Principles, Mechanisms, and Selected Results. *Chemical Reviews* **1995,** *95* (3), 735-758.
190. Ferguson, J., Absorption and Emission Spectra of the Perylene Dimer. *The Journal of Chemical Physics* **1966,** *44* (7), 2677-2683.
191. Kasha, M.; Rawls, H.; El-Bayoumi, M. A., The exciton model in molecular spectroscopy. *Pure Appl Chem* **1965,** *11* (3-4), 371-392.
192. Katoh, R.; Sinha, S.; Murata, S.; Tachiya, M., Origin of the stabilization energy of perylene excimer as studied by fluorescence and near-IR transient absorption spectroscopy. *J Photoch Photobio A* **2001,** *145* (1-2), 23-34.
193. Auweter, H.; Ramer, D.; Kunze, B.; Wolf, H. C., The Dynamics of Excimer Formation in Perylene Crystals. *Chemical Physics Letters* **1982,** *85* (3), 325-329.
194. Deacon, G. B.; Phillips, R. J., Relationships between the Carbon-Oxygen Stretching Frequencies of Carboxylato Complexes and the Type of Carboxylate Coordination. *Coordin Chem Rev* **1980,** *33* (3), 227-250.
195. Nara, M.; Torii, H.; Tasumi, M., Correlation between the vibrational frequencies of the carboxylate group and the types of its coordination to a metal ion: An ab initio molecular orbital study. *J Phys Chem-Us* **1996,** *100* (51), 19812-19817.
196. Dobson, K. D.; McQuillan, A. J., In situ infrared spectroscopic analysis of the adsorption of aromatic carboxylic acids to TiO2, ZrO2, Al2O3, and Ta2O5 from aqueous solutions. *Spectrochim Acta A* **2000,** *56* (3), 557-565.